

Barker

Science

Science
Extension
Journal



Scientific Research
in School

Volume 2 Number 1 September 2020



Barker
College

Honor Non Honores

Mission

An Anglican community inspiring
every learner
every experience
every day

Vision

To be a leader in Christian education
that is characterised by a global vision
that inspires hope

Values

Commitment
Compassion
Courage
Integrity
Respect



We acknowledge the Dharug, Darkinjung and Wonnarua peoples who are the traditional custodians of the land on which Barker College, Darkinjung Barker and Ngarralingayil Barker stand. We pay respect to the Elders past, present and emerging of the Dharug, Darkinjung and Wonnarua nations and extend that respect to other Indigenous people within the Barker College community.

Introduction

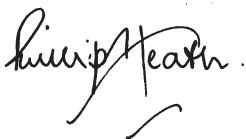


Science seeks to give reason to our perceptions in a way that is coherent and beautiful.

It is a gift to know and understand more about our world. Astronomer Johannes Kepler (1751-1630) eloquently described this privilege as “merely thinking God’s thoughts after him”. 2020 is a year where scientists continue to seek a better understanding of God’s world while yearning for a population that might trust their conclusions as COVID-19 is suppressed and a vaccine sought. Our students, who personally have been effected by the consequences of the global pandemic, have not taken a backward step but are instead continuing the cause of science as researchers themselves as part of the Science Extension course.

Research is typically the remit of university academics, but for the second year in a row we are proud to be able to publish genuine contributions to the scientific literature from students at Barker College. These students will go on to do great and wonderful things, but we do not have to wait to see what they can offer as in this journal they present new work in medicine, microbiology, education, engineering, physics, nutrition, environmental science and beyond.

Congratulations to the student researchers, their families and friends, and their supervising teachers for another outstanding year of scientific research in school.



Mr Phillip Heath AM
Head of Barker College



Science Extension invites students to become practising scientists as they think deeply about the history, philosophy and methods of science.

As they completed their research they have learned many valuable skills relevant across the sciences and beyond which will prepare them well for further study or careers in research or communication fields. I am excited by what the Barker College Science Extension research group has been able to produce in the last two years and I look forward to seeing how this growing body of work, produced by high school students, will continue to play its role in our scientific understanding.

Science is a team effort and the students and staff have demonstrated this in all aspects of the course. I am thankful to Dr Terrett, Dr Gates and Dr Hill who have continued to lead and support these students, with amazing results.



Mr Robert Paynter
Head of Science



Dr Matthew Hill
Director of The Barker Institute
Physics Teacher



Dr Katie Terrett
Chemistry Teacher



Dr Alison Gates
Agriculture & Science Teacher

Undertaking proper scientific research takes curiosity, capacity and commitment. These students found research questions that they were passionate about and worked hard to implement the scientific research process to answer them. They demonstrated a high capacity for scientific thinking, inquiry and communication resulting in these high-quality journal articles. It was a joy and a privilege to work with these fine young scientists. We are incredibly proud of them and we are excited to share their work with you in this journal.

Editors

Dr Matthew Hill
Dr Katie Terrett
Dr Alison Gates

Creative Direction

Mrs Susan Layton
Dr Matthew Hill

Printing

Barker Print Room

Contents

Part 1: Physics

Optimal length of a propeller duct Tom Harper	03
Emotions in the student Physics laboratory Arabella Crowley	13
A study of a marble's chaotic motion on a pinboard Max van Grecken	21
A general vector theory of the dynamics of a rapidly rotating top Alexander Gray	27

Part 2: Chemistry

Synthesis of a pyrimethamine analogue Kai Wong	47
Storage temperature and its effect on the concentration of lycopene extracted from tomatoes Alexander de Montemas	61
Synthesis of pyrimethamine and statistical analysis of product formed, assessing reliability of Sydney Grammar's published method (2016) Jasmine Sims	67

Part 3: Biology and Environmental Science

Escherichia Coli filtration using Casuarina xylem Laura Redman	79
Comparison of the antimicrobial properties of manuka honey vs store bought honey Cormac Sutherland	87
An investigation of the concentration of microplastics in the beaches of Lizard Island Jacob Kalnins	93
Microplastics in the gastrointestinal tract of prawns from Vietnam compared to Australia Yana McTeigue	99
The effect of temperature and salinity on the growth of Anabaena Jed Tomlinson	105

Part 4: Conference Presentations

Emotions in the Physics student laboratory: The impact of colour and story on secondary school student emotions during physics practical tasks Arabella Crowley, Dr Matthew Hill Australasian Science Education Research Association Conference, 2020	117
A new frontier in secondary science education: scientific research to high school students Dr Matthew Hill, Dr Alison Gates & Dr Katie Terrett Australasian Science Education Research Association Conference, 2020	121



Physics

Physics underpins all that we observe, and this year four students took very different approaches to produce unique developments in our understanding of the physical world.

In the scientific spirit of research leading to further investigations, Tom built on former Science Extension student, Alex Marlin's 2019 paper (comparing ducted and non-ducted propellers) by exploring the optimum duct length for producing maximum air flow through a propeller using computer simulations supported by practical data with 3D printed components. Similarly, Alex used a combination of computational and practical methods to produce some highly sophisticated work describing a more generalised model of forces on spinning tops. Alex's project is particularly interesting because it is a novel project developed around trying to understand the complex motion of the commonly accessible toys known as Beyblades. This is an example of how anytime we wish to know more about objects or motions around us we might consider the scientific research process we might use to develop our knowledge. Another project that considered the Physics behind toys was Max's research into the somewhat unpredictable motion of a marble falling through a pin-board component of a plastic marble run. He sought to ask whether there were predictable patterns, performed hundreds of trials, and proposes some interesting analysis.

Reading reports with complicated Physics concepts and equations arouses various emotions. Arabella's project investigated Year 11 student emotions in the Physics laboratory, a growing area of research at the academic level. She collaborated with researchers at The University of Sydney to bring research at the university to the high school classroom and presented her work as a poster at the Australasian Science Education Research Association conference in June. The poster is printed at the back of this journal. Her results are relevant for Barker Science teachers who are research led when it comes to their classroom approach. This project is part of Barker's growing work in the area of Science Education, along with former Science Extension student Jordan Guyot's project on enthusiasm in Chemistry education in 2019.

The Optimal Length of a Propeller Duct

Tom Harper

Barker College

Aeronautical engineers seek to design propellers with maximum efficiency. One motivation is derived from the pursuit of reducing the 915 million tonnes per year of carbon emissions from air-based travel (Air Transport Action group, 2020). One way to increase efficiency involves surrounding the propeller with a cylindrical duct which changes the efficiency of that propeller as the duct's length is varied. As research into the aerofoil profile indicates that an increased length enhances the effect of an aerofoil, this project examined whether increasing the length of a duct (which utilises the aerofoil profile) will further increase the efficiency of a propeller. Output air velocity was measured for five different duct lengths from 5cm to 11cm (at intervals of 1.5cm) of a standard three blade, 5-inch (12.7cm) diameter propeller, through both 3D Computational Fluid Dynamics simulations and a practical analysis of 3D printed prototypes. The results consistently demonstrated that as the duct length was increased, the produced air velocity also increased until a maximum point (around 9.5cm length), from where air velocity decreased again. It is proposed that resultant air flow is maximised when the duct length is 0.75 times the propeller diameter.

Literature review

Propellers are devices consisting of thin aerofoil-shaped blades which rotate around a central axis. They are designed to increase the flow-rate of an incoming fluid, producing a forward thrust (Lee & Lin, 2002) (Figure 1). Propellers are used in many real-world applications from planes to model drones (Gao, Hou & Zhu, 2015). A propeller uses an aerofoil shape that rotates to produce thrust in a desired direction (National Aeronautics and Space Administration, 2010). However, a standard propeller has design flaws yet the implantation of a duct can dramatically improve their resultant efficiency (Bhattacharyya, 2015). Three ways a duct can increase efficiency include the prevention of wing-tip vortices, the increase in air-flow rate through the duct and the prevention of turbulent thrust (Engstrand, 1927; Burge, 1988).

What is a propeller duct?

A propeller duct is a cylindrical object that encases the propeller (Figure 2). The cross-section of the duct is designed in the shape of an aerofoil. An aerofoil is a 2-Dimensional shape characterised by its rounded leading edge and tapered tail (Masters et al., 2016).

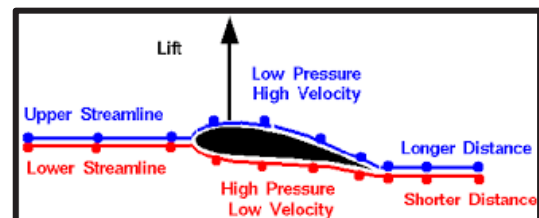


Figure 1: Aerofoil Cross-section demonstrating air-flow around it and the subsequent Bernoulli principle.

Source: Miller, 2017

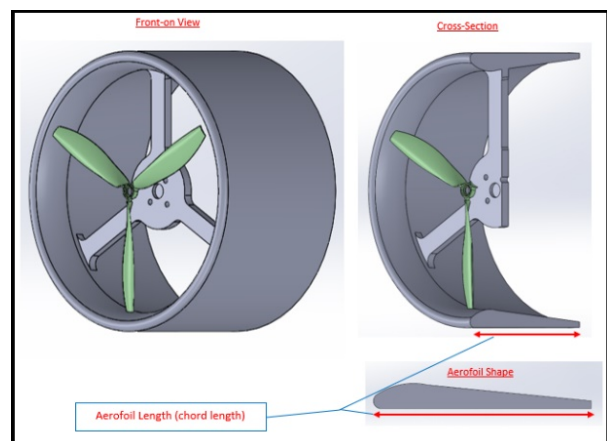


Figure 2: A Diagram of the shape of a propeller duct demonstrating the aerofoil cross-section design.

The shape of an aerofoil directs air rapidly over the longer top side and slowly underneath the shorter edge to cover a further distance in the same time (Figure 1). Since the air is moving slower below the aerofoil, it is of higher pressure and thus by the Bernoulli principle, it generates a lift force (National Aeronautics and Space Administration, 2010). A simple propeller has a cross sectional shape of an aerofoil that is rotated to produce a thrust force downwards by the Bernoulli principle. Similarly, the intention behind a propeller duct is to adopt this same Bernoulli principle and as it encases a propeller, the oncoming air is accelerated through the inside of the duct as the diameter of the duct decreases towards the propeller due to the Venturi effect (Vadaje, 2018) (Figure 3)¹. Thus, a propeller duct is a hollow tube shape with an aerofoil cross-section rotationally extruded around the propeller with the top curved edge on the inside of the duct (Masters et al., 2016) (Figure 2).

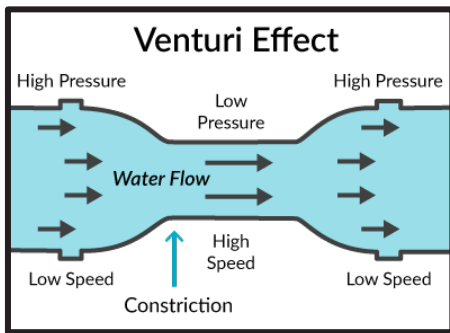


Figure 3: Diagram demonstrating the Venturi Effect whereby a constriction in a fluids path increases the velocity of the fluid. Source: Vadaje, 2018

Aerofoil Design and Efficiency

The current findings into optimising aerofoil design suggest that the 'NACA 1415' design and its proportions are the most efficient aerofoil for small scale aeronautical applications (Bontempo & Marcello, 2016) (Figure 4).

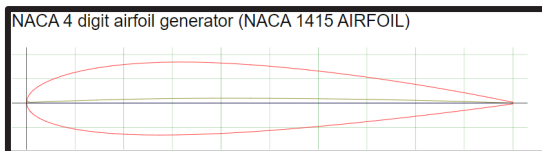


Figure 4: The NACA 1415 Aerofoil Shape which was used in Part 1 and Part 2 of the Methodology as the foundation of all duct designs. Source: Airfoil Tools, 2020

Current research into aerofoils (not ducts) suggests that increasing the length (often referred to as the chord length) of an aerofoil can greatly increase the thrust

produced while only minimally increasing the weight (Nagpurwala, 2015; Hu et al., 2018) (Figures 5 & 6). To be clear, this cited research is not for a duct or a propeller, rather simply the efficiency of the aerofoil shape. The proposal is that this can be applied to new context, by considering how increasing the length of the duct aerofoil might increase the efficiency of the propeller and duct.

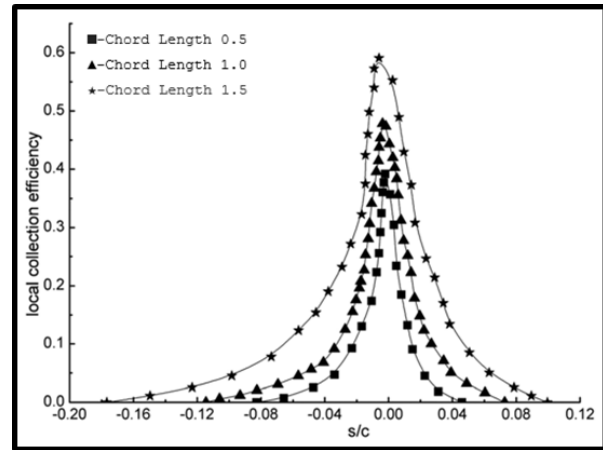


Figure 5: A graph of 3 aerofoils of increasing chord length demonstrating the increased efficiency of the longer aerofoil. Source: Saimee, 2018

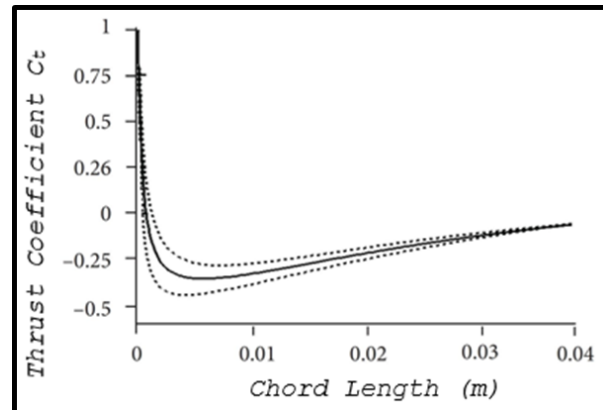


Figure 6: A graph of 3 aerofoil shapes demonstrating the increased thrust coefficient as the chord length is increased. Source: Saimee, 2018

Propeller Inefficiencies & Duct length

Wing-tip vortices

Wing-tip vortices occur because the rotational inertia acting on the air particles above the propeller blade forces them to the tips of the blade where this low-pressure diffuses with the high-pressure air below as they 'fall off' the blade, ultimately creating a wake of turbulent vortices which waste energy from the propeller and make the thrust produced turbulent (Red, 2015). Figures 7-8 demonstrates the adverse effects of wing-tip vortices on

¹ The same principles hold true for both marine and aeronautical applications of a propeller duct due to the consistent behaviour of water and air as a fluid.

the C-130 Hercules Aircraft. The addition of a propeller duct has been demonstrated to almost completely eliminate such wing-tip vortices from forming by encasing the tips of the propeller and preventing the low/high-pressure areas from diffusing (Eleshaky, 1993).

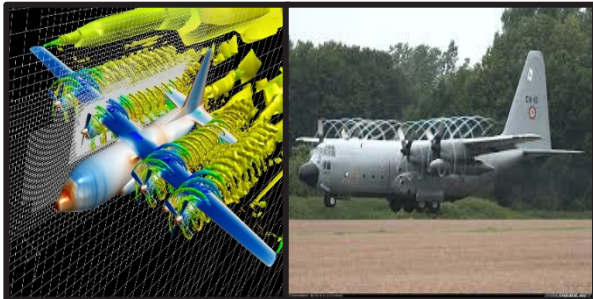


Figure 7 & 8: Computational and visual depiction of the wing-tip vortices formed by the propellers on a C-130 Hercules aircraft. The helical trail is indicative of the wing-tip vortices and demonstrates the significance of their inefficiency. Source: Reddit Aviation, 2008, Aviation Stack Exchange, 2016

In a recent study, Marlin (2019) measured the air velocity of various propellers with and without ducts, demonstrating the increase in efficiency generated by adding a duct, particularly due to the reduction of wing-tip vortices. Figure 9 shows heatmaps produced by Marlin which indicates the air speed that makes obvious the wing-tip vortices for the non-ducted propeller and the elimination of the vortices for the ducted propeller. Less turbulent air-flow means increased efficiency due to less unnecessary particle collisions (Shieh & Morris, 2001).

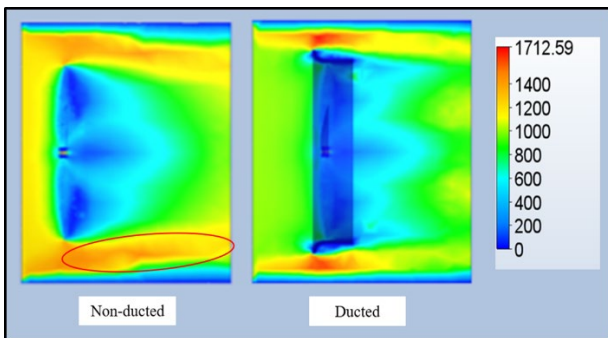


Figure 9: Fluid (Air) Velocity Heat Map of propeller with and without a duct. Wing tip vortices are circled on the non-ducted image. Source: Marlin, 2019

Slow intake air-flow speed

One real-world issue that significantly reduces the efficiency of a non-ducted propeller particularly on cruise-efficient aircraft is the limitations of incoming air-flow speed (Muller et al., 2014). Propellers typically produce more thrust when the air being directed into the propeller (such as when the propeller is moving forwards

through the air) is increased (Kweder et al., 2014). To increase intake air speed, a propeller duct is designed so that the aerofoil shape has the longer curved face on the inside of the duct (Vadaje, 2018). Since this air travels a further distance in the same time period, the duct naturally accelerates it to a higher speed and creates a funnel towards the propeller. Additionally, the Venturi effect occurs as the funnel shape of the duct reduces in diameter and subsequently increases the air velocity towards the propeller (Figure 10). Whilst the incoming air is pre-accelerated by the duct, the propeller is then able to accelerate the same air even further and produce a higher thrust (more efficient) than a non-ducted propeller and perhaps, a longer duct can do this to a greater extent (Muller et al., 2014; Kweder et al., 2014).

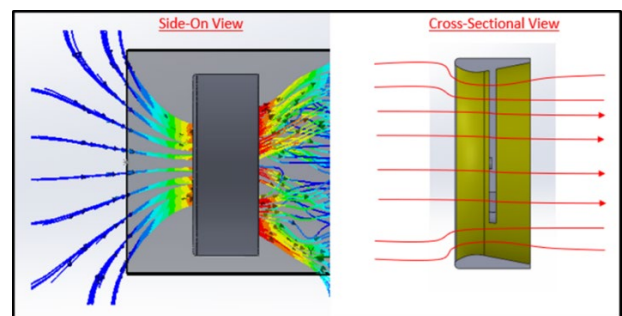


Figure 10: A propeller duct exhibiting the Venturi effect and channelling the incoming air through the duct rather than around it simulated in the SOLIDWORKS™ Flow Simulation Software.

Turbulent Thrust

In a traditional non-ducted propeller, the incoming air and thrust produced are usually very turbulent which leads to inefficiencies and excess noise (this occurs even if wing-tip vortices are eliminated) (Emiet, 1977). Turbulence in air-flow is directly related to loss of energy through heat, noise and eddies (Schetz & Jakubowski, 1975). The addition of a duct is theorised to direct the outgoing air in a more laminar flow. Rather than allowing the thrust force to spread out omnidirectionally after exiting the propeller blade, a duct channels it straight down for a longer period of time (Sánchez-Caja, 2001) (Figure 11). The effects are therefore theorised to increase with a longer duct as there is a longer period of forced laminar flow.

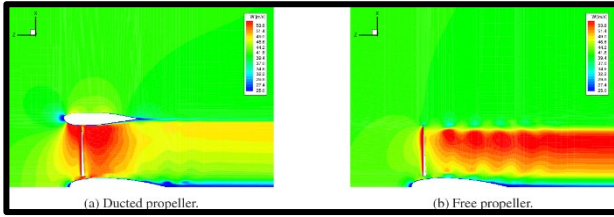


Figure 11: A cross-sectional comparison of a ducted vs non-ducted propeller which clearly demonstrates the resultant thrust of the free propeller as turbulent and the ducted propeller as streamlined.

Source: Biava & Barakos, 2016

Efficiency and air velocity

There are many specific definitions of efficiency of a propeller depending on the purpose, however, all are associated with the value of air velocity produced by the propeller (Cho & Lee, 1998). Therefore, in this experiment, the focus will be on the air velocity directly behind the propeller through visual and quantitative depictions whereby higher air velocities correlate to higher efficiencies.

Summary

Surrounding a propeller with a duct may greatly increase the efficiency but this is dependent on the shape and size of the duct. Research suggests that as duct length increases, efficiency increases but we hypothesise there may be a decrease in efficiency when the duct length increases beyond a certain length. For this experiment, just one element of efficiency will be investigated, the air flow behind a propeller rotating at a designated rate.

Scientific research question

To investigate the effects of varying the length of a propeller duct on its air-flow velocity and subsequent efficiency.

Scientific hypothesis

That the air-flow velocity of a ducted propeller will increase as the duct length increases until a point where air-flow velocity will decrease again.

Methodology

While this paper is reporting on a different property of ducted propellers, a similar experimental design was used in this research as done by Marlin (2019).

Part 1: Duct Design and Preliminary Computational Analysis

Five duct models were designed in the Computer Aided Design (CAD) program SOLIDWORKS™ as a 3D geometry file. The scale of these files was kept relatively small to allow a 1:1 comparison to the practical simulation of Part 2 and allow model drone components to be used. Thus, a 3 bladed propeller of 5 inches ($P = 12.7\text{cm}$) diameter was designed in conjunction with ducts of slightly larger diameter ($D = 15\text{cm}$) (Figure 12). The shape of the cross-sectional aerofoil was based off the ‘NACA 1415’ design and only the length component was changed between ducts (Bontempo & Marcello, 2016). The range of the 5 lengths was determined to be 5-11cm (1.5cm increments) based off the aerofoil scaling research described in the literature review (Krasilnikov, Steen & Bhattacharyya, 2016).

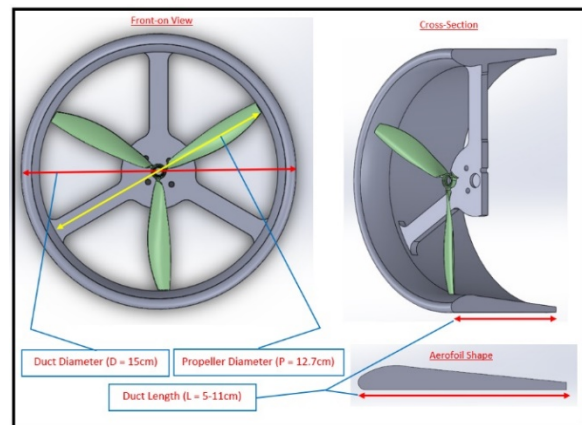


Figure 12: The propeller and one of the ducts used in Parts 1 & 2 of the Methodology. The relevant dimensions are indicated.

The inbuilt Flow Simulation software was then used with constant environment parameters of a 10m.s^{-1} laminar air-flow with a propeller angular velocity of 500 radians/s ($\sim 4800\text{rpm}$). Each of the five simulations were run under these same conditions. Repetition was not required for each model as the software produces a constant output with identical input conditions. A velocity heat map was produced which showed the cross-sectional air speed with shaded coloured regions². Three air velocity ‘trap points’ were established under the bladed side, the axis of rotation and the non-bladed side all in line with the trailing edge at 10mm from each duct (Figure 13). The air velocity value was averaged from these three points on each of the cross-sectional heatmaps to produce an average air velocity value. These results were recorded and compared visually and graphically.

² Note, air-flow velocity is directly proportional to thrust, which is directly proportional to efficiency (Cho & Lee, 1998)

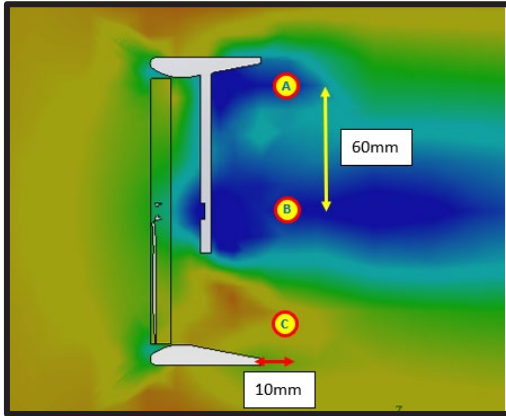


Figure 13: The three air velocity 'trap points' were established as shown above with 60mm vertical spacing and 10mm spacing from the trailing edge of the duct.

Part 2: Duct Manufacture and Practical Simulation

Each of the five propeller ducts was 3D Printed out of PLA plastic at a 1:1 scale³. These models were attached to a brushless DC drone motor and a propeller. The duct was then suspended on a bracket and the anemometer was placed 30cm from the front of each duct with the central axis aligned to the centre of the propeller. An Arduino micro-computer was used to power the motor via a 12 Volt battery. The code used generated a PWM (Pulse Width Modulation) signal required for the brushless motor to spin. The diagram in Figure 14 demonstrates this set up. Each of the ducts was spun up to 80% power (9.6 Volts) using the potentiometer by regulating the voltage at 9.6 Volts and the anemometer recorded the max air velocity after 10 seconds. This process was repeated five times for each of the five ducts. The battery voltage was checked to be between 12 and 12.2 volts after each test.

To account for the dangers associated with propellers spinning at ~5000rpm, throughout the practical experimentation, safety glasses were worn and adjustments were only made when the propeller was not rotating.

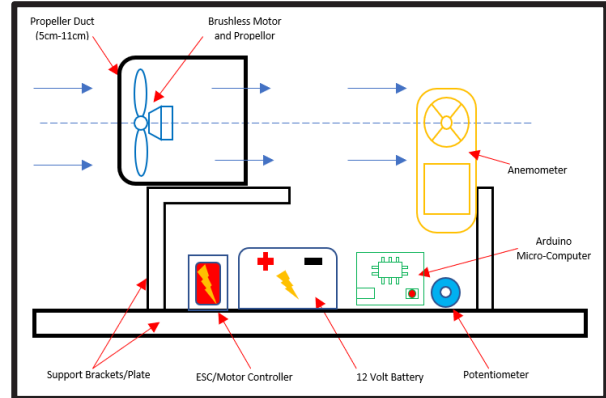


Figure 14: A scientific diagram of the set up used in Part 2 of the methodology

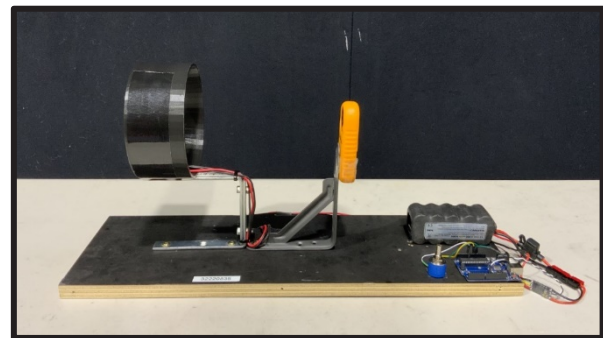


Figure 15: A photograph of the set up used in Part 2 of the methodology

Results & Analysis

Part 1 Computational Results

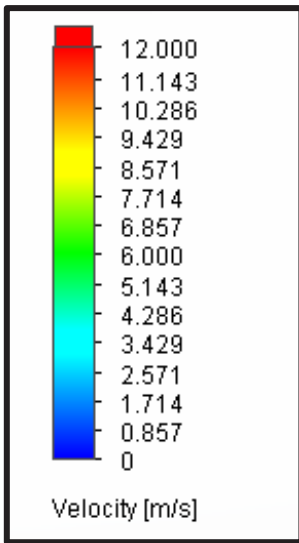
Cross-sectional heat maps were generated from the respective 5 propeller ducts from a side angle allowing for direct comparison of the air-flow through the propeller for each length Figure 1 (A-E).

The images were captured when 1 of the 3 propeller blades (pointing downwards in this cross-section) was vertically opposite 1 of the 3 motor supports (pointing upwards). The white duct, with the aerofoil cross section, can clearly be seen, as well as the motor support (pointing upwards). The propeller blades cannot be seen due to their thin profile. Higher air velocity is expected in the lower half of the diagram, as this is directly behind the propeller blade⁴.

³ The 3D Printer used was an AnyCubic i3 Mega and the filament layer height was 0.1mm

⁴ Since the propeller is rotating at a fast speed of 500 rad/s, the thrust produced is aligned with the rotation of the propeller, making the characteristic helix spiral of thrust. Interestingly, the high air flow is from the previous blade which is now 1/3rd of a revolution away, whereas there is not time for air flow to be increased at the top where the propeller blade passed through the space only 1/6th of a revolution ago.

The chosen unit being displayed is air velocity whereby the different colours represent certain air velocities as per the key. The dark blue areas represent slow moving air which typically corresponds with decreased efficiency whilst the yellow and red areas represent the fastest moving air (increased efficiency).



A
5.0cm

B
6.5cm

C
8.0cm

D
9.5cm

E
11.0cm

Non-Ducted
0.0cm

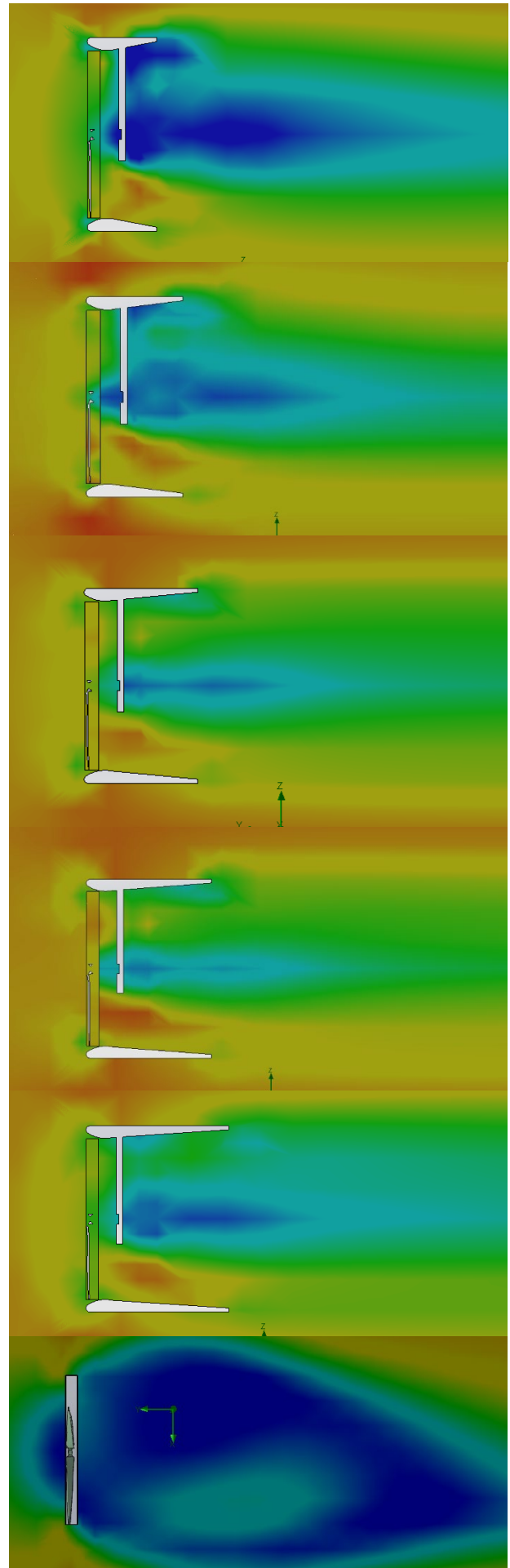


Figure 16: The non-ducted cross-sectional air velocity heat map compared to the 5 different duct lengths heat maps

Visual Analysis

The central area in Figure 16A is dark blue and large. This central dark blue area gets smaller in A through D, demonstrating an increase in overall air velocity. However, this central increase in area in Figure 16 E, suggests that the total thrust has peaked between D and E and is now following a decreasing trend. The wing-tip vortex is most evident in Figure 16A in the dark blue patch at the top and the size of this low air velocity patch varies consistently with the central low-velocity patch, increasing from 5.0-9.5cm then decreasing by 11cm. The trailing air in Figure 16A can be considered highly turbulent due to the wavy boundary between red/yellow and green/blue areas. This boundary is observed to become much more linear and defined through to D and overall trend towards faster and more linear resultant thrust. However, E again sees a reversal of the previous trend as the boundary becomes much less laminar in its flow and reverts overall towards the slower green/blue air. Additionally, a non-ducted simulation air velocity has been included which demonstrates the wing-tip vortices (dark blue area) and how large this area is when no duct is introduced. The resultant air velocity and thrust of a non-ducted propeller is also observed to be highly turbulent in nature, consistent with Marlin (2019). Therefore, Figure 16A-E provides supporting evidence for the hypothesis that the resultant air velocity of a ducted propeller increases as the length increases until a point (Duct D, 9.5cm) and then decreases again.

Quantitative Analysis

Velocity trap points were set up as demonstrated in Figure 13 and their instantaneous air-velocities were recorded and averaged in Table 1 and plotted as a graph in Figure 17.

Table 1: The air velocity values for each duct taken by the software from the 3 points and then averaged

Duct Length (cm)	A	B	C	D	E
	5.0	6.5	8.0	9.5	11.0
	Velocity (m·s ⁻¹)				
A) Top	1.5	2.5	4.0	5.0	3.0
B) Center	1.0	1.5	3.0	4.0	1.5
C) Bottom	8.0	9.0	10.0	11.0	9.0
Average	3.5	4.3	5.7	6.7	4.5

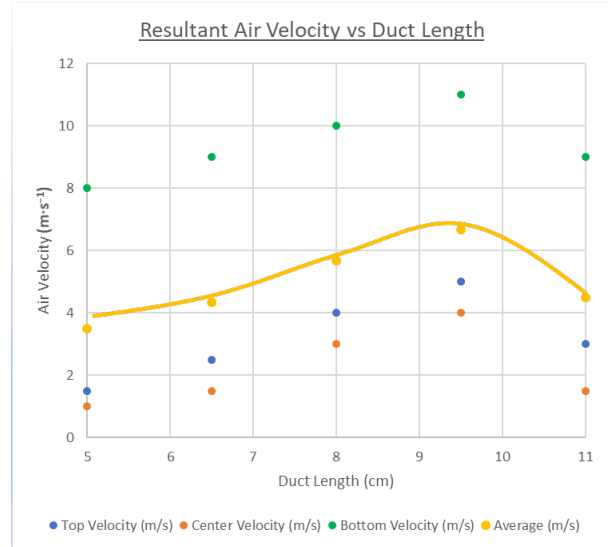


Figure 17: A plot of the air velocity point values versus the Duct Length. The average air velocity was also plotted in gold against duct length and a curve of best fit produced. The peak of the average air velocity clearly occurs at the 9.5 cm duct.

Part 2: Practical Results

Each of the five 3D printed propeller ducts were secured to the support plate using a loop of duct tape and run at a 9.6 Volt input. The anemometer was placed at a constant position from the duct and was able to measure the maximum air velocity produced by the duct five times for each duct. The results are presented in Table 2 and Figure 18.

Table 2: The air velocity values produced by the anemometer for each of the five tests of the five ducts. The average air velocity for each duct lengths is also included.

Duct Length (cm)	A	B	C	D	E
	5.0	6.5	8.0	9.5	11.0
	Velocity (m·s ⁻¹)				
Test 1	9	9.1	9.4	9.5	9.3
Test 2	8.9	9.3	9.3	9.7	9.2
Test 3	8.8	9.2	9.4	9.7	9.4
Test 4	9.0	9.3	9.4	9.6	9.2
Test 5	8.8	9.2	9.5	9.7	9.4
Average	8.9	9.2	9.4	9.6	9.3

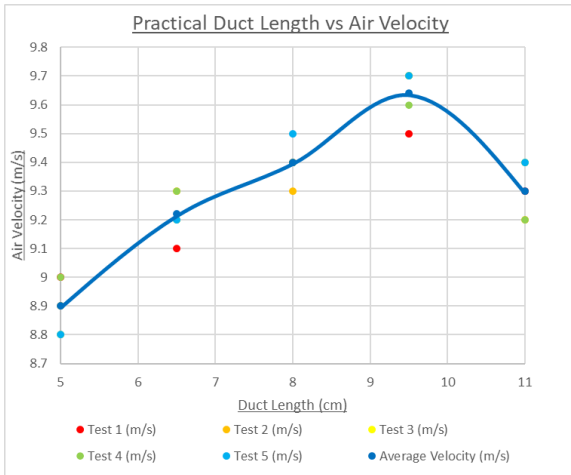


Figure 18: A plot of the practical air velocity values for the five tests across each of the five ducts. The average air velocity was also plotted in blue against duct length and a curve of best fit produced. The peak of the average air velocity also clearly occurs at the 9.5cm duct.

Again, consistent with the simulation, Figure 18 demonstrates a linear increase in air velocity until a peak at 9.5cm.

Part 3: Ideal Ratio Calculation

Both the computational and practical experiment demonstrated a peak air velocity value for the 9.5cm duct. Since both methods agreed that the 9.5cm duct produced the greatest air velocity, this is an approximation of the ideal duct length for 12.7cm diameter propeller.

$$R = \frac{\text{Duct Length (L)}}{\text{Propeller Diameter (P)}}$$

$$R = \frac{0.095m}{0.127m}$$

$$R = 0.7480314960629921$$

$$R \approx 0.75$$

This is a ratio of Duct Length (L): Propeller Diameter (P) of 0.7480 ≈ 0.75 (Appendix 1).

Discussion

It was demonstrated that for a 2D aerofoil, increasing the length of it will increase the thrust produced (Nagpurwala, 2015; Hu et al., 2018; Bontempo & Marcello, 2016). However, this report is not about ducts but about aerofoils in general. When combined with research from Marlin and other sources (Bhattacharyya, 2015; Eleshaky, 1993; Muller et al., 2014), it was

described how a duct of any length would address particular propeller inefficiencies. Hence, the hypothesis that increasing the length of a propeller duct will also increase its produced air velocity was formed.

In Figure 16, the introduction of a duct was shown to reduce wing-tip vortices (Marlin, 2019), reduce central turbulence (Sánchez-Caja, 2001) and increase intake air flow velocity (Kweder et al., 2014).

Ducts have the profile of an aerofoil, research into the 2D aerofoil profile in general (however, not applied specifically to ducts in the extant literature) demonstrates that increasing the length will increase the effect of the aerofoil shape (Nagpurwala, 2015; Hu et al., 2018; Marlin, 2019). If an aerofoil shaped duct can improve the output air flow of a propeller, the procedure in this report investigated the hypothesis that increasing the length of the aerofoil shaped duct around a propeller would increase the output air velocity.

The computational analysis provided multiple points of evidence supporting the hypothesis. It was shown that the wing-tip vortices would reduce in size as the duct length increased until it peaked at a length of 9.5cm, and this was true for the central turbulence behind the propeller also. Similarly, the average air velocity produced was seen to increase until the peak at 9.5cm. With these three areas all increasing in efficiency until the same mark at 9.5cm, it was made very clear that a longer duct is better at addressing all the inefficiency areas, but only to a point. Since the graphs had a peak, it suggested that there is an optimal ratio between the duct length and diameter of its propeller.

The practical analysis was primarily designed to confirm the validity of the results of the computational analysis. In order to achieve this, the same models used in the computational analysis were 3D printed at a 1:1 scale and all other components were mimicked as to provide the most consistent testing. The air velocity results similarly demonstrated an increase in average air velocity as the duct length increased until they both peaked at the same value of 9.5cm.

It was therefore concluded that of the five duct lengths, the 9.5cm duct produced the maximum air velocity from the propeller. Taking this value, the optimal duct to propeller diameter ratio is equal to 0.75 times the diameter. This ratio may apply for propellers of varying diameters.

Future Research

Another factor that relates to the efficiency of a propeller is its thrust to weight ratio. For a stationary propeller, weight is irrelevant and therefore this research on air velocity concludes that around 9.5cm is the optimal length for efficiency, however in many propeller applications weight must be considered. A preliminary analysis in Table 3 shows that the thrust to weight ratio may peak earlier than 9.5cm for this propeller duct combination. Further analysis should be considered.

Table 3: A preliminary analysis of the thrust to weight ratio formed using the experimental data and weights. These results suggest that the optimal thrust to weight duct may occur closer to the 8.0cm duct

Duct length (cm)	5.0	6.5	8.0	9.5	11.0
Average computational velocity (m/s)	3.5	4.3	5.7	6.7	4.5
Mass of duct (kg)	0.097	0.116	0.136	0.16	0.183
Air-flow to weight ratio (m·s ⁻¹ ·N)	3.7	3.8	4.3	4.3	2.5

Whilst this experiment was able to determine a most efficient duct length, the spacing between data points was considerably large in order to ensure the peak fell between the overall range. This experiment could be conducted again but with a focus on the range from 8-11cm (where the peak occurs) to determine an even more precise ratio.

Conclusion

Through use of computational simulations which were verified by practical results, it was determined that output air velocity increased with increasing duct length from 5.0 to 9.5cm before decreasing by 11cm. The peak for a 12.7cm diameter propeller was observed to be between 8.0 and 10.5cm. It is proposed that the ideal duct length may be 0.75 times the propeller diameter, and this relationship should now be explored for various diameters of propeller.

Acknowledgements

Thank you to Dr Hill for providing assistance, guidance and advice throughout my project. I would also like to thank Mr Becker and Mr Pilley for providing assistance during the practical simulations and duct manufacturing

process. I would also like to thank Mr Paynter for proof-reading the report.

References

Air Transport Action Group 2020, Facts & Figures. <https://www.atag.org/facts-figures.html>.

Allen, C.B. Masters, D. Poole, D.J. Rendall, T. Taylor, N.J. 2016. ‘A Geometric Comparison of Aerofoil Shape Parameterisation Methods’. American Institute of Aeronautics and Astronautics Journal, Vol. 55, No. 1, pp. 1575-1589.

Aviation Stack Exchange, 2016. Can These Vortices Be Dangerous? Photograph. <https://aviation.stackexchange.com/questions/25024/can-these-vortices-be-dangerous>.

Biava, M. Barakos, G.N. 2016. ‘Optimisation of Ducted Propellers for Hybrid Air Vehicles Using High-Fidelity CFD’. Aeronautical Journal, Vol.120, pp. 1632- 1657.

Bontempo, R & Marcello, M. 2016, ‘Effects of Duct Cross Section Camber and Thickness on the Performance of Ducted Propulsion Systems for Aeronautical Applications, International Journal of Aerospace Engineering, 2016 Volume.

Burge, C.O. 1988. ‘Propeller Assembly’. Patent: US4936803A.

Bhattacharyya, A., Abdel-Maksoud, M., Krasilnikov, V., Neitzel, J.C., Steen, S. 2015. ‘Influence of Flow Transition on Open and Ducted Propeller Characteristics’. Fourth International Symposium on Marine Propulsors, Austin, Texas, USA. pp. 1-9.

Cho, J. Lee, S. 1998. ‘Propeller blade shape optimization for efficiency improvement’. Computers and Fluids, Vol. 27, No. 3, pp. 407-149.

Eleshaky, M.E. Baysal, O. 1993. ‘Airfoil Shape Optimization Using Sensitivity Analysis on Viscous Flow Equations’. Journal of Fluids Engineering, Vol. 115, No. 1, pp. 75-84.

Emiet, R.K. 1977. ‘Noise Produced by Turbulent Flow into a Propeller or Helicopter Rotor’. American Institute of Aeronautics and Astronautics Journal, Vol. 15, No. 3.

Engstrand, G.C. 1927. ‘Propeller’. Patent: US1767786A.

Gao, Y., Hou, Q. & Zhu, Y. 2015. ‘Modelling and Control of a Magnus-effect-based Ducted Fan Aerial Vehicle’. International Journal of Control, Automation and Systems, Vol. 13, No. 1, pp. 934-941.

Hu, L. Zhu, X.C. Hu, C. Cheng, J. 2018. ‘Calculation of the Water Droplets Local Collection Efficiency on the Wind Turbines Blade’. Journal of Energy Resources Technology, Vol. 139, No. 5.

Krasilnikov, V. Steen, S. Bhattacharyya, A. 2016. ‘A CFD-based scaling approach for ducted propellers’. Ocean Engineering, Vol. 123, No. 1, pp. 116-130.

Kweder, J. Zeune, C.H. Geiger, J. Lowery, A.D. Smith, J.E. 2014. ‘Experimental Evaluation of an Internally Passively Pressurized Circulation Control Propeller’. Journal of Aerodynamics, 2014 Vol.

- Lee, Y. and Lin, C. 2002. 'Optimized Design of Composite Propeller'. *Mechanics of Advanced Materials and Structures*, Vol. 11, No. 1.
- Marlin, A. 2019. 'The Efficiency of Ducted Propellers'. *Scientific Research in School*, Barker College, Volume 1, pp. 71-76.
- Miller, C 2017, Bernoulli's Equation, Diagram, Owlcation. <https://owlcation.com/stem/Aerodynamics-The-Theory-of-Lift>.
- Müller, L. Heinze, W. Kožulović, D. Hepperle, M. Radespiel, R. 2014. 'Aerodynamic Installation Effects of an Over-the-Wing Propeller on a High-Lift Configuration'. *American Institute of Aeronautics and Astronautics Journal*, Vol. 51, No. 1.
- NACA 1415 AIRFOIL 2020, Diagram, Airfoil Tools. <http://airfoiltools.com/airfoil/naca4digit?MNaca4DigitForm%5Bcamber%5D=1&MNaca4DigitForm%5Bposition%5D=40&MNaca4DigitForm%5Bthick%5D=15&MNaca4DigitForm%5BnumPoints%5D=81&MNaca4DigitForm%5BcosSpace%5D=0&MNaca4DigitForm%5BcosSpace%5D=1&MNaca4DigitForm%5BcloseTe%5D=0&yt0=Plot>.
- Nagpurwala, Q, 2015. Ducted Fans and Propellers, Ramaiah School of Advanced Studies, Bangalore, pdf, <http://164.100.133.129:81/econtent/Uploads/09-%20Ducted%20Fans%20and%20Propellers%20%5BCompatibility%20Mode%5D.pdf>.
- National Aeronautics and Space Administration, 2010, Bernoulli's Principle, United States of America Government. https://www.nasa.gov/sites/default/files/atoms/files/bernoulli_principle_k-4.pdf.
- Red, U. 2015, Why Ducting A Propeller Makes It More Efficient, Flite Test, <https://www.flitetest.com/articles/why-ducting-a-propeller-makes-it-more-efficient>.
- Reddit Aviation 2008, Simulation Graphic, Reddit. https://www.reddit.com/r/aviation/comments/cm90i/since_were_talking_c130_propeller_tip_vortices/.
- Saimee, A. 2018. 'Improvement of Airfoils Aerodynamic Efficiency by Thermal Camber Phenomenon at Low Reynolds Number'. *Journal of Aerospace Technology and Management*, Vol. 10, No. 1.
- Sánchez-Caja, A. 2001. 'Simulation of Incompressible Viscous Flow Around a Ducted Propeller Using a RANS Equation Solver'. *Symposium on Naval Hydrodynamics (2001)*, Vol. 23, No. 1, pp. 527-538.
- Schetz, J.A. Jakubowski, A.K. 1975. 'Experimental studies of the turbulent wake behind self-propelled slender bodies'. *American Institute of Aeronautics and Astronautics Journal*, Vol. 13, No. 12.
- Shieh, C. Morris, P. 2001. 'Comparison of two- and three-dimensional turbulent cavity flows'. *American Institute of Aeronautics and Astronautics Journal*, 39th Aerospace Sciences Meeting and Exhibit.
- Vadaje, Y. 2018, Venturi Effect Explained, Engineering Fact. <https://www.engineeringfact.com/venturi-effect-explained/>.

Emotions in the Student Physics Laboratory

Arabella Crowley

Barker College

Facilitating positive student emotions in the classroom is important for many reasons including supporting emotional wellbeing and better allowing for meaningful learning to occur. Physics is a discipline associated with diverse emotions; some enjoy it, some even detest it. This study uses an adaptation of the Achievement Emotions Questionnaire (PhysicsPrac-AEQ) to assess the emotional impact of the implementation of colour and story in high school physics students' practical instruction material. Results are presented on six achievement emotions: Pride, Enjoyment, Anger, Anxiety, Hopelessness and Boredom. Previously the PhysicsPrac-AEQ has only been used to measure emotions at a university level. 69 Year 11 students at a secondary school in Sydney Australia, in their penultimate year of high school, completed a practical activity using instructional material that was either in black and white (adapted from existing practical instructional material) or a new set of material that incorporated green coloured checkpoints, a colourful image, and a historical narrative background information, along with the standard practical instructions. For these students, those completing the intervention involving colour and story reported more positively on all six of the measured emotions, however, unlike a similar test at the university level, statistical tests did not show the results to be significant so various options for further exploring this topic are proposed.

Literature review

Emotional links to engagement

Education researchers have referred to student engagement as a resource that 'once established, builds on itself, thereby contributing to increased improvements in core distal outcomes of interest' (Fredericks, Blumenfeld & Paris, 2004). Positive achievement emotions can aid in increasing students' engagement in science classrooms, making the learning experience more fulfilling for both the teacher and the student. Student engagement is needed for ongoing interest and substantial success in a particular subject (Bhansali & Sharma, 2020). Physics education research has revealed that the implementation of colour and storytelling in physics helps to increase student engagement and motivation (Kuh et al., 2008), attention retention and memory performance (Olurinola & Tayo, 2015), and increase positive emotions towards physics (Lim, 2019). Thus, by using colour and story we can not only increase positive emotions but also engagement. The question then arises, how can positive emotions be invoked when it comes to subjects such as physics which are often associated with particularly diverse emotions, for

instance boredom or hopelessness, and can be difficult for students to find interesting (Pekrun et al., 2002; Williams et al., 2003)?

Survey selection

The Achievement Emotion Questionnaire (AEQ) is an established survey on student emotions implemented in diverse contexts with sound statistical results (Pekrun et al., 2011). The AEQ has also been modified for use in specific contexts (e.g. the Mathematics AEQ (Pekrun, Goetz, & Frenzel 2005)) and recently for use in the context of students completing physics practicals (Bhansali & Sharma 2020). Bhansali chose the AEQ-M as the basis for the AEQ-PhysicsPrac survey as mathematics is allied to physics, hence making it likely to arouse similar emotions. The emotions selected for the AEQ-PhysicsPrac were pride, enjoyment, anger, anxiety, hopelessness, and boredom. These emotions cover all three relevant quadrants of emotions frequently experienced in the Physics laboratory, considering their valence (positive vs negative) and activity level (activating vs deactivating). The AEQ-PhysicsPrac was used in this investigation.

Storytelling in science

Neuroscience research has discovered that emotions play a large role in engaging students in science classrooms and concludes that stories are a tool which can be effectively used as a framing device for learning, increasing positive achievement emotions, and making the learning of physics more effective (Lim, 2019). The research reveals that ‘concept learning occurs when networks of neuronal connections are created in our brains’ (Lim, 2019, p1). Thus, drawing connections between concepts or problems and real-life scenarios (e.g. Galileo experimenting with acceleration due to gravity) evokes student curiosity and engagement, allowing neuronal networks to be build off existing networks, therefore activating stronger network connections upon recall, increasing retention and the effectiveness of learning in physics.

Despite this research, the focus for physics education researchers and teachers tends to be on conceptual development, rather than affective factors (McDermott & Redish, 1999).

Storytelling and science education

Experiments conducted by Stinner (1995) demonstrate the positive impacts on motivation and engagement were a result of presenting content as ‘science stories’ which included the history of science. They also revealed that appropriate contextual information can attract students’ interest and increases the motivation to learn science. Students readily relate to the human aspiration and thought process behind particular discoveries and science understandings.

Psychology of colour

The psychology of colour explains that each colour stimulates a particular emotion (e.g. blue is associated with sadness, white with purity, and orange with enthusiasm and attention) (Mayer & Bhikha, 2014). While perceptions of colour are somewhat subjective, there are universal meanings to most which evoke a variety of emotions. Alter (2001) gives numerous examples of how individuals can feel ‘agitated and even believe that technology is working slower when using a red or yellow webpage rather than one with a blue background. This research revealed trends that link directly to the theory of colour.

The colour theory ‘explains how humans perceive colour; and the visual effects of how colours mix, match, or contrast with each other’. It also involves the messages

colours communicate (Decker, 2017). Colours are categorized into six groups: warm colours, cool colours, happy colours, sad colours, calming colours, and energizing colours (Gremillion, 2019). The emotional reactions linked with colour are rooted in psychological effects, biological conditioning and cultural imprinting. According to psychologists, ‘we’re able to bury coloured scenes deeper in our memory, and later retrieve them more effectively than identical scenes presented in black and white’ (Alter, 2001, p170-171).

Similarly, the implementation of colour in science materials aids in enhancing learning and motivating students. Olurinola & Tayo (2015) demonstrate how the use of congruent colours (e.g. reds when describing high temperatures) in graduate learners has been found to increase retention rates, as compared to achromatic colours (black and white) and incongruent colours. It was also found that the use of colour can have a positive effect in learning on retention rates and memory performances. In this study, the student practical instruction material for the intervention feature science stories and include colour. Muller and Sharma (2005) also conducted experiments looking at the positive effects of colour in Physics videos. The results discovered that the ‘wide palate of bright colours to create complicated and colourful scenes and background added to the visual appeal.’ (Muller & Sharma, 2005, p503).

Colour and story in the university Physics Laboratory

The basis of this experiment is to test whether storytelling and colour work in a Year 11 high school context, extending off Bhansali and Sharma’s work in a university context. The intervention used in their study was a newly developed practical on ‘heat and thermodynamics’ and contained a colourful historical science story. The rest of the student notes were in black and white. The control was an established practical on ‘ultrasound’, having a theoretical background with no colour, science story or historical context. The student notes were entirely in black and white. Bhansali and Sharma found that students reported significantly higher positive emotions, and significantly lower negative emotions for students completing the intervention rather than the control in the undergraduate Physics 3-hour laboratory session. They also found positive correlations between both the positive emotions and negative emotions. Their work focused on undergraduate Physics students, 18-21-year old’s, with about 25% females. Each student, out of a 406 total, was allocated one 3-hour laboratory session for one topic per week. Completion of the AEQ-PhysicsPrac was

voluntary with a total of 71% responses for the control and 86% responses for the intervention. The question then remains, does the use of colour and storytelling work in other contexts, as measured by the AEQ-PhysicsPrac model (Bhansali & Sharma, 2020)?

Scientific research question

Does use of storytelling and colour have an impact on student emotions in the high school Physics laboratory?

Scientific hypothesis

That, following the results of Bhansali and Sharma (2020), introducing colour and storytelling in high school students' Physics practical manuals will increase positive achievement emotions and decrease negative emotions in the Physics laboratory.

Method

Sample and procedure

The proposed method is an experimental, small-scale quasi-experiment using convenience sampling to include 69 Year 11 students studying Physics as an elective, 15 to 17 years old, with around 15% females. The study was conducted at a single Pre-Kindergarten to Year 12, Independent, coeducational School in Sydney, Australia. The cohort constitutes of 5 mixed ability classes with different teachers, each class having already completed two practical tasks prior to the 'Measuring Acceleration Due to Gravity' practical. One-hour practical sessions run during a single period throughout the week, each class is timetabled for one practical lesson per week. Students work in teams of three to five, seeking assistance from their classroom teacher who teaches and facilitates student activities and learning.

Across the five classes, two classes were randomly allocated the experimental instructional material, two were randomly allocated the control instructional material, and one had a random half of the class use the experimental material and half use the control. The reason for allocating whole classes to different treatments was that in the school setting the procedure needs to be simple for the individual teachers to implement. This means that an uncontrolled variable is the emotions and experiences that the students have with their particular teacher. However, this is minimised by the instructional material being fully sufficient to explain the task to the students. All 69 students in attendance of the practical classes completed the task and the survey. 32 students

completed the control experiment (black and white), 37 completed the intervention (colour and story). Consent was provided by each of the students' parents, and the students themselves, allowing the anonymous data to be used for research. The study has ethics approval from the Barker Institute.

The Intervention

An existing practical activity for Year 11 was selected for this investigation. The activity chosen was on 'Measuring Acceleration due to Gravity' which required students to drop tennis balls from various heights while measuring the time taken to reach the ground. The students would plot a graph of height vs time squared and use the gradient to determine a value for local acceleration due to gravity.

The practical instructional material was modified by including an introduction and concluding with the AEQ-Physics survey.

The experimental group (colour and story) consisted of an introduction as a colourful historical science story of how Galileo demonstrated free-falling objects experience the same acceleration. This section of the booklet also contained a colourful image of Galileo's discovery in 16th Century. The checkpoints throughout the practical booklet for this experiment are green (because of the colour's association with the human ideas of growth, optimism, peace and harmony (Kurt & Kingsley Osueke, 2014). The rest of the content in the student notes is black and white.

The control had an introduction focussing on the physics principles and uses of acceleration due to gravity, providing a theoretical background without any historical context or science story. The practical booklet was entirely in black and white.

Other than the introduction, and the green 'Checkpoints' for the experimental group, all elements of the instructional material were identical including layout, procedure and analysis. Both also had a question at the start of the task inviting students to record their emotion upon beginning the activity to establish an emotional baseline. A summary of the two treatments is depicted in Figure 1.

Colour & Story Version

Experiment 1.3: Measuring Acceleration due to Gravity (First-Hand)

(Time allocated: 1 period)

Please circle the emotion that best describes how you are feeling right now at the start of this practical activity:



Background (5 Minutes)



The remarkable observation that all free-falling objects fall with the same acceleration was first proposed by Galileo Galilei nearly 400 years ago.

Galileo conducted experiments using a ball on an inclined plane to determine the relationship between the time and distance travelled.

He found that the distance depended on the [square of the time](#) and that the velocity increased as the ball moved down the incline.

The relationship was the same regardless of the mass of the ball used in the experiment.

The experiment was successful because he was using a ball for the falling object and the friction between the ball and the plane was much smaller than the gravitational force. He also used a very shallow incline, so the velocity was small and the drag on the ball was very small compared to the gravitational force.

The story that Galileo demonstrated his findings by dropping two cannon balls off the Leaning Tower of Pisa is probably just a legend.

At four points in the instructional material students reached a checkpoint (below)

CHECKPOINT 1:

STOP HERE AND GET YOUR TEACHER'S INITIALS _____

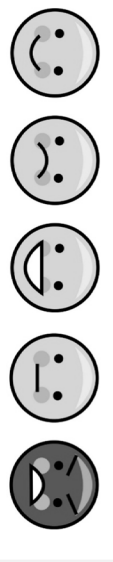
All students then completed the AEO-PhysicsPrac

Black & White Version

Experiment 1.3: Measuring Acceleration due to Gravity (First-Hand)

(Time allocated: 1 period)

Please circle the emotion that best describes how you are feeling right now at the start of this practical activity:



Background (5 Minutes)

Newton's second law states that the net force on an object is equal to its mass times its acceleration ($F = ma$). This can be used to explain why, even though objects of varying masses have different gravitational forces on them drawing them to the ground they will have the same acceleration towards the ground (ignoring air resistance).

This acceleration due to gravity is often referred to as " g " and is approximately 9.8 m/s^2 at the earth's surface. So ignoring air resistance, all objects will accelerate to the ground at $9.8/s^2$.

If g is constant, the equations of constant acceleration can be used to describe the falling object's motion. Particularly helpful for this experiment, the equation $s = ut + \frac{1}{2}at^2$ can be applied.

It turns out that the value of g can vary for different places on the earth's surface. For example, it is greater at the poles of the earth than the equator and it is lower for places of higher altitude above sea level.

CHECKPOINT 1:

STOP HERE AND GET YOUR TEACHER'S INITIALS _____

All students then completed the AEO-PhysicsPrac

Figure 1: Comparison of content for the intervention (colour and story) and control (black and white).

Administration, data collection and analysis

Physics teachers chose a lesson to complete this practical task. The individual teachers provided a brief introduction prior to students starting their practicals, including specific instruction that the students are to thoroughly read through the ‘Background’ section. At this point, the AEQ-PhysicsPrac survey was also introduced, and the students were told to complete the booklet as usual (including the survey). The surveys were completed after the students completed the practical, as part of the learning activity, and collected as students left the laboratory.

The data were curated by removing the responses which had three or more items left blank. The data from the 69 responses were entered into Excel. The Likert scale was interpreted as: Strongly Agree=5, Agree=4, Neutral=3, Disagree=2, Strongly Disagree=1.

Results and Analysis

Following the work of Bhansali and Sharma (2020), the student responses to the AEQ-PhysicsPrac have been quantitatively analysed to determine the effects of storytelling and colour on Year 11 High School Physics students.

Correlation between emotions

Table 1 shows this investigation’s correlation coefficients (Pearson’s r) for the six emotions measured by the AEQ-PhysicsPrac. Each correlation is colour coded to allow for easy comparison.

Colour coding indicates both the strength of correlation and whether there is a positive or negative correlation. A stronger green indicates a stronger positive correlation, a stronger red indicates a stronger negative correlation (yellow indicates a very weak correlation). All correlations were significant to at least $p < 0.05$.

It is helpful to compare the correlations for this research with previous research in the university context using the same survey instrument. Table 2 shows the correlations from Bhansali and Sharma (2020) and has been modified to have the same colour coding as in Table 1. The strong positive correlations in Table 2 indicate that students responded affirmatively to experiencing feelings of Pride and Enjoyment, and Anger and Hopelessness.

There are many similarities between the two correlation tables. Bhansali and Sharma noted strong positive correlations between pride and enjoyment; and between anger, boredom and hopelessness (Table 2). While positive correlations between pride and enjoyment, and anger and hopelessness are also seen in this investigation (Table 1), it is interesting that there was a weaker positive correlation with anxiety for the other two emotions of anger and helplessness for the Year 11 students. Perhaps this may be due to students’ desire to achieve well and be diligent with their work ethic, increasing general anxiety but not necessarily other negative emotions including hopelessness and anger. Another similarity was that the strongest negative correlation for both studies was between enjoyment and boredom and these are much

Table 1: Correlations between the emotions for the intervention (above the diagonal) and control (below the diagonal in Italics).

	Pride	Enjoyment	Anger	Anxiety	Hopelessness	Boredom
Pride	-	0.543	-0.294	0.012	-0.344	-0.121
Enjoyment	<i>0.545</i>	-	-0.504	-0.424	-0.424	-0.536
Anger	<i>-0.616</i>	<i>-0.58</i>	-	0.145	0.826	0.253
Anxiety	<i>-0.34</i>	<i>-0.258</i>	<i>0.443</i>	-	0.179	0.042
Hopelessness	<i>-0.459</i>	<i>-0.545</i>	<i>0.689</i>	<i>0.625</i>	-	0.208
Boredom	<i>-0.346</i>	<i>-0.69</i>	<i>0.37</i>	<i>0.082</i>	<i>0.293</i>	-

Table 2: Correlations between the emotions for the intervention (above the diagonal) and control (below the diagonal in Italics) (Bhansali and Sharma, 2020) Modified to use colour to identify strength and direction of the correlation.

	Pride	Enjoyment	Anger	Anxiety	Hopelessness	Boredom
Pride	-	0.654	-0.268	-0.028	-0.16	-0.287
Enjoyment	<i>0.834</i>	-	-0.293	0.075	-0.252	-0.474
Anger	<i>-0.164</i>	<i>-0.188</i>	-	0.537	0.711	0.576
Anxiety	<i>0.083</i>	<i>0.07</i>	<i>0.472</i>	-	0.547	0.139
Hopelessness	<i>-0.243</i>	<i>-0.227</i>	<i>0.707</i>	<i>0.517</i>	-	0.541
Boredom	<i>-0.284</i>	<i>-0.375</i>	<i>0.502</i>	<i>0.171</i>	<i>0.522</i>	-

stronger in this study with Year 11 students (-0.690 and 0.536) than with the university students (-0.375 and -0.484). Other strong negative correlations in this study included enjoyment and anger, and enjoyment and hopelessness, and pride and anger. Interestingly the negative correlation between pride and anger was much stronger for the control group (-0.646) than the intervention group (-0.294). Three conclusions can be drawn from the data:

1. Many of the correlations are expected (positive emotions positively correlate with positive emotions, but negatively with negative emotions).
2. The typically strong correlations mean that if changing the instructional material results in a change in one emotion, it is likely to also have affected other emotions.
3. There is generally consistency between the emotions of the Year 11 students and the university students increasing the likelihood that Bhansali and Sharma’s research can apply to the secondary school context.

Averages

Table 3 shows statistics relevant for comparing initial emotion and six achievement emotions, as quantified by the AEQ-PhysicsPrac, for the control and the intervention. Figure 2 provides a visual representation of the means comparing the control and intervention for easy comparison.

Table 3: Comparing intervention with control for each emotion: descriptive statistics

Emotion	Mean (SD)		Range
	Intervention (n=37)	Control (n=32)	
Initial Emotion	3.1 (0.9)	3.5 (0.6)	1-5
Pride	14.1 (2.1)	13.5 (2.4)	9-19
Enjoyment	17.4 (2.4)	16.8 (2.6)	11-22
Anger	6.5 (1.3)	6.8 (2.4)	3-12
Anxiety	6.6 (2.1)	6.7 (2.0)	3-13
Hopelessness	3.9 (1.5)	4.0 (1.7)	2-9
Boredom	5.2 (1.6)	5.7 (1.8)	2-10

Table 3 and Figure 2 reveal that the on average, students who completed the intervention (colour and story) reported higher positive emotions and lower negative emotions in relation to the task. This is despite having an overall less positive initial emotion at the start of the activity. However, a series of student t-tests (with the appropriate Bonferroni corrections) did not indicate significant differences between students in the intervention and control for any of the emotions.

Table 4 has been reproduced from Bhansali and Sharma (2020) for comparison. It is helpful to compare the control and intervention for this research with previous research in the university context using the same survey instrument.

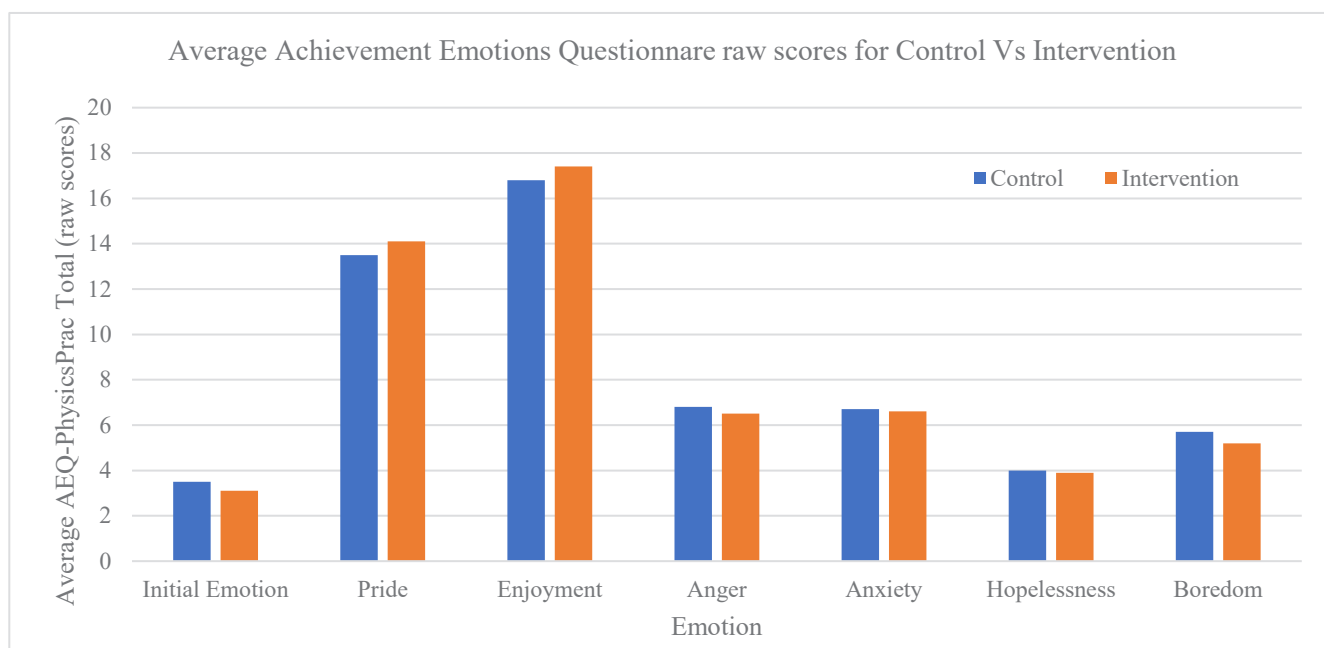


Figure 2: Comparison between achievement emotions for control and intervention. The Average AEQ-Physics Prac Totals are the raw scores associated with how many items related with each item

Table 4: Bhansali and Sharma (2020) Comparing intervention with control for each emotion for university students

Emotion	Mean (SD)		Range
	Intervention (n=37)	Control (n=32)	
Pride	15 (2)	14 (3)	4-20
Enjoyment	18 (3)	17 (4)	5-25
Anger	8 (2)	9 (2)	3-15
Anxiety	7 (3)	8 (3)	2-15
Hopelessness	5 (2)	6 (2)	1-10
Boredom	5 (2)	6 (2)	1-10

The results for positive emotions, pride and enjoyment are consistent across both experiments. The means are higher for the intervention than the control. For negative emotions, anger, anxiety, hopelessness, and boredom, the means are lower for the intervention when compared with the control. Comparing the intervention with colour and a historical 'science story' with the control which is a standard monochromatic practical, we find that the intervention attracts more positive emotions and less negative emotion. This demonstrates that the use of colour and story in High School Physics may aid in increasing positive achievement emotions in the science laboratory. The results also help further validate the applications of the AEQ-PhysicsPrac (Bhansali and Sharma, 2020) in a high school context to assess and understand students' emotions towards physics in laboratory situations.

The important difference between the two sets of results is that the similar study in the university context reported significant differences between each group for each emotion, however the present study is reporting a null result. Despite all the consistency between the two sets of results this is an important inconsistency where the similar effect was unable to be repeated.

Discussion

Implications for research

This study suggests that the findings of Bhansali and Sharma (2020) can be applied more universally by finding results with a similar direction in a secondary school context. It aids in the understanding of how storytelling and colour impact a student's achievement emotions based on age. It does reveal some differences between the university and school students, such as heightened anxiety in school students, which may be a result of less familiarity with the subject, more pressure from schools, and overall pressure to do well leading up to their final examinations.

Most importantly, the significant findings at university were not replicated in the school context. This leads to four main avenues for further research.

1. The smaller sample size was a likely contributor to the p-values from the t-test yielding non-significant results. The same instructional material can be used in future years with Year 11 students and the data combined to increase the sample size.
2. There were other differences between this study and the university study due to a variety of factors that are difficult to control for. These include the time of day or day of the week that the class occurred, and the teacher who supervised the class. While not ideal, this was necessary for the particular context. Dividing each class into students who completed the control and the intervention goes towards mitigating this however further strategies could be considered to increase the similarities with the university study to more validly attempt to replicate the results.
3. The research can be expanded to other practical investigations in Year 11 Physics, or practical investigations in other Scientific domains.
4. There was more data collected including how students completed the practical activities and qualitative responses to some questions that could be analysed to provide further information about the impact of introducing colour and story in Physics laboratory instructional materials.

Implications for Physics teaching in secondary schools

From these results, it is evident that some students are feeling anxious, hopeless, bored, and even angry in the physics practical classroom regardless of the formatting of their practical experimental booklets. This should be of some concern to instructors. However, one way of addressing this may be to include story and colour in Physics practical instructional material. This research about Physics teaching in secondary school with a smaller sample size (which likely contributed to the lack of significant results) produced results in a similar direction to the significant findings in the university context (Bhansali & Sharma, 2020). Perhaps, even in secondary schools, adding colour and story in the booklets helps increase pride and enjoyment of the experiment itself, and decreases anger, anxiety, hopelessness and boredom. Implementing colour is a relatively simple exercise and should be an easy step for teachers. Including story could take more work but it may

be worth the effort, especially if further research demonstrates significant effects in schools.

Conclusion

The outcomes of this experiment continue the work of Bhansali and Sharma (2020) and find that, for a group of high school students, including the use of colour and a 'science story', resulted in more positive achievement emotions and less negative ones overall. Unlike the university study, this study achieved a null result which is confidently shared as a springboard for further research into 'deciphering how and why certain techniques are more effective than others and how we can apply these techniques to other contexts' (Georgiou & Sharma 2012). The consistent correlations imply that the validated AEQ-PhysicsPrac does allow for a quantitative analysis of student's emotions in the high school Physics laboratory.

Acknowledgements

I would like to thank Dr Terrett and Dr Gates for providing insights into my scientific project. I would also like to especially thank Dr Hill for being a great mentor and sharing his extensive knowledge in Physics education research. A special thanks goes to Mr Paynter (Head of Science) and the team of Year 11 Physics teachers and students who supportively engaged with my research. Aesha Bhansali and Manju Sharma's work in the field of Physics education research also greatly influenced me, and I would like to thank them both for continued interest, encouragement and interaction with my project.

References

Alter, A. (2001). 'Drunk Tank Pink: And Other Unexpected Forces that Shape How We Think, Feel, and Behave.' East Rutherford, New Jersey.

Bhansali, A., & Sharma, M. D. (2020). 'The Achievement Emotions Questionnaire: Validation and implementation for undergraduate physics practicals.' *International Journal of Innovation in Science and Mathematics Education (Formerly CAL-Laborate International)*, 27(9), Article 9.

Cherry, K (2019). 'How Colours Impact Moods, Feelings, and Behaviours', <https://www.verywellmind.com/color-psychology-2795824>.

Decker, K (2017), 'The Fundamentals of Understanding Colour Theory', <https://99designs.com.au/blog/tips/the-7-step-guide-to-understanding-color-theory/>.

Fredricks, J.A., Blumenfeld, P.C., Paris, A.H. (2004). 'School Engagement: Potential of the Concept, State of the Evidence.' *Review of Educational Research*, 74 (1), 59-109.

Georgiou, H. and Sharma, M., 2012. 'Why it is important to publish 'null' results: A project involving no change in learning gains from Interactive Lecture Demonstrations in first year thermal physics.' *In World Conference on Physics Education, Istanbul*.

Gremillion, A (2019), 'Colours and Emotions: How Colours Make You Feel', <https://99designs.com.au/blog/tips/how-color-impacts-emotions-and-behaviors/>.

Kuh, G. D., Cruce, T. M., Shoup, R., Kinzie, J., & Gonyea, R. M. (2008). 'Unmasking the effects of student engagement on first-year college grades and persistence.' *The Journal of Higher Education*, 79(5), 540-563.

Kurt, S., Kingsley Osueke, K. (2014). 'The Effects of Colour on the Moods of College Students.' *Sage Open Journals*.

Lim, B. (2019). 'The Story of Physics: Storytelling for High School Physics Teaching.' *Ontario Association of Physics Teachers Newsletter*.

Mayer, L., Bhikha, R. (2014). 'The Physiology and Psychology of Colour'. *A Science of Medicine, The Art of Care*, 3, 1-14.

McDermott, L.C., & Redish, E.F. (1999). 'Resource letter: PER-1: Physics education research'. *American Journal of Physics*, 67 (9), 755-767.

Muller, D.A, Sharma, M.D. (2005). 'Determining the factors affecting student perception of a popular science video'. *Australasian Journal of Educational Technology* 2005, 21(4), 491-509

Olurinola, O., & Tayo, O. (2015). 'Colour in Learning: Its Effect on the Retention Rate of Graduate Students'. *Journal of Education and Practice*, 6(14), 1-5.

Pekrun, R., Goetz, T., Frenzel, A. C., Barchfeld, P., & Perry, R. P. (2011). 'Measuring emotions in students' learning and performance: The Achievement Emotions Questionnaire (AEQ)'. *Contemporary Educational Psychology*, 36(1), 36-48.

Pekrun, R., Goetz, T., & Frenzel, A. C. (2005). 'Achievement Emotions Questionnaire—Mathematics (AEQ-M). User's manual.' *Munich: University of Munich, Department of Psychology*.

Pekrun, R., Goetz, T., Titz, W., & Perry, R. P. (2002). 'Academic emotions in students' self-regulated learning and achievement: A program of qualitative and quantitative research.' *Educational Psychologist*, 37(2), 91-105.

Ponnambalam, M. (2018). 'Emotional Component in Teaching and Learning'. *The Physics Teacher Journal*, 6 (2).

Stinner, A. (1995). 'Contextual settings, science stories, and large context problems: Toward a more humanistic science education'. *Science Education*, 79(5), 555-581.

Williams, C., Stanisstreet, M., Spall, K., Boyes, E., & Dickson, D. (2003). 'Why aren't secondary students interested in physics?' *Physics Education*, 38(4), 324-329.

A study of a marble's chaotic motion on a pinboard

Max van Grecken

Barker College

In this article, chaos theory is explored through the manipulation of the probability of different outcomes in a chaotic system. This investigation examined how changes in starting conditions can affect the random motion of a marble on a pinboard. This process involved a total of 1200 trials of dropping a marble through a marble run component which was elevated to various angles. For each angle, the paths taken by the marble was recorded. A comparison of the results has shown that at low angles, the system is very bias towards four main paths. However, increasing the angle of inclinations lead to a greater variability of pathways, and a reduction in the frequency of the top four paths. In layman's terms, this means that the system grew more random and chaotic at larger angles.

Literature review

'Chaos theory' is the study of dynamic systems and how their seemingly random nature is in actuality the system's susceptibility to small changes in starting conditions, leading to drastic effects on the end result (Batterman, 1993). It is proposed that chaotic systems contain no 'true' randomness, rather, slight modifications to the starting conditions in a system will have drastic effects on the end result. A well-known instance of a chaotic system is Edward Lorenz's mathematical model of Atmospheric convections, 'The Lorenz attractor' (Bourke, 1997). The results of the Lorenz attractor, however, outwardly appeared to be random when graphed, which, at certain values, took the rough shape of a butterfly (Figure 1). Because of the seemingly random nature of the outcome due to its sensitivity to small changes in starting values, today, the 'Butterfly effect' is a metaphor for 'chaotic' systems & is commonly conveyed with the analogy that 'A butterfly flapping its wings could cause a hurricane on the other side of the globe.' (Forbes, n.d.). This investigation will similarly demonstrate how minute changes to starting conditions can have drastic effects on the outcome. In this study, the angle of inclination will be intentionally varied to investigate the effect it had on the system.

An example of a system with chaotic motion is the many potential routes a marble could take when dropped into a sloped, cloud shaped, pinboard (Figure 2). If we assume that air resistance and friction are negligible, there are three main forces that will act on the marble.

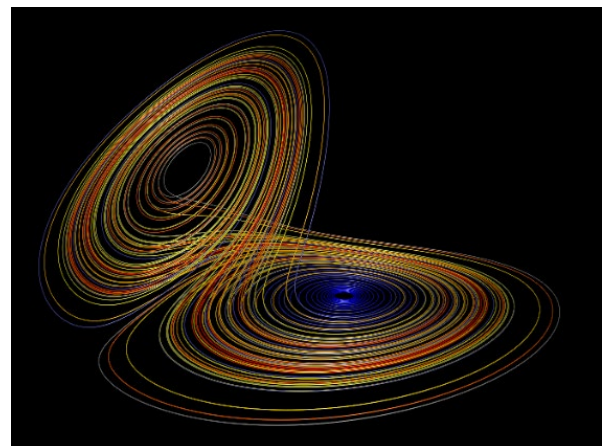


Figure 1: The Lorenz attractor in 3D.
Source: Bourke, 1997



Figure 2: The cloud-shaped pinboard Marbleworks component used in this experiment.

These forces include a weight force due to gravity, a normal force from the inclined plane of the cloud-shaped pinboard, and a reaction force/ricochet which retards the motion occurring any time a marble comes in contact with a plastic pin on the pinboard (or the sides of the pinboard).

The first two are the force due to gravity and the normal force (Figure 3). These two forces combine to form the net force acting on the marble, which will accelerate it down the slope. The acceleration on a slope is less than the acceleration due to gravity due to the normal force. The acceleration of the object on a slope equal to $g \cdot \sin(\theta)$ (where θ is the angle of the slope relative to the horizontal and g is the acceleration due to gravity, 9.8ms^{-2} .)

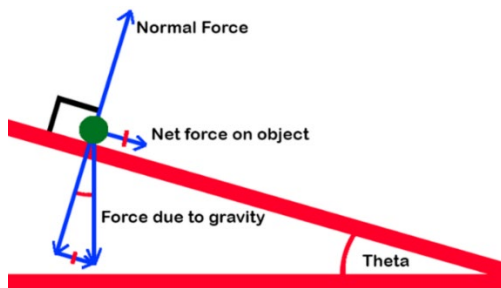


Figure 3: A free body diagram depicting the forces acting on an object on an inclined plane.

As a consequence, the greater the angle, the greater the acceleration of the object, such that it is likely to be travelling at a higher velocity when it collides with a pin. These impacts result in the third main force that may act on the marble, reaction force, which result in ricochets. A ricochet is defined as a ‘Shot or hit that rebounds off a surface’ (Oxford dictionary, 2020). Such a rebound can occur when a round object collides with a pin or side of a surface. As momentum must be conserved, if the object does not collide with sufficient force to move the object it collided with, a reaction force will accelerate the object in a different direction, resulting in a ricochet. As the force of impact, and subsequent reaction force, will be greater at larger angles, they are expected to become more powerful at higher angles during this experiment. Based on this information, it was my belief that the greater the angle of a track with multiple slopes, the less likely a marble would be to stray from the centre.

Scientific research question

How will the angle of inclination of a pinboard track effect the frequency of the various paths taken?

Scientific hypothesis

That the greater the angle of a track with multiple paths the greater the probability that the marble will take one of the four most used paths.

Methodology

Central to this investigation was a symmetrical, cloud shaped, marble toy by Marbleworks (Figure 2). It consisted of a plastic inclined slope with eight pins that can divert a passing marble to take one of 72 potential paths. It was affixed to three other pieces of marblework’s plastic tubing. Varying the angle of inclination allowed for comparison between the frequency of various paths taken.

The marble track apparatus was attached to a variable slope that allowed the ramp’s angle of inclination to be changed. To ensure that the angle of inclination was accurate, a protractor was affixed to the system and checked every 50 runs to ensure that the apparatus had not been bumped or compromised. Ensuring that the cloud was not tilted to either side was performed using a level meter.

The variable base was initially set so that the angle of inclination for the slope was 5° and a marble was dropped from a point centred immediately above the red tube 200 times. The path was recorded using the Key (Figure 4a, b & c) for each run. The angle was then increased by 5° and this step repeated until the apparatus had reached 30° .

In order to effectively record the path taken by the marble during each test, each of the 72 pathways has a four-letter designation as allocated by this recording system (Figure 4a). For example, if the marble falls to the left of the first pin, the first letter of its designation will be ‘A’. If a marble that takes the leftmost path all the way down, its designation would be ‘AAAA’ (Figure 4b) and a marble that takes the rightmost path would be ‘BCDC’ (Figure 4c).

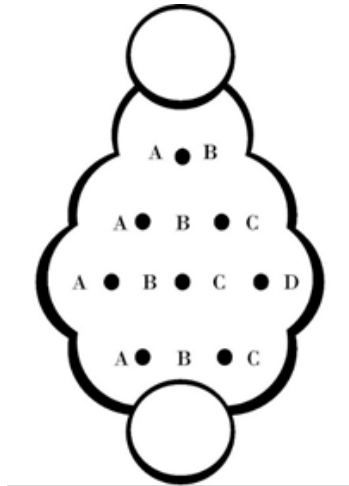


Figure 4a: Path Key

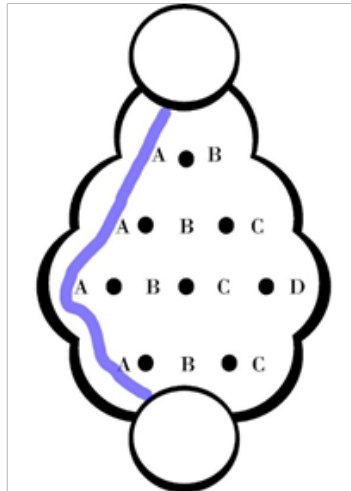


Figure 4b: Path AAAA

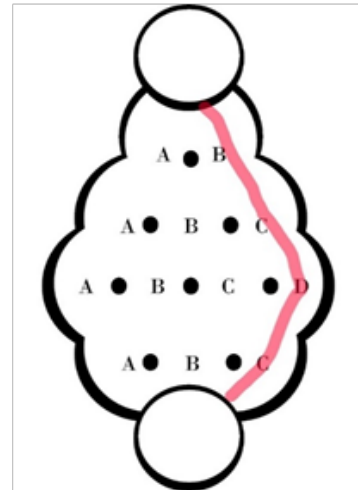


Figure 4c: Path BCDC

Results

Table 1: The frequency of each path taken from 200 trials for each angle. Paths are ordered from most to least frequent, excluding paths that did not occur.

5°	Route	ABCB	ABCC	BBBA	BBBB	BBCB	AABB	BBCC	ABBA	ABBB	AABA				
	Count	43	42	26	23	17	13	12	9	9	6				
10°	Route	BBBB	BBBA	BBCC	ABCC	ABCB	ABBA	BBCB	ABBB	BBAA	BCCC	BCBB	AABB		
	Count	37	29	25	25	24	22	21	10	4	1	1	1		
15°	Route	ABCB	BBBB	BBCB	ABCC	ABBA	ABBB	BBCC	BBBA	ABDC	BBAA	BABB	AABB		
	Count	38	27	25	24	21	17	15	14	11	5	2	1		
20°	Route	ABBB	ABBA	BBCB	BBBB	BBBA	ABCB	ABCC	BBAA	BBCC	ABDC	ACCB	AABA		
	Count	44	25	24	24	22	16	13	12	12	6	1	1		
25°	Route	BBCB	BBBB	BBBA	ABBB	BBCC	ABCC	ABBA	ABCB	ABDC	BBAA	BBDC	AABC	BAAB	ACCB
	Count	33	26	24	21	19	19	18	14	14	5	3	2	1	1
30°	Route	BBBB	BBCB	ABCC	ABBA	BBBA	BBCC	ABCB	ABBB	ABDC	BBAA	BBBC			
	Count	34	30	23	23	22	21	17	17	7	5	1			

Analysis

The average number of unique paths taken was 11.8 for each angle, however the specific paths that the marble took at different angles varied wildly. Many paths such as BCBB, occur once or twice at one angle and then not at all in subsequent angle/s. These paths may be different for each of the angles. For example, Route BBBB occurred 37 times at 10 degrees, but only 27 times at 15 degrees. Interestingly, the most frequent path for each angle is not always the same, as the frequency of

individual routes often varies wildly, however, the frequency of the lesser used routes generally increases with the angle of inclination. In contrast, chaotic systems lend themselves to unpredictability.

In order to use this data to provide evidence for or against the hypothesis, that the greater the angle of inclination, the greater the frequency of the 4 most used paths, a graph can be produced of the percentage of the trials that resulted in the marble taking any of the four most commonly used paths for that angle (Figure 4). The Frequency in percentage that the marble took one of the four most used paths for each angle can be found in Table 2 and plotted in Figure 5.

Table 2: Table of frequency of the four most common paths for each angle tested

Angle (°)	Percentage of four most common paths (%)
5	67
10	58
15	57
20	58.5
25	52
30	55

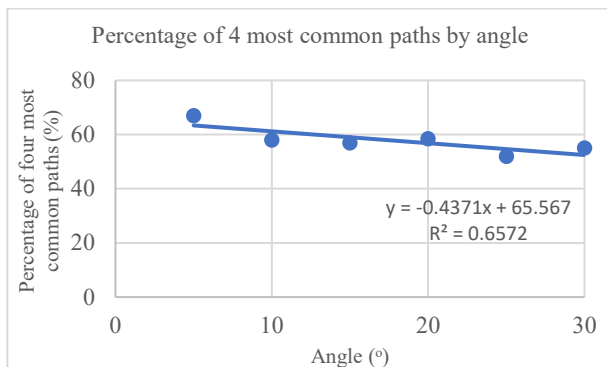


Figure 5: A graph of the percentage of the runs that the marble takes one of the four most frequented paths (as opposed to the remaining paths) for each angle

It can be seen from Table 2 and Figure 5 that the average frequency of the top 4 paths decreased as the angle increased, indicating that the frequency of the lesser paths was actually increasing as the angle increased, directly opposing the hypothesis.

A Pearson’s r test was used to calculate the correlation coefficient between the angle of inclination and the percentage the marble taking the top four paths. There is a strong negative correlation ($r = -0.810679$), with a r^2 value of 0.6572 which shows that 65% of the variance in one variable can be accounted for by the variance in the other. Because this is a strong negative correlation, this means that as the angle increases the frequency of the top four paths decrease which is evidence against the hypothesis, which indicated that the frequency of the four most common paths would increase as the angle increased.

Discussion

The frequency of the marble taking the more common paths can be used as a measure for chaos or randomness. The greater the distribution of paths (and conversely, the reduction of frequency of the more common paths), then the greater the susceptibility to initial variations, i.e.

chaos. With that in mind, the strong negative correlation between angle of inclination and the frequency of the four most common paths have shown that the initial hypothesis, is incorrect. This because of new paths occurring only at greater angles, which is due to an increase in routes resulting from large ricochets. In this experiment, I have defined ‘Routes resulting from a large Ricochet’ as pathways that involved the marble colliding with a pin with sufficient force to ‘jump’ over a gap, such as route ABDC (Figure 6). The results show that large ricochets occur at greater angles and occur with greater frequency at higher angles. They have been highlighted as shaded cells in table 3. A larger angle of inclination results in a greater force down the incline, and therefore a greater acceleration of the marble and higher velocities. When a collision with a pin changes the direction of the velocity, it is still at a higher velocity for higher angles due to conservation of momentum.

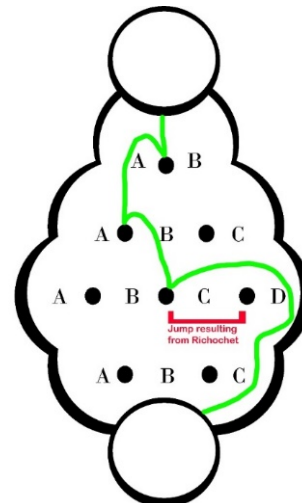


Figure 6: path ABDC, a path resulting from a ricochet

When it is launched horizontally at these higher velocities, the marble occasionally jumps a gap, such as in route ABDC, where the marble collides with the pin between the 3rd rows’ B and C, and ‘jumps’ over C.

To explore this theory as the cause of the decreased likelihood that a marble rolling down a steeper slope will use the most common paths, a deeper analysis can be made by investigating which taken routes involved jumps resulting from a ricochet (e.g. ABDC). Table 3 is a reproduction of Table 1 with shaded cells indicating routes involving jumps after a ricochet.

Table 3: Table 1 with route resulting from a ricochet shaded

5°	Route	ABCB	ABCC	BBBA	BBBB	BBCB	AABB	BBCC	ABBA	ABBB	AABA				
	Count	43	42	26	23	17	13	12	9	9	6				
10°	Route	BBBB	BBBA	BBCC	ABCC	ABCB	ABBA	BBCB	ABBB	BBAA	BCCC	BCBB	AABB		
	Count	37	29	25	25	24	22	21	10	4	1	1	1		
15°	Route	ABCB	BBBB	BBCB	ABCC	ABBA	ABBB	BBCC	BBBA	ABDC	BBAA	BABB	AABB		
	Count	38	27	25	24	21	17	15	14	11	5	2	1		
20°	Route	ABBB	ABBA	BBCB	BBBB	BBBA	ABCB	ABCC	BBAA	BBCC	ABDC	ACCB	AABA		
	Count	44	25	24	24	22	16	13	12	12	6	1	1		
25°	Route	BBCB	BBBB	BBBA	ABBB	BBCB	ABCC	ABBA	ABCB	ABDC	BBAA	BBDC	AABC	BAAB	ACCB
	Count	33	26	24	21	19	19	18	14	14	5	3	2	1	1
30°	Route	BBBB	BBCB	ABCC	ABBA	BBBA	BBCC	ABCB	ABBB	ABDC	BBAA	BBBC			
	Count	34	30	23	23	22	21	17	17	7	5	1			

Table 3 shows that ricochets occur at greater angles and occur with greater frequency at higher angles. These paths did not occur at lower angles. As these pathways occurred more frequently the greater the angle was, it has indicated the force required to ricochet in such a way, was only possible, or at least more likely to occur, when the angle was greater.

Conclusion

In conclusion, it can be drawn from the strong negative correlation between an increase in angle and frequency of the top routes that the initial hypothesis ‘That the greater the angle of a track with multiple paths the greater the probability that the marble will take one of the four most used paths’ must be rejected. As the angle of inclination grew, the system’s spread of paths increased. The strong ricochets which came as a result of the greater force of collision at higher angles lead to a range of paths that can’t occur at lower angles, such as ABDC. As this increases the variability, it can be said that the system becomes more chaotic at larger angles. Indicating that, until shown otherwise, that it should be accepted that the greater the angle of a track with multiple paths, the lower the probability that a marble will take the one of the four most frequency paths. This consequently allows for parallels to be drawn between known chaotic systems, such as the Lorenz attractor and this experiment, as small changes in the starting conditions of this system, led to dramatic changes in the outcome, the spread of paths taken.

Acknowledgements

I would like to thank Dr Hill for providing the apparatus used to perform the experiment and for his expert advice on both the writing of a scientific report and the scientific thinking aspect of the study which he drew from his experience in this field.

References

Batterman R., 1993, Defining chaos, Vol. 60, pp 43-66.

Bishop R., 2003, On separating predictability and determinism, pp 170-186.

The Lorenz attractor in 3D, 1997, <https://paulbourke.net/fractals/lorenz/>.

Encyclopedia Britannica, 2019, viewed 9 February 2020, Chaos theory, <https://www.britannica.com/science/chaos-theory>.

Fractal foundation n.d., What is Chaos theory, viewed 9 February 2020, <https://fractalfoundation.org/resources/what-is-chaos-theory/>.

Forbes n.d., Chaos Theory, The Butterfly Effect, And The Computer Glitch That Started It All, viewed 9 February 2020, <https://www.forbes.com/sites/starwithabang/2018/02/13/chaos-theory-the-butterfly-effect-and-the-computer-glitch-that-started-it-all/#748a244269f6>.

myPhysicslab, 2002, double pendulum viewed 9 February 2020, <https://www.mypysicslab.com/pendulum/double-pendulum-en.html>.

NCBI, 2007, a simple guide to chaos and complexity, viewed 9 February 2020, <https://www.ncbi.nlm.nih.gov/pmc/articles/PMC2465602/>.

Science buddies, 2020, Marble Roller Coaster: Converting Potential Energy to Kinetic Energy, viewed 9 February 2020, <https://www.sciencebuddies.org/science-fair->

projects/projectideas/Phys_p037/physics/roller-coaster-marbles-converting-potential-energy-to-kineticenergy#background.

Wolfram mathworld, 2020, Lorenz attractor, viewed 9 February 2020, <http://mathworld.wolfram.com/LorenzAttractor.htm>.

A General Vector Theory of the Dynamics of a Rapidly Rotating Top

Alexander Gray

Barker College

Previously, the motion of tops has been studied on flat surfaces with either pointed or rounded bases. These models are insufficient as they only apply in specific situations and are unable to adequately describe the motion of tops in other contexts and their real-world applications. This research investigates the behaviour of a top with a flat base on a spherical surface to develop a generalisable model for the forces and torques on a top. The model is based on five defined forces (gravity, the normal force, friction, rolling resistance, air resistance) and is partially verified through comparison between experimental and simulated results.

Background

Beyblades¹ are toy tops designed to spin for long periods of time, move with high linear velocity, and continue to spin despite contacting another Beyblade while battling in a hemispherical-shaped plastic dish known as a stadium (See Appendix 1 and Figure 1).

The type Beyblades used in this research can be split into three main, customizable parts – the top layer; the weight disk; and the driver (Figure 2). Many drivers have a flat, cylindrical base (Figure 3).

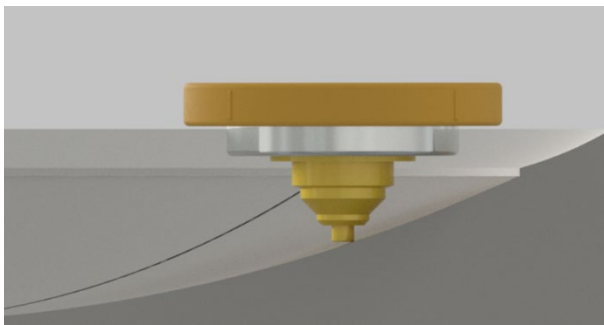


Figure 1: A cross section of a stadium with a computationally modelled Beyblade in motion at some point on the surface.



Figure 2: A 'Beyblade Burst' Beyblade split into its 3 core parts and put together.

After: Worthpoint, 2020; Millgrove, 2020

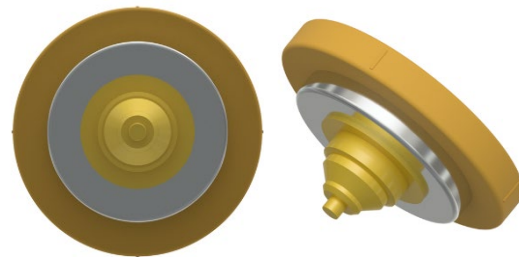


Figure 3: A 3D model of a simple Beyblade with a flat cylindrical base

¹ Beyblades originated in Japan and are produced by Takara Tomy. There have been many iterations in the general design of Beyblades over the years, however the Beyblades used in this research are from the 'Beyblade Burst' generation (although the physics which govern each generation are nearly identical).

Literature Review

The limited range of research into spinning tops

Spinning objects have been subject to physical and mathematical analysis since Newton (Newton, Koyré, & Cohen, 1972), with basic analysis of gyroscopes and spinning tops being a common section of first-year university Physics courses (Sears, Zemansky & Young 1987). However, there are few journal articles describing the motion of spinning tops suggesting that while some features of spinning tops are well understood, a comprehensive model is still undefined. A brief summary of the contributions of five main journal articles are below.

Braams (1952) presents a theoretical mechanism for friction causing the rising centre of mass (COM) of a top, such that it lies along the vertical axis through the contact point. Hugenholtz (1952) described a similar theoretical mechanism for the rising COM of a ‘tippe top’ (which paradoxically flips over during its motion) and standard top due to friction. More recently, Soodak (2002) gave a simple theory for the motion of a standard top with a demonstration of its equivalence for the well-known motion of a gyroscope. He also provided further exploration of a tippe top.

Two recent papers have sought to provide a more comprehensive understanding of a top in a specific set of circumstances. Klein and Sommerfeld (2012) provided a deep analysis of the effects of gravity, friction, rolling resistance and air resistance on the motion of a top on a flat surface. Their analysis includes both theoretical and mathematical derivation. Their description of rolling resistance is discussed later, and their derivations are helpful for constructing the generalisable model (despite being applied in the context of a specific set of assumptions). Similarly, Cross (2013) assumed a flat surface but provided a model for a standard top (with a rounded base) and tippe top which incorporated friction, rolling resistance and gravity. Experimental data presented supported this model.

Three limitations of this body of research are:

1. Only the motion of a top on a flat horizontal surface is studied, neglecting the effects of a slope on the motion of a top,
2. A realistic top, with a flat base, has not been described, and
3. The analysis only applies at particular stages of a top’s motion (e.g. rolling without slipping) which simplifies the problem, rather than providing a general theory for the motion.

This report aims to provide a general theory of forces and torques on a top, using vectors to define a model which is generally applicable to any cylindrically or point based top, at any stage of the motion, that can be translated to a surface of any curvature.

The Physics of Rotational motion

Along with drawing on theories in extant literature on tops, there are physics principles on rotational motion required for the justification of the model proposed in this report, particularly concerning gyroscopic motion, friction, and rolling resistance.

Gyroscopic Precession

A gyroscope or spinning top with any small deviation of its COM from the vertical axis through the contact point will result in precession or ‘wobble’ motion (Cross, 2013; Soodak 2002). This precession, when a gyroscope is horizontal (Figure 4), is defined as $\Omega = \frac{wR}{I\omega}$ where w is the gyroscope’s weight, R the distance between pivot and COM, I the gyroscope’s moment of inertia, ω its angular velocity (Cooper, 1988).

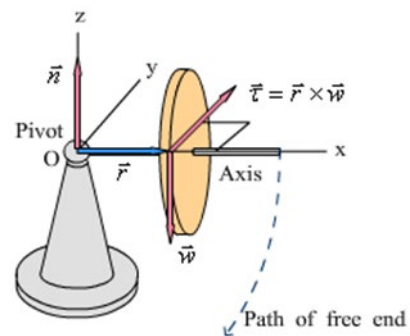


Figure 4: Diagram of a gyroscope rotating about a point. Source: Hong Kong Polytechnic University 2008

There are two methods of determining the torque that results in precession.

- (1) Gravity acting on the COM, at a distance from a pivot point produces a torque:

$$\vec{\tau}_g = \vec{r} \times \vec{F}_g \tag{1}$$

- (2) Alternatively, the normal force acting on the point of contact with the surface, at a distance from the COM, produces a torque about the COM:

$$\vec{\tau}_N = -\vec{r} \times \vec{F}_N \tag{2}$$

Either method will yield the same torque, but only if a top is on a flat surface:

$$\vec{\tau}_N = -\vec{r} \times \vec{F}_N = -\vec{r} \times -\vec{F}_g = \vec{r} \times \vec{F}_g = \vec{\tau}_g \quad (3)$$

The symmetry of these torques is broken when the top is considered on a slope due to the changed direction of the normal force such as in a generalised model of a top's motion.

Friction

Due to the top's rotation, relative motion arises at the point of contact and sliding friction will act at the base to oppose this motion (Cross 2013, Braams 1952, Hugenholtz, 1952). If there is no relative motion (i.e. the top is rolling without slipping) there is the potential for static friction to act at the base (Cross, 2013).

Rolling Resistance

There are two models used to describe rolling resistance which provide equivalent results when applied to rolling balls, however only one is sufficient to describe rolling resistance on spinning tops.

While the model that involves the normal force and rolling resistance force acting through the COM works for rolling balls (Klein & Sommerfeld, 2012; Vozdecký, Bartoš & Musilová, 2014), Cross (2013, 2016, 2017) demonstrated that for tops it is required to model these two forces acting at a distance from the COM (Figure 5) based on experimental evidence verifying the presence of more than simply kinetic friction (Parkyn, 1958; Cross, 2013) contrary to (Crabtree, 1909).

The two models are equivalent for the case of a ball rolling on a surface but lose their equivalence for a top and, as such, Cross' experimental validation of the model presented in Figure 5 makes it the most accurate existing model of rolling resistance.

The force causing the reduction in linear momentum in all models is given by

$$F_{rr} = C_r F_N = \frac{\mu_r}{r} F_N \quad (4)$$

Where μ_r (with units m) is the distance in front of the COM through which the normal force acts (D in Figure 5).

A question remains as to whether rolling resistance occurs when there is rolling with slipping motion. Each model describes the phenomenon using surface deformations and are each presented as only being valid when there is no slipping, however no reasoning is given for this. It is possible that this is merely because the effect cannot be measured when there is rolling with slipping. Despite this, it appears logically consistent with the models presented that this effect would persist even when there is rolling with slipping, provided there is some linear motion.

The Force Model

Defining vectors

To propose a generalised force and torque model for a top, a specific situation (with a sufficient level of complexity) needs to be described. Here, a Beyblade

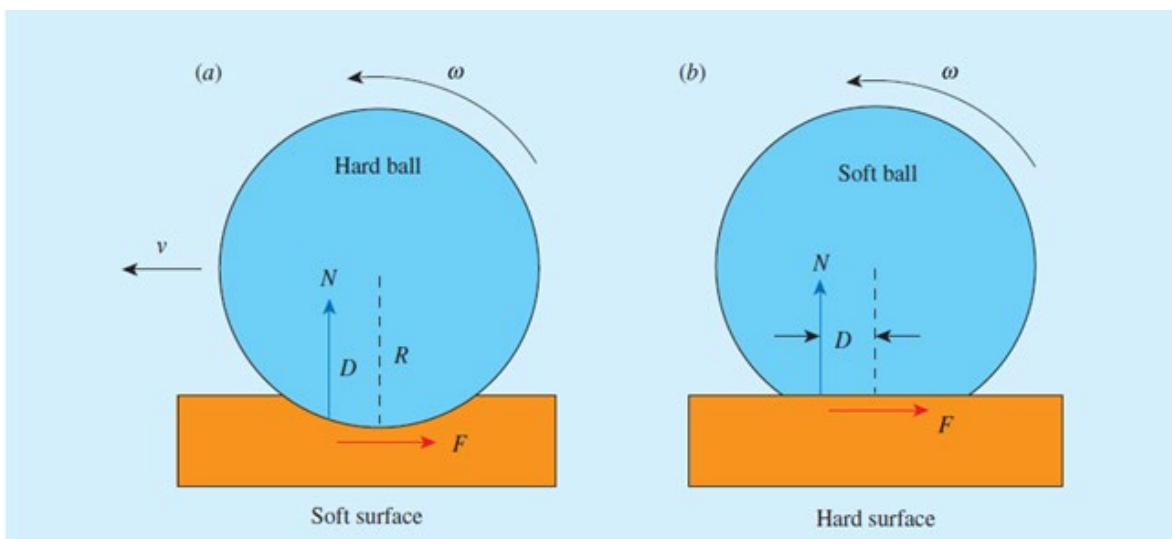


Figure 5: A ball rolling along a surface while rolling without slipping. The net forces and their locations are shown. Source: Cross, 2017

rotating on a cylindrical base, in a segment of a sphere will give the parameters for the simulation.

A cartesian coordinate system is defined with the origin at the stadium's centre, and lowest point (Figure 6) with positive \hat{z} direction pointed upwards. A radius vector, \vec{r}_s , is given by its position in the x - y right-handed plane i.e. (x, y) (Figure 7). Occasionally, spherical coordinates are also utilised for simplicity.

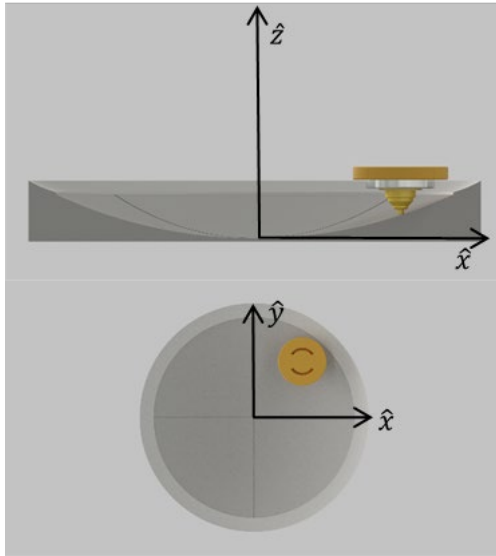


Figure 6: Diagram of a Beyblade in a stadium defined with cartesian coordinates

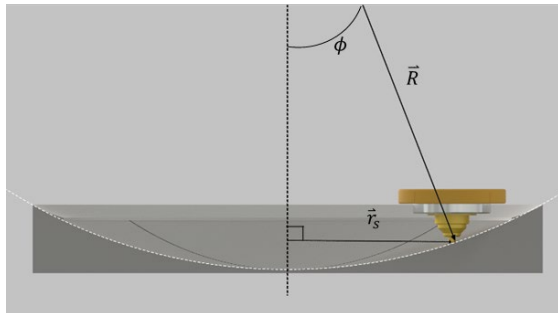


Figure 7: A Beyblade in motion in a stadium with a horizontal position vector and spherical position vector

If R is the spherical radius then the vector from the centre of the sphere to the position of the Beyblade is:

$$\vec{R} = (x, y, z - R)$$

$$\text{And, } \vec{N} = -\hat{R}$$

² It is worth noting that although this general form for \vec{r}_c is true for all tops, a different equation must be used for each component ($\vec{\sigma}$ and \vec{r}_d) than presented here. For example, a top with a rounded peg (as investigated by Cross (2013)) would have $\vec{\sigma}$ and \vec{r}_d vectors of variable sizes dependent on the tilt angle.

The height of the stadium is given by:

$$S(r_s) = R - \sqrt{R^2 - r_s^2}, \quad 0 \leq r_s \leq 0.123 \text{ (Figure 7)}$$

The radius of the Beyblade's cylindrical base is \vec{r}_d directed towards the point of contact with the stadium (Figure 8).

$$\vec{r}_d = r_d((\vec{N} \times \hat{\omega}) \times \hat{\omega}), \quad (\hat{\omega} = \text{angular velocity})$$

Pointing downward from the Beyblade's COM, directly through its axis of rotation, to the base of the driver is assigned $\vec{\sigma}$. (Figure 8).

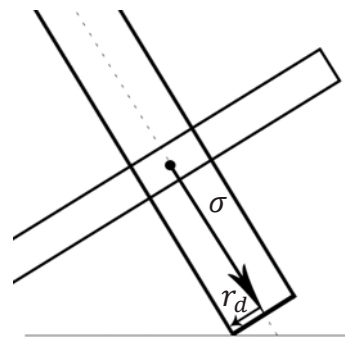


Figure 8: Diagram of a top with contact radius r_d and COM distance σ

Therefore, the vector from the COM, to the point of contact is $\vec{r}_c = \vec{\sigma} + \vec{r}_d$ ²

Velocity Vectors

Spherical coordinates $((R, \theta, \phi); \phi = \tan^{-1} S'(r_s))$ assist in defining velocity which is perpendicular to the spherical radius \vec{R} utilising the cross product (see Figure 7).

The velocity of the Beyblade's COM is given by the vector (\vec{v}).

$$\text{The velocity in the } (x, y) \text{ plane: } \vec{v}_h = \frac{d\theta}{dt} \times \vec{r}_s$$

$$\text{The velocity up / down the slope: } \vec{v}_s = \frac{d\phi}{dt} \times \vec{R}$$

The angular momentum $\vec{L} = I\hat{\omega}$, where I is the moment of inertia about the spin axis.

\vec{v}_d is the relative velocity due to rotation at the point of contact defined as: $\vec{v}_d = \vec{\omega} \times \vec{r}_d$.

The rate of precession of the axis of rotation about the COM is $\vec{\Omega} = \frac{\hat{\omega} \times \vec{\tau}_{net}}{|\omega|}$ where $\vec{\tau}_{net}$ is the net torque.

The base's motion due to precession is given by

$$\vec{v}_p = \vec{\Omega} \times \vec{r}_c.$$

The velocity at the contact point, \vec{v}_{net} , is therefore the sum of

- 1) The COM's velocity (\vec{v})
- 2) The relative velocity due to rotation (\vec{v}_d), and
- 3) The base velocity due to precession (\vec{v}_p).

$$\vec{v}_{net} = \vec{v} + \vec{v}_d + \vec{v}_p$$

The distance from the point of contact where the normal force acts due to effects of plastic deformation, shown as the distance D in Figure 5, is:

$$\vec{r}_N = \mu_r \left(\frac{\vec{v} \cdot \vec{v}_d}{|\vec{v} \cdot \vec{v}_d|} \right) \hat{v}_d$$

The five forces contributing to the force model

Summary

It has been determined from this background research that the five main forces on a Beyblade moving in a stadium consist of (1) gravity, (2) friction, (3) rolling resistance, (4) the normal force and (5) air resistance. Following are definitions and calculations of these five forces (and relevant torques).

1. Gravity

The force due to gravity is defined as:

$$\vec{F}_g = m\vec{g}, \quad \vec{g} = -9.8\hat{z} \text{ m s}^{-2} \quad (4)$$

No torque due to gravity occurs as the sum of all forces due to gravity acts at the COM, which results in no net torque about the COM.

2. Friction

Friction is most easily defined in two parts, regarding kinetic and static friction. Kinetic friction opposes relative motion and is defined as:

$$\vec{F}_k = -\mu_k F_N \hat{v}_{net} \quad (5)$$

Where \vec{F}_N is the normal force.

This force does also act as a torque defined as:

$$\vec{\tau}_k = \vec{r}_c \times \vec{F}_k \quad (6)$$

Static friction was considered, however, due to the difficult nature of modelling, it was ignored. This was justified with the observation that a Beyblade always moves either outwards or inwards with respect to the stadium's vertical axis, meaning it is likely always slipping up or down the slope.

3. Rolling Resistance

As determined by Cross (2013), rolling resistance acts at the point of contact as a force opposing the linear motion of the contact. The force due to rolling resistance can be given by:

$$\vec{F}_r = -\frac{\mu_r}{r_d} F_N \hat{r}_N \quad (7)$$

A torque will also arise due to this force about the point of contact and is therefore given by

$$\vec{\tau}_r = \vec{r}_c \times \vec{F}_r \quad (8)$$

4. Normal Force

The normal force for a moving object on a spherical surface is not defined in literature or textbooks. The normal force is made up of two terms. The first is the same as for an object on an inclined plane, $F_g \cos \phi$. However, as the Beyblade is also undergoing circular motion the normal force must also contribute a centripetal force of $\frac{mv^2}{R}$ (see Appendix 2 for the original derivation).

In vector form:

$$\vec{F}_N = \left(F_g \cos \phi + \frac{mv^2}{R} \right) \hat{N} \quad (9)$$

This normal force acts a distance from the COM and therefore acts as a torque:

$$\vec{\tau}_N = (\vec{r}_c + \vec{r}_N) \times \vec{F}_N \quad (10)$$

5. Air Resistance

The force due to Air Resistance on the COM is defined as:

$$\vec{F}_A = -C_D v^2 \hat{v} \quad (\text{NASA 2015}) \quad (11)$$

However, as in projectile motion, the air resistance drag force is often ignored due to the relatively low linear velocities so only the torque must be accounted for.

The torque due to air resistance from the rotational motion can be given by:

$$\vec{\tau}_A = -C_\tau \omega^2 \hat{\omega} \quad (12)$$

(Where C_D and C_τ are constants with units $kg\ m^{-1}$ and $kg\ m^2$ respectively).

Model Summary

The purpose of this report was to propose and assess a more comprehensive model for spinning tops. Everything in this report up to this point has been to justify and produce the four force, and four torque model that describes the changes to velocity and angular velocity of a cylindrical-based spinning top in a spherical stadium.

Now we can take all of this and combine the forces into a general vector form.

Net force (on COM) = weight force + normal force + kinetic friction + rolling resistance

$$\begin{aligned} \vec{F} &= \vec{F}_g + \vec{F}_N + \vec{F}_k + \vec{F}_r = m\vec{a} \\ &= m\vec{g} + \left(F_g \cos \phi + \frac{mv^2}{R} \right) \hat{N} - \mu_k F_N \hat{v}_{net} - \frac{\mu_r}{r_d} F_N \hat{r}_N \end{aligned} \quad (14)$$

Net torque (about COM) = air resistance + normal torque³ + kinetic friction + rolling resistance

$$\begin{aligned} \sum \vec{\tau} &= \vec{\tau}_A + \vec{\tau}_N + \vec{\tau}_k + \vec{\tau}_r = I\vec{\alpha} \\ &= -C_\tau \omega^2 \hat{\omega} + (\vec{r}_c + \vec{r}_N) \times \left(F_g \cos \phi + \frac{mv^2}{R} \right) \hat{N} \\ &\quad + \mu_k F_N \hat{v}_{net} \times \vec{r}_c + \frac{\mu_r}{r_d} F_N \hat{r}_N \times \vec{r}_c \end{aligned} \quad (15)$$

The rest of the report focusses on exploring the accuracy of this model through simulation and physical testing.

Scientific research question

What are the forces on a rapidly spinning top applicable to various parameters and situations?

Scientific hypothesis

That the motion of a spinning top in a generalised context is sufficiently described by the proposed force and torque models:

$$\sum \vec{F} = \vec{F}_g + \vec{F}_N + \vec{F}_k + \vec{F}_r \quad (16)$$

$$\sum \vec{\tau} = \vec{\tau}_A + \vec{\tau}_N + \vec{\tau}_k + \vec{\tau}_r \quad (17)$$

Methodology

The Simulation

To test the model proposed, a computer simulation was created in Visual C#. Inputs included the stadium and Beyblade’s parameters, initial position, and angular velocity. The main outputs included the changing position and velocity. The simulated motion can be compared to experimental (real-world) tests of Beyblades with identical properties. To allow for effective comparison, simulated results were computed for three different base radii to match three different Beyblade bases used.

Table 1: The names and values of constants used in the simulation

Name	Symbol	Value	Source
Coefficient of Kinetic Friction	μ_k	0.2	(Engineering Toolbox 2004)
Coefficient of Rolling Resistance	μ_r	$0.0002\ m$	(Hibbeler 2007) ⁴
Coefficient of Air Resistance Torque	C_τ	$2.105 \times 10^{-9}\ kg\ m^2$	(See Appendix 3)
The Stadium’s Spherical Radius	R	$0.29\ m$	Measured
Initial Angular Velocity	$\vec{\omega}_i$	$(0, 0, -345)\ rad\ s^{-1}$	Measured

³ The normal torque was chosen over the gravity torque as it is logically consistent with the rest of the model which assumes all forces acting at a distance from the C.O.M. act as torques.

⁴ This value was taken from the source as the coefficient for rolling resistance between hardened steel bearings and steel but doubled.

Table 2: The values of driver-specific constants used in the simulation

Base radius (m)	Mass - m_{r_d}		Moment of Inertia - I_{r_d}		C.O.M. Radius - σ_{r_d}	
	Symbol	Value (kg)	Symbol	Value ($kg\ m^2$)	Symbol	Value (m)
$r_d = 1.3mm$	$m_{1.3}$	5.590×10^{-2}	$I_{1.3}$	2.085×10^{-5}	$\sigma_{1.3}$	2.26×10^{-2}
$r_d = 1.6mm$	$m_{1.6}$	5.608×10^{-2}	$I_{1.6}$	2.089×10^{-5}	$\sigma_{1.6}$	2.25×10^{-2}
$r_d = 2.3mm$	$m_{2.3}$	5.608×10^{-2}	$I_{2.3}$	2.089×10^{-5}	$\sigma_{2.3}$	2.24×10^{-2}

Parameters of the Beyblades (See Appendix 4)

The Beyblade used for this research was constructed from the same top layer and weight disk but changing drivers (bases) with each driver having a driver radius (r_d) of 1.3mm, 1.6mm and 2.3mm respectively (see Table 2 and Figure 9).



Figure 9: The three drivers with varying base radii.

Experimental (Real-World) Testing

To validate the simulated results, a real-world situation with identical parameters was constructed for experimentation. A bespoke automatic Beyblade Launcher (Figure 10) (Appendix 6) ensured each Beyblade had consistent initial angular velocity, dropping close to the stadium’s centre.

Each Beyblade was filmed using an iPhone 6s at 720p resolution, 240Hz. The recordings were analysed in Tracker⁵.

Results

Figures 11 to 16 present the radial position (r_s) and speed (v) as functions of time since the Beyblade hit the stadium surface.

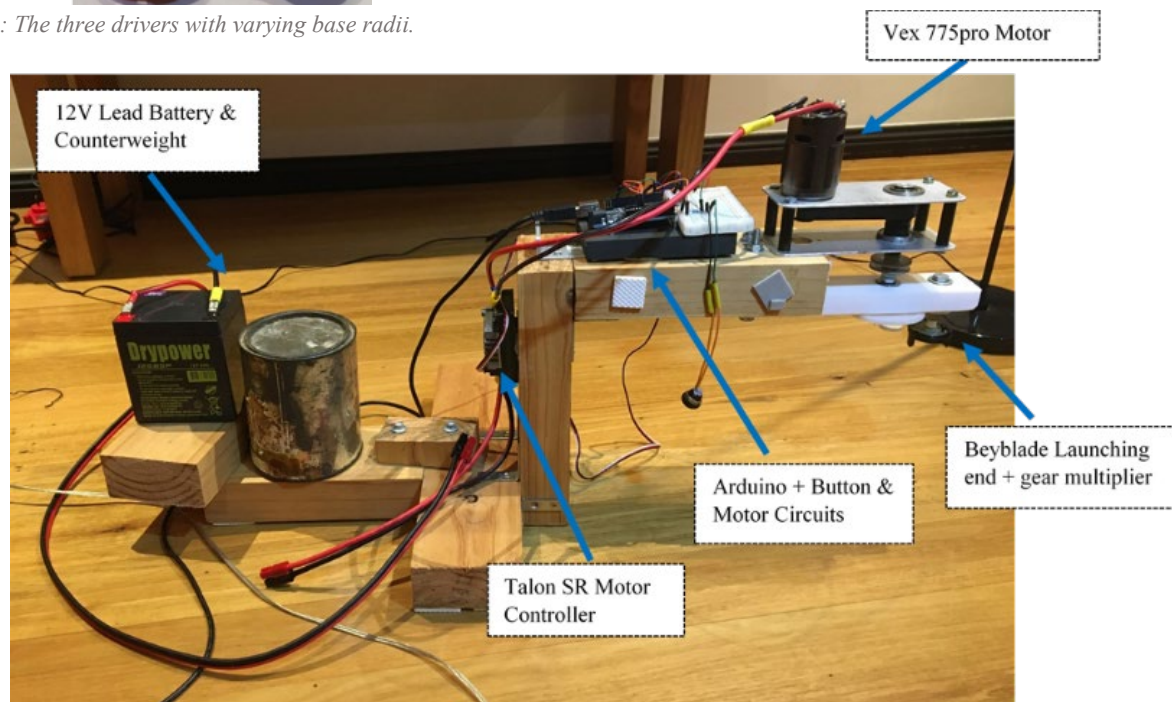


Figure 10: The Automatic Beyblade Launcher used to launch the Beyblades (See Appendix 6 for further information)

⁵ Tracker is a free video analysis tool built for use by Physics students. It was created by Doug Brown and can be found at <https://physlets.org/tracker/>.

1.3mm Radius Driver (Top 1)

Initial Velocity⁶: (0.0873, 0.0452) ms^{-1}

Initial Radial Position: 0.0363 m

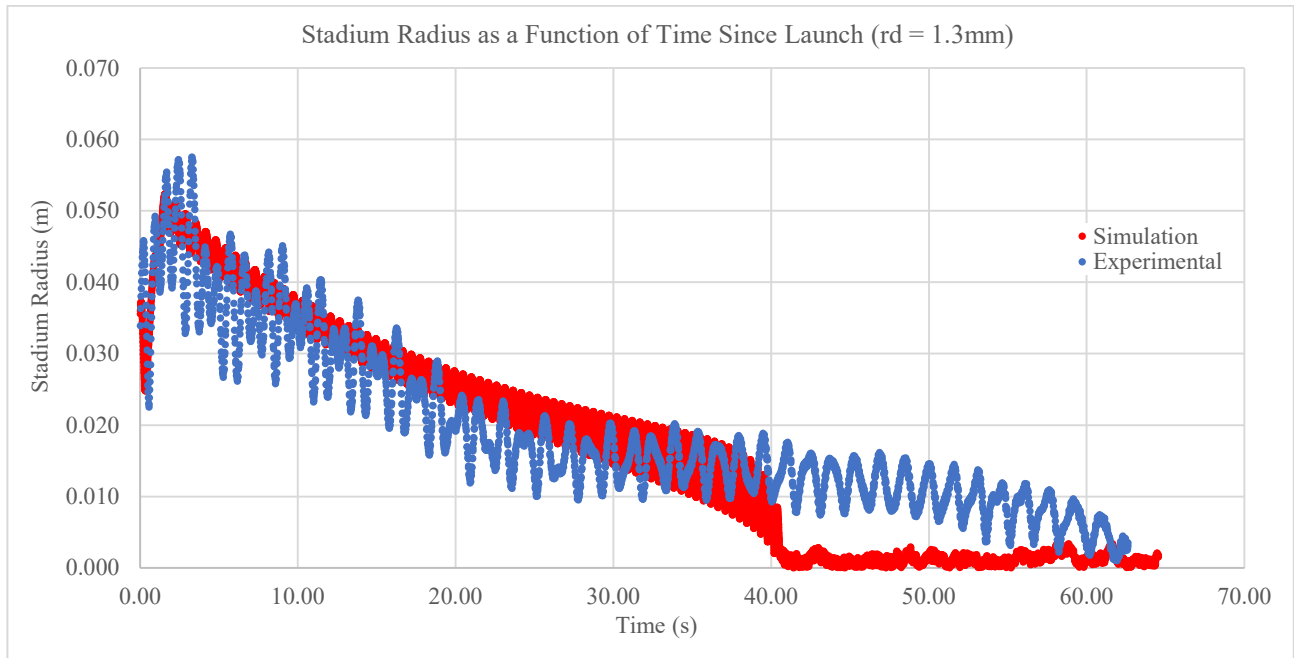


Figure 11: Graph of horizontal position (stadium radius) of the Beyblade as a function of time since it was launched for both experimental and simulated results (Top 1).

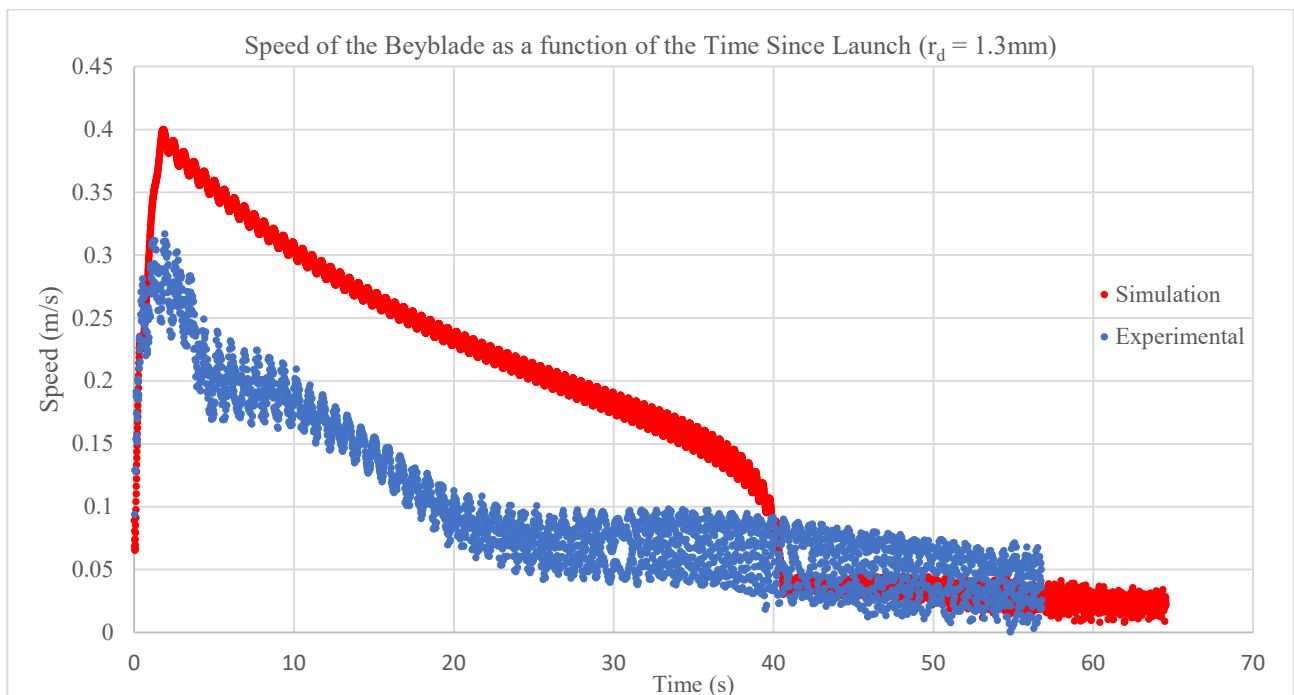


Figure 12: Graph of linear velocity of the Beyblade as a function of time since it was launched for both experimental and simulated results (Top 1).

⁶ One might expect the initial velocity and position to be zero, however this was unlikely to be the case due to minor fluctuations in the forces associated with the launcher. Therefore, the small initial velocity and position were measured, recorded, and input into the simulation as the initial velocity and position to allow for a valid comparison.

1.6mm Radius Driver (Top 2)

Initial Velocity: $(-0.1566, -0.0448) \text{ ms}^{-1}$

Initial Radial Position: 0.0389 m

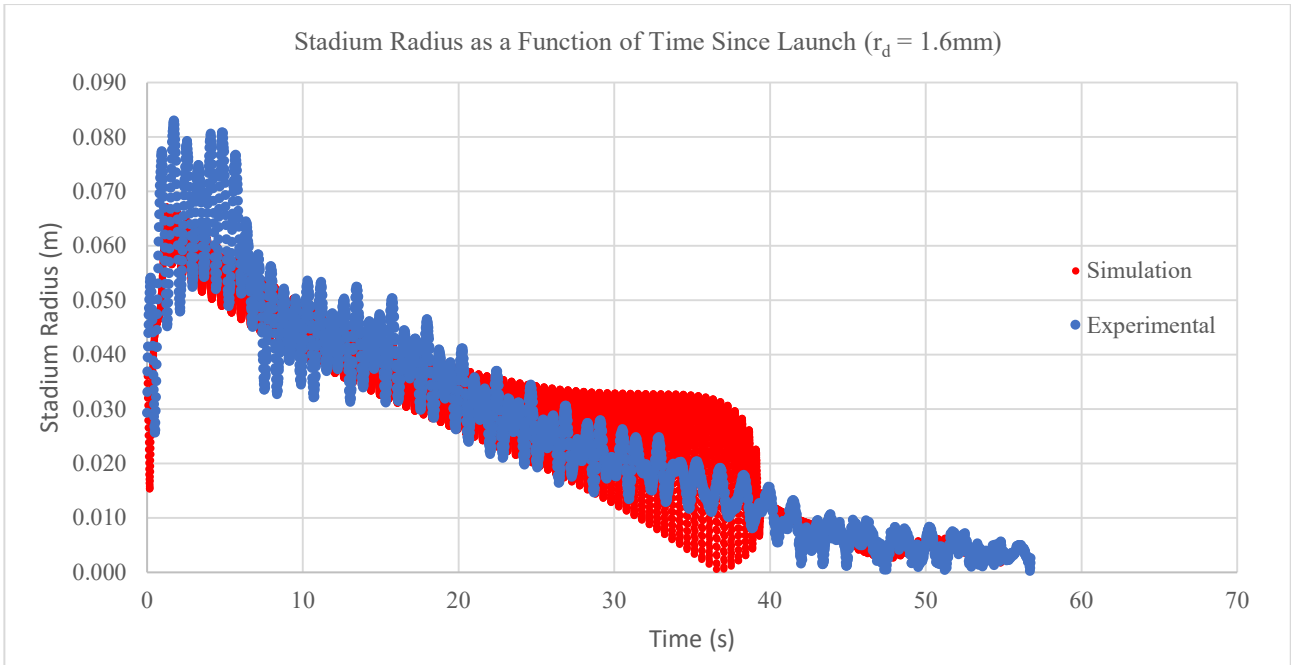


Figure 13: Graph of horizontal position (stadium radius) of the Beyblade as a function of time since it was launched for both experimental and simulated results (Top 2)

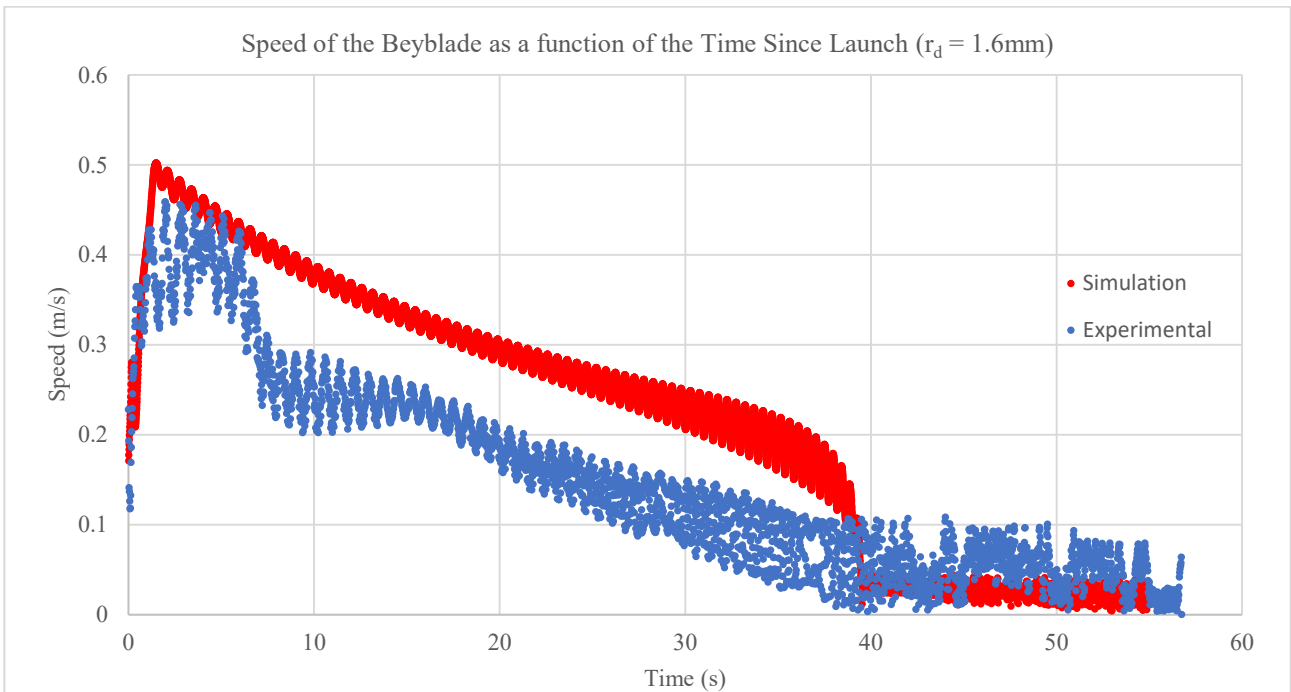


Figure 14: Graph of linear velocity of the Beyblade as a function of time since it was launched for both experimental and simulated results (Top 2)

2.3mm Radius Driver (Top 3)

Initial Velocity: $(-0.0293, 0.2258) \text{ ms}^{-1}$

Initial Radial Position: 0.0313 m

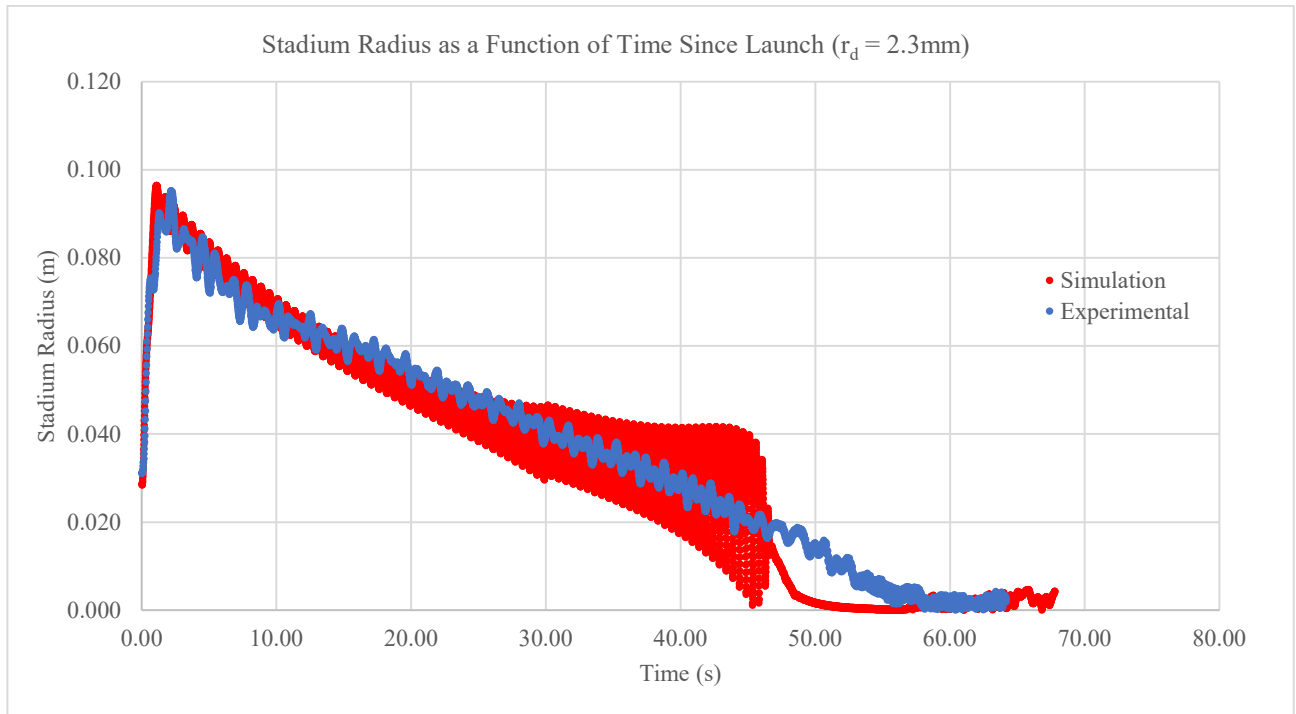


Figure 15: Graph of horizontal position (stadium radius) of the Beyblade as a function of time since it was launched for both experimental and simulated results (Top 3).

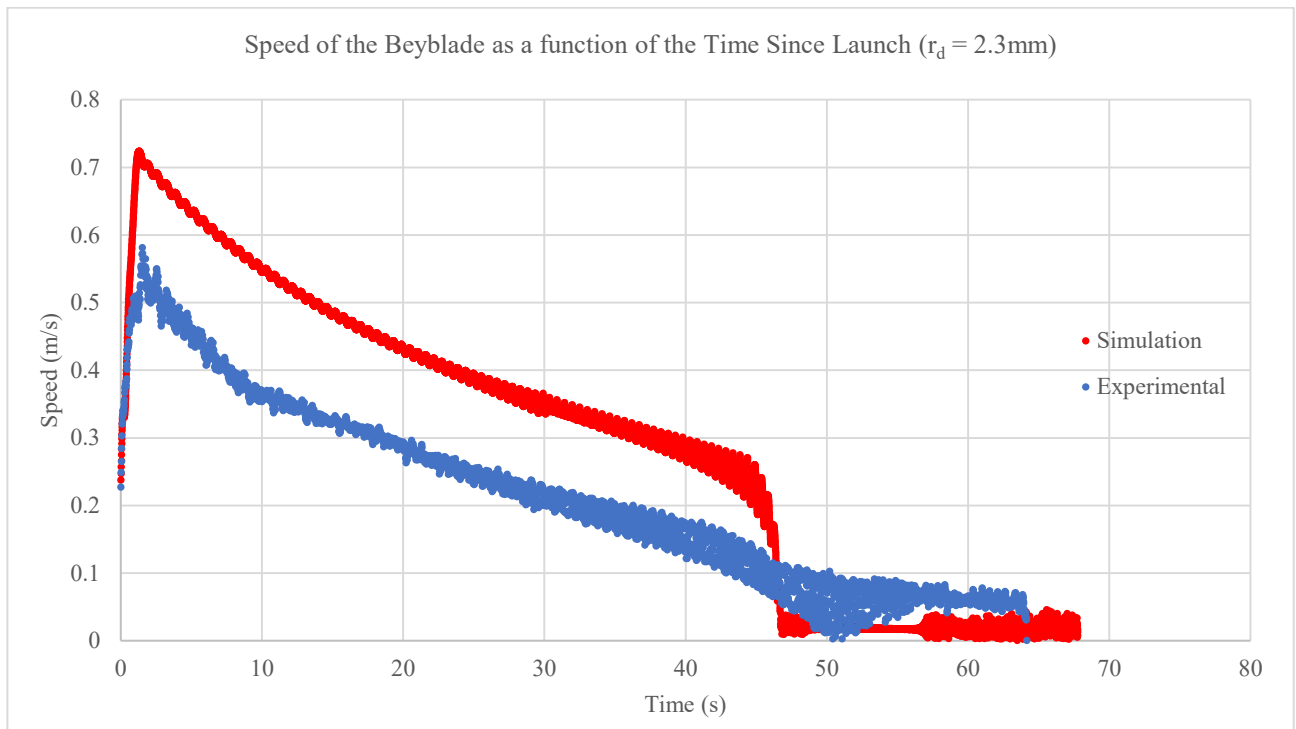


Figure 16: Graph of linear velocity of the Beyblade as a function of time since it was launched for both experimental and simulated results (Top 3).

Summary of Results

From figures 11, 13 and 15:

- a. For the radial position, the simulated data tends to match the experimental data for the first half of the motion.
- b. At around the halfway point however, the differences between the model and experiment become much greater where the simulation has a lower radial position than the experiment.
- c. Both the experimental and simulated results oscillate with a general downward trend.

In figures 12, 14 and 16:

- d. The experimental speed is clearly much lower than the simulated speed for the majority of the motion, but it follows a similar trend indicating that there is an alignment but a key factor that is inadequately represented in the model.

Discussion

The discussion begins with an explanation of the four observations from above. They appear in the order that best suits the explanations.

Observation a) - Consistent radial position from simulated and experimental data for the majority of the motion.

The consistency for the majority of the motion is a positive result for the model suggesting a moderate degree of accuracy for the model, with a high degree of accuracy at fast rotational speeds.

Observation c) – Oscillation of the graphs

The basic features of the oscillation in both the simulated and the experimental results is an expected consequence of gyroscopic precession. This is because precession causes a fluctuation in the direction of the relative motion at the point of contact.

Observation b) – Inconsistencies arise later in the motion

Further data can be used to investigate this result. By logging the net simulated velocity of the base, it was determined that the relative velocity at the point of contact becomes approximately zero during the simulation. Static friction occurs when there is no relative motion so should be present in the simulation.

In the first half of the motion, where the simulations closely resemble experiment, the experimental graphs show an unstable oscillation of the Beyblade's radial position which is consistent with a theoretical

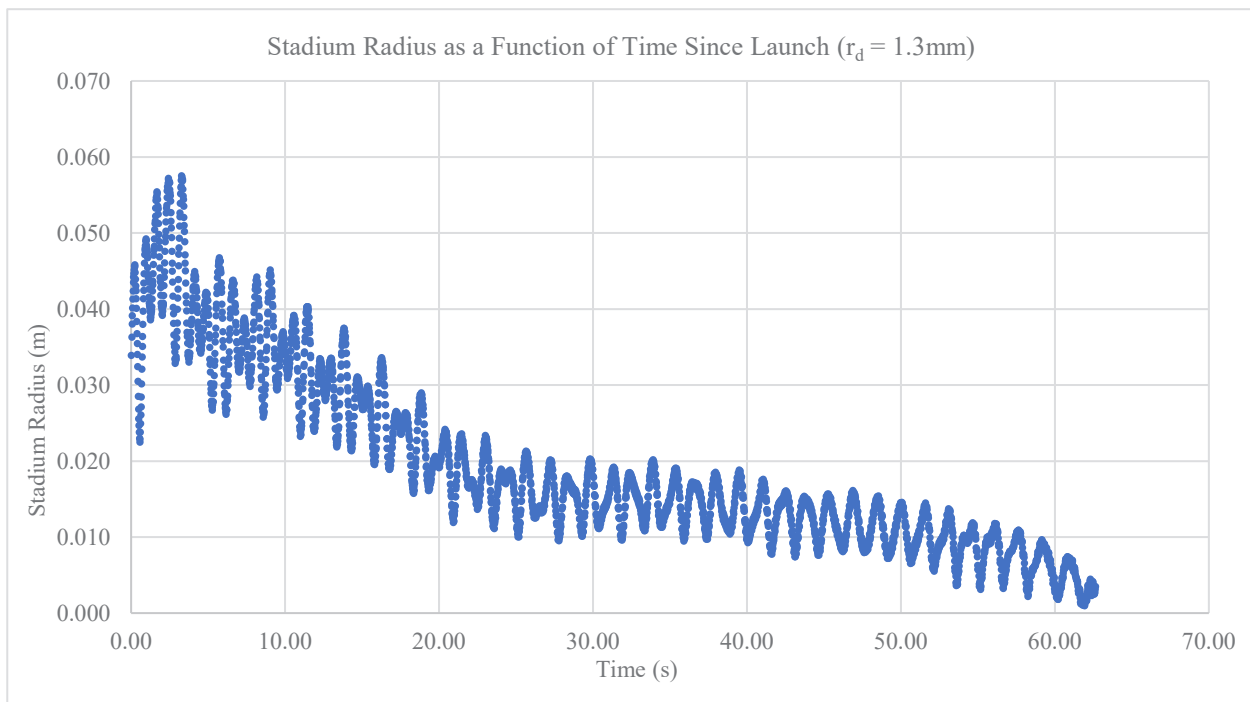


Figure 17: The experimental graph of Stadium Radius as a function of Time for Top 1.

understanding of the effects of kinetic friction and rolling *with* slipping (Figures 11 and 17).

In the second half of the motion, where the simulations lose their congruence, there is a clear transition to a more regular oscillation of the radial position which is consistent with an understanding of static friction and rolling *without* slipping.

This suggests that the assumption that static friction is absent during the motion is incorrect and is likely the primary cause for the discrepancies between the two in the second half of the motion.

Despite the desire to have included static friction as a force and torque maintaining rolling without slipping, as it does in theory (Sears, Zemansky & Young, 1987), modelling this formula is far more complex than the other vector models and can only be an area for further research.

Observation d) – linear velocity is lower for experimental than simulated data

It is assumed that the Beyblade is at least close to rolling without slipping. Because of this condition, from a particular experimental angular velocity, the expected linear velocity (if rolling without slipping) can be calculated and compared to the actual experimental linear velocity (see Table 3 for two examples).

Table 3: Table of results taken at random points from the experimental data (Top 3). The angular velocity, the expected velocity if the top was approximately rolling without slipping and the actual velocity are shown.

Time (s)	Experimental ω (rad s^{-1})	Expected v (m s^{-1})	Experimental v (m s^{-1})
10	215.4	0.50	0.36
20	167.6	0.39	0.29

The expected linear velocity is much greater than the actual experimental linear velocity which means that either:

- (i) It cannot be rolling without slipping (however, this is unlikely because there would be a noticeably high linear acceleration); or
- (ii) There are other factors allowing the Beyblade to roll without slipping, but with a lower than expected linear velocity, possibly due to surface deformation.

A mechanism for low experimental velocity

Over a century ago, Reynolds (1876) noted that a rolling object temporarily stretches material as it passes over it (Figure 18). This creates the impression that the object is moving with a slower apparent velocity as it is in contact with a greater distance of material than it appears to be covering. This is a possible explanation for the observed slower than predicted motion but is not yet quantitatively modelled.

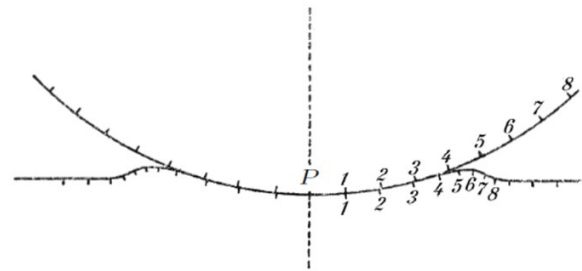


Figure 18: A cross section of the deformation of a soft surface being rolled over by a hard wheel.

Source: Klein and Sommerfeld, 2012

The Amended Model

Therefore, there appear to be two changes to the proposed model.

1. A model for the effects of surface deformation on the speed of a moving top must be developed to fully describe the linear motion of a top.
2. The force and torque components must be amended to include static friction.

Conclusion

The proposed vector model of the forces and torques on a spinning top provides an accurate computational result when compared to experimental results with the same parameters for high rotational speeds. However, there are inaccuracies at lower speeds, explained by the absence of static friction and surface deformation in the model.

The lack of clear experimental research behind the true nature of rolling resistance in relation to tops makes the additional details of the model hard to theoretically derive. Further experimentation into assumptions of rolling resistance and characteristics of surface deformation is required.

Despite these difficulties, this generalised model represents a more complete understanding of the motion of real-world tops on varying surfaces.

Acknowledgements

I would like to thank Dr Hill for his assistance with developing the model and the writing of this report. I would also like to thank the Barker College Robotics Team for assisting in making the motorised Beyblade Launcher.

Reference List

Braams, C.M. 1952. 'On the influence of friction on the motion of a top'. *Physica*. Vol. 18, no. 8-9, pp. 503-514.

Crabtree, H, *An Elementary Treatment of the Theory of Spinning Tops and Gyroscopic Motion* (Longman Green, London, 1909, reprinted by Chelsea, 1967).

Cross, R. 2013. 'The rise and fall of spinning tops'. *American Journal of Physics*. Vol. 81, no. 4, pp. 280-289.

Cross, R. 2016. 'Coulomb's law for rolling friction'. *American Journal of Physics*. Vol. 84, no. 3, pp. 221-230.

Cross, R. 2017. 'Origins of rolling friction'. *Phys. Educ.* Vol. 52, no. 055001, pp. 1-4.

Cooper, M. 1988, *Rotational Motion*, Brooks Waterloo, Sth Melbourne, Victoria.

Engineering Toolbox 2004, *Friction and Friction Coefficients*, Engineering Toolbox, viewed 15 January 2020, https://www.engineeringtoolbox.com/friction-coefficients-d_778.html.

Hibbeler, R.C. 2007, *Engineering Mechanics: Statics and Dynamics*, Pearson Prentice Hall, Singapore, Singapore.

Hong Kong Polytechnic University 2008, *Gyroscopic Precession*, Hong Kong Polytechnic University, Hong Kong, viewed 13 May 2020.

Hughenoltz, N.M. 1952. 'On tops rising by friction'. *Physica*. Vol. 18, no. 8-9, pp. 515-527.

Klein, F, Sommerfeld, A 2012, *The Theory of the Top Volume III: Perturbations. Astronomical and Geophysical applications*, Springer Science + Business Media, New York, New York.

Millgrove 2020, *Kids Toys Beyblade Burst B-48 Starter Zeno Excalibur .M.I (Xeno Xcalibur .M.I) with launcher Beyblade spinner B-66 kids toys*, Millgrove Heavy Equipment Service, Viewed 20 April 2020, <http://www.millgroveheavyequipmentservice.ca/Kids-Toys-Beyblade-Burst-B48-Starter-Zeno-Excalibur-MI-Xeno-Xcalibur-MI-with-launcher-beyblade-spinner-B66-kids-toys-qIhVkkTh-p-4097.html>.

NASA 2015, *Forces on a falling object*, NASA, Washington D.C. viewed 4 February 2020, <https://www.grc.nasa.gov/WWW/K-12/airplane/falling.html>.

Newton, Isaac, Alexandre Koyré, and I B. Cohen. 1972, *Philosophiae Naturalis Principia Mathematica*, Cambridge, Mass.: Harvard University Press.

Parkyn, D.G. 1958. 'The rising of tops with rounded pegs'. *Physica*. Vol. 24, no. 1-5, pp. 313-330.

Reynolds, O. 1876. 'On Rolling-friction'. *Royal Society*. Vol. 166, no. 6, pp. 155-174.

Sears, F, Zemansky, M & Young, H 1987, *University Physics Seventh Edition*, Addison-Wesley, Boston, Mass.

Soodak, H 2002. 'A geometric theory of rapidly spinning tops, tippe tops, and footballs'. *American Journal of Physics*. Vol. 70, no. 8, pp. 815-828.

Vozdecký, L., Bartoš, J. and Musilová, J. 2014. 'Rolling friction – models and experiment. An undergraduate student project'. *European Journal of Physics*. Vol. 35, no. 055004, pp. 1-16.

Worthpoint 2020, *Beyblade Burst B-48 Starter Xeno Xcalibur M.I Beyblades with Launcher Starter*, Worthpoint, Viewed 19 April 2020, <https://www.worthpoint.com/worthopedia/beyblade-burst-48-starter-xeno-1867478308>.

Appendix 1



Figure 19: Beyblade Burst Stadium (B-76)

Appendix 2

Two situations aided in the construction of the model for the normal force on a moving Beyblade: (1) A mass on a string undergoing horizontal circular motion and (2) a mass on a string undergoing vertical circular motion. This model is useful as it is less complex but contains the same type of motion relevant to the normal force.

In horizontal circular motion where: L is the length of the string; ϕ is the angle of the string from the vertical and; v_h is the horizontal speed of the mass, the tension in the string is given by:

$$F_T = F_g \cos \phi + \frac{mv_h^2}{L} \quad (18)$$

The second situation is a mass on a string undergoing vertical circular motion with the similar characteristics, with circular velocity v_c . Instantaneously, the tension is given by

$$F_T = F_g \cos \phi + \frac{mv_c^2}{L} \quad (19)$$

Clear parallels can be drawn to the two forms of motion and the movement of the Beyblade up and around the stadium. As a result, it would reason that these formulae could be combined to give the normal force for a Beyblade in a stadium. i.e.

$$F_N = F_g \cos \phi + \frac{mv_h^2}{R} + \frac{mv_s^2}{R} \quad (20)$$

This formula can also be simplified using the result $v = \sqrt{v_s^2 + v_h^2}$:

$$F_N = F_g \cos \phi + \frac{mv^2}{R} \quad (21)$$

It is worth noting that this formula is accurate for a flat slope, where a flat slope is defined as a sphere with spherical radius of ∞ :

$$F_N = \lim_{R \rightarrow \infty} \left(F_g \cos \phi + \frac{mv^2}{R} \right) = F_g \cos \phi \quad (22)$$

Appendix 3

Determining the Coefficient of Air Resistance Torque

To establish the coefficient of Air Resistance torque on the Beyblade, a digital tachometer was held in place and pointed at a Beyblade with a small piece of reflective tape on the top layer, pointing radially from its centre. The Beyblade used the same top layer and weight disk ('Glide Ragnaruk 1S' and 'Outer') however the driver used was Orbit Metal (B-149). This driver was used due to its low friction properties (the contact point is made of metal which has a lower coefficient of friction and the metal contact is a sphere which can rotate freely) and due to its shape which gives it a very small driver radius (approximately a point). This small contact point allows the effects of friction torque to be ignored. An iPhone 6s was then used to film the tachometer at 240Hz and every time the display updated; the reading was recorded. The data was then used to construct a graph of torque against angular velocity squared to find the coefficient.

$$\begin{aligned} \tau = -C_\tau \omega^2 &\Rightarrow \frac{\tau}{\omega^2} = -C_\tau \Rightarrow C_\tau \\ &= 2.105 \times 10^{-9} \text{ kg m}^2 \end{aligned} \quad (23)$$

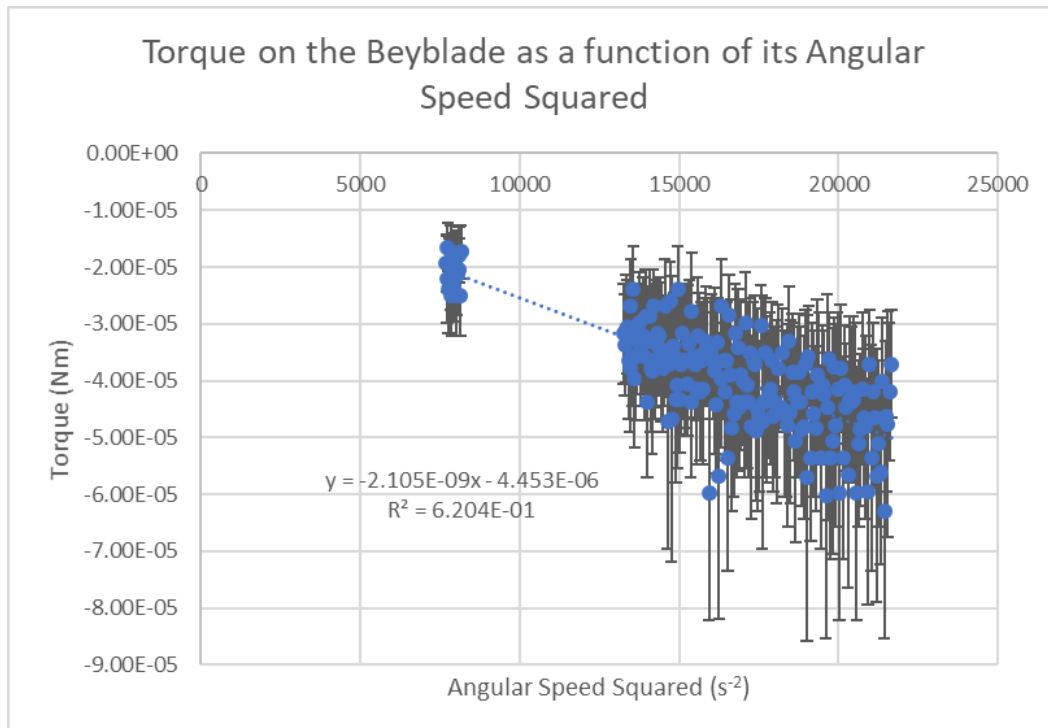


Figure 20: The gradient of torque over angular speed squared ($\frac{\tau}{\omega^2}$) represents the coefficient of air resistance torque for a Beyblade with a driver radius $r_d \cong 0$. This is then the air resistance coefficient for all drivers.

Appendix 4

Determining Moment of Inertia

To measure the moment of inertia of the Beyblade, each piece was separated and approximated to its closest regular geometrical counterpart and assumed to have uniform mass distribution. As a result, a slightly different moment of inertia value was determined for each Beyblade combination due to slight variations in the mass of each driver.

Table 4: Table describing the mass, approximate regular geometric shape, approximate moment of inertia and measurement error of the moment of inertia for each Beyblade part used as part of this research.

	Part	Mass (kg)	Shape	Moment of Inertia (kg m²)	Measurement Error (kg m²)
Layer	Ragnaruk	3.00E-03	Disk	3.04E-07	±7.00E-10
	Glide	8.79E-03	Ring	5.21E-06	±4.02E-09
	1S	1.67E-02	Ring	7.34E-06	±3.44E-09
Disk	Outer	2.17E-02	Torus	6.72E-06	±5.78E-09
Drivers	Orbit Metal	7.90E-03	Cone	1.70E-06	±1.39E-09
	Blow	5.71E-03	Cone	1.23E-06	±1.31E-09
	Accel	5.89E-03	Cone	1.27E-06	±1.32E-09
	Assault	5.89E-03	Cone	1.27E-06	±1.32E-09

Appendix 5

The Beyblade



Ragnaruk Chip

https://beyblade.fandom.com/wiki/Superking_Chip_-_Ragnaruk

Glide Ring

https://beyblade.fandom.com/wiki/Ring_-_Glide

IS Chassis

https://beyblade.fandom.com/wiki/Chassis_-_IS

Outer Weight Disk

https://beyblade.fandom.com/wiki/Forge_Disc_-_Outer

Figure 21: Glide Ragnaruk IS Outer - Exploded view

The top layer used was 'Glide Ragnaruk 1S' (B-161⁷) and the weight layer used was 'Outer (Ω)' (B-128). The drivers used were 'Blow' (B-130), 'Accel' (B-146) and 'Assault' (B-00), with each driver having a driver radius (r_d) of 1.3mm, 1.6mm and 2.3mm respectively

⁷ Beyblade products have an item number which will be indicated in brackets after describing the item. All Beyblade products used in this experiment are manufactured by the company Takara Tomy.

Appendix 6

The Launcher

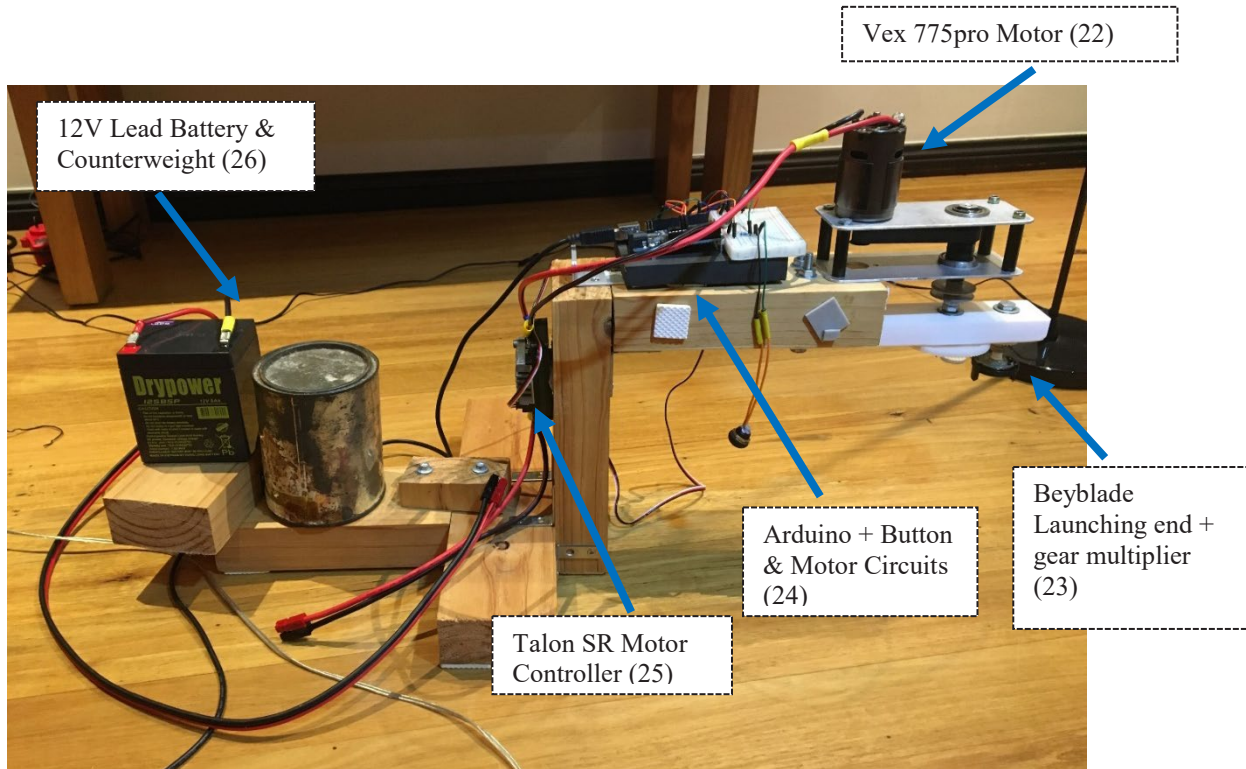


Figure 22: The motorised Beyblade Launcher

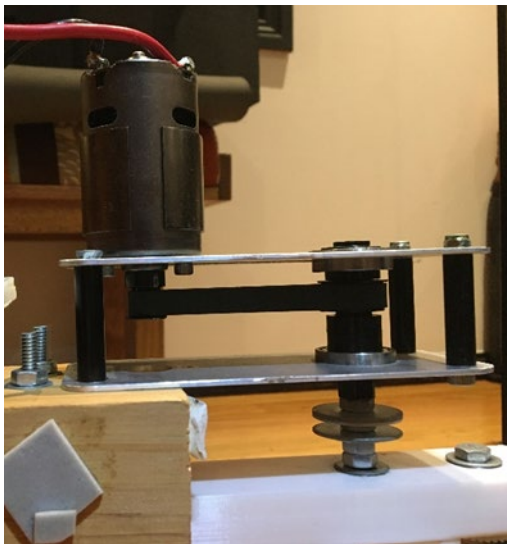


Figure 23: The 775pro motor attached to a belt system



Figure 24: The gear multiplier and Beyblade launching end

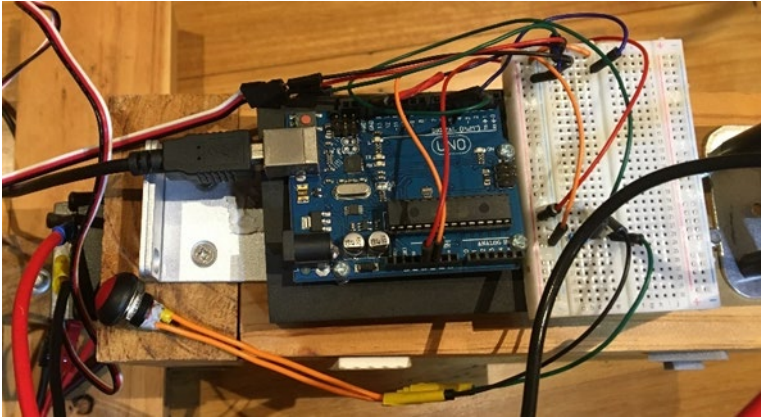


Figure 25: Arduino and breadboard circuit

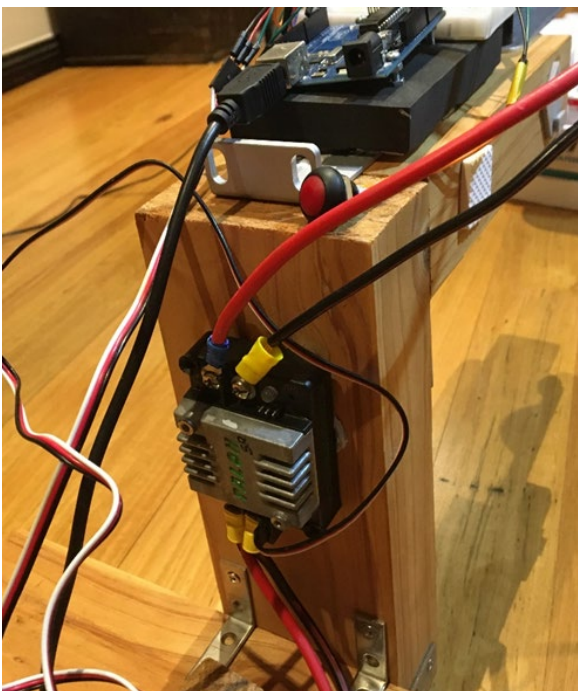


Figure 26: Talon SR motor controller



Figure 27: 12V Lead Battery



Chemistry

Chemistry is concerned with the study of the composition, properties and reactivity of matter.

This year's chemistry projects were focused in the area of medicinal chemistry, a vitally important research area with the potential to unlock new pathways to treat diseases. Alex's project aimed to investigate the effect of storage temperature on the lycopene concentration in tomatoes. Due to the potent medicinal properties of lycopene and the analysis method developed by Alex, this area of research will surely facilitate future Science Extension projects.

Both Kai and Jasmine were part of the Breaking Good project; a citizen science project targeting the availability and cost of essential medicines. Building on a project from last year, Kai was able to synthesise a new analogue of the antimalarial drug, pyrimethamine. This research is vital in the fight against drug resistance, which is a significant issue with malaria treatments. Jasmine focused on confirming the reliability of the synthesis of this drug, pyrimethamine, which has been developed by Sydney Grammar School. Assessing the reliability of this new synthetic pathway represents an important development in showcasing the unnecessary high price point of some essential medicines like these, which continues to be an issue in society.

These chemistry projects are traditionally reserved for university level research and require a significant jump in knowledge from the HSC Chemistry course. These students have taken to this difficult task with passion and focus and we congratulate them on these impressive scientific contributions.

Synthesis of a Pyrimethamine Analogue

Kai Wong

Barker College

Since its introduction in 1952, the efficacy of pyrimethamine as an anti-malarial agent has declined significantly due to a mutation in the dihydrofolate reductase enzyme of *Plasmodium falciparum*, the most prevalent malaria pathogen. The present study highlights the potential to overcome this drug resistance by changing the nature of the substituents on the pyrimethamine ring. Utilising an established synthetic pathway for the synthesis of pyrimethamine, this report describes the successful synthesis of the novel 4-iodopyrimethamine analogue and its possible applications in cross-coupling reactions.

Literature review

Malaria is a protozoan vector-borne disease transmitted by the female *Anopheles* mosquito. It is caused by five species of *Plasmodium* parasites, of which *Plasmodium falciparum* is the most severe and widespread (Talakpo et al., 2019). *P. falciparum* causes the surface of red blood cells to become “sticky”, so they clump together and obstruct blood flow to vital organs (Ashley et al., 2018). If not treated within 24 hours, *P. falciparum* malaria can progress to severe illness, often leading to death (WHO Global, 2019).

According to the World Health Organisation, in 2018, an estimated 228 million cases of malaria occurred worldwide, with 213 million in the African Region alone (WHO, 2019). Alarmingly, *P. falciparum*, the most potent malaria causing species, accounted for 99.7% of cases within the region. Additionally, in 2018, there were approximately 405 000 global malaria deaths, which is a 30% decrease from the 585 000 deaths in 2010 (WHO, 2019). Although this is a considerable improvement, since 2016, the rate of reduction in both morbidity and mortality in the African Region has slowed dramatically (Figure 1) (WHO, 2019).

Trends in malaria case incidence rate (cases per 1000 population at risk) globally and by WHO region, 2010–2018 The WHO European Region has reported zero indigenous cases since 2015. Source: WHO estimates.

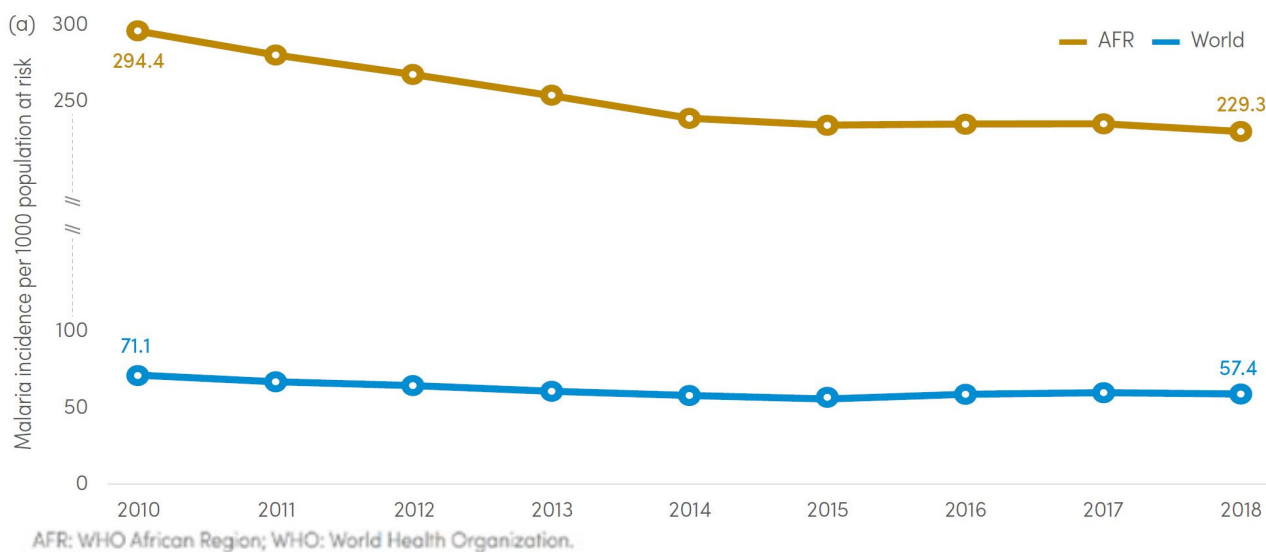


Figure 1: Graph displaying the trends in malaria mortality rate
Source: WHO, 2019

This slowed progress may be explained by recent changes in two key areas. Firstly, increased temperatures and wetter conditions caused by climate change have optimised mosquito breeding conditions in endemic areas (Endo et al., 2017). Both historical evidence and future malaria modelling suggest that changes in climate and weather patterns could even lead to the migration of mosquito vectors to previously unreported areas (WHO, 2019). Secondly, rapid mutations within plasmodium parasites have led to an increased occurrence of antimalarial drug resistance, thereby rendering many conventional treatment options largely ineffective (Nattee et al., 2017). Resistance of *P. falciparum* to previously potent medicines has undermined malaria control efforts and reversed gains in child survival (WHO, 2019). These reasons highlight the urgent need for high potency drug solutions.

The anti-malarial drug pyrimethamine (Figure 2) is a specific derivative of 2,4-diaminopyridine and is sold under the trade name Daraprim. Since being developed in 1952, pyrimethamine has seen widespread use as an anti-malarial and anti-protozoal agent (Falco et al., 1951). It has been particularly effective in treating immuno-suppressed patients who have the highest risk of infection from microorganisms such as *Toxoplasma gondii* and *P. carinii*, which result in toxoplasmosis and pneumonia, respectively. Furthermore, the drug is well tolerated by pregnant women and young children who are most vulnerable to *P. falciparum* infection (Oaks et al., 1991). As such, these three micro-organisms have been successfully treated by pyrimethamine in the past.

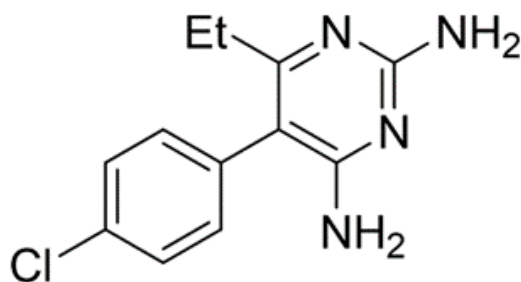


Figure 2: Pyrimethamine (1)

The mechanistic function of pyrimethamine against these microorganisms lies in its ability to inhibit key enzyme pathways (Tropak et al., 2015). Pyrimethamine is an antagonizing agent which is highly effective in binding to the parasitic enzyme dihydrofolate reductase (DHFR), crucial for cell growth and reproduction (Bloland, 2001).

More specifically, the drug prevents DHFR from catalysing the hydrogenation of dihydrofolate to form tetrahydrofolate with NADPH (Figure 3). This pathway is part of the biosynthesis of purines, a class of precursor molecules necessary for DNA and RNA synthesis (Ashley & Phyo, 2018). Thus, inhibition of this enzyme disrupts nucleic acid synthesis and prevents further proliferation of the plasmodium.

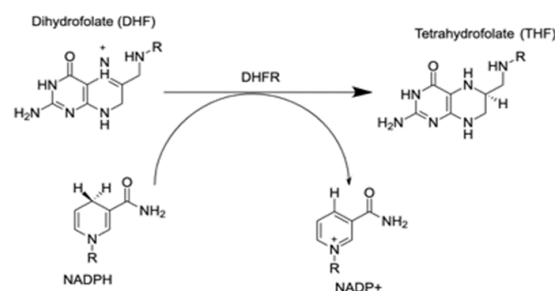


Figure 3: Bio-synthetic pathway of DHFR catalysed hydrogenation of dihydrofolate

Source: Tropak et al., 2015

Unfortunately, new mutations in the DHFR gene have led to resistant strains of these microorganisms, thereby compromising the efficacy of pyrimethamine (Okombo et al., 2018). To overcome this drug resistance, it is imperative that further research is undertaken to better understand the differences in pyrimethamine's interactions with the mutated DHFR as opposed to the wild-type DHFR enzyme. Current literature on this subject is still relatively limited; pyrimethamine's direct interaction with *P. falciparum* DHFR is a complex, multi-faceted process, and the exact structure of the bio-functional enzyme is not yet known (Imwong et al., 2017). Molecular modelling suggests that pyrimethamine's structural similarity to DHF allows it to effectively bind to DHFR and stabilize the folded enzyme within the endoplasmic reticulum (Figures 4 & 5) (Birdsall et al., 1990). In wild-type DHFR, the key interaction with pyrimethamine is the hydrogen bonding which occurs at the active site. The enzyme-inhibitor complex is formed by the two amino groups on the heterocyclic pyrimidine component which form three hydrogen bonds with the active site amino acids D290, D240 and E491, and the two amino functional groups on the ring which interact with R211 and D354 (Figure 4). The ethyl group on the pyrimidine ring is most commonly found in the non-polar pocket of W405 and W424 (Figure 4) (Tropak et al., 2015)

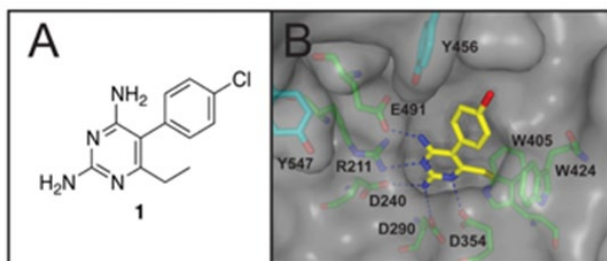


Figure 4: A) Structure of pyrimethamine B) 3D modelling of enzyme-inhibitor complex at the active site between pyrimethamine and wild-type DHFR ligand
Source: Tropak et al., 2015

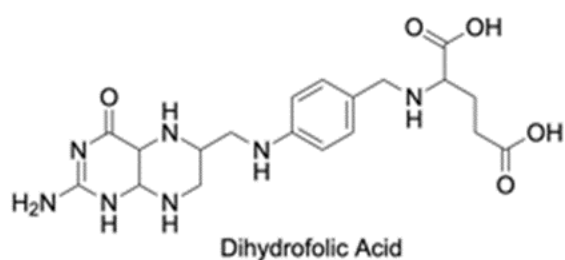


Figure 5: Structure of DHF

However, in the mutated DHFR enzyme active site, there is a steric clash between the chlorine atom of pyrimethamine and an amino acid that was not present in the wild-type DHFR. This explains how mutated *P. falciparum* has developed resistance against pyrimethamine, drastically reducing its clinical utility (Tropak et al., 2015). Likewise, through other mutations, *P. falciparum* has developed resistance against nearly all available antimalarial drugs, and it is likely that the parasite will eventually become resistant to any widely used medicine (Bloland, 2001). For these reasons, long-term success against malaria will depend on a continuous supply of new and affordable drugs.

One common approach to creating novel medicines is through the development of analogues of drugs which have lost their potency. Small structural alterations to the original compound can lead to significant improvements in drug efficacy. Previous studies indicate that substitution at the R4 position (Figure 6) with alternative atoms or functional groups may greatly increase binding affinity (Tarnchompoo et al., 2002). Thus, there has been significant effort into the synthesis of various pyrimethamine analogues, as well as the collection of biological data via testing of these analogues against both mutant and wild-type *P. falciparum* (Nattee et al., 2017). As stated previously, pyrimethamine is a pyrimidine-2,4-diamine, substituted at the C5 position by a *para*-

chlorophenyl ring. This phenyl ring, and more specifically the R3 and R4 positions, are the most common locants for variations to be introduced during synthesis (Nattee et al., 2017). The majority of analogues which have been synthesised to date include combinations of halogen substitutions on the phenyl ring. Other analogues consist of more complex methylbenzoprism substitutions (Yuthavong et al., 2004). The variation in effectiveness of each analogue as an antagonist of DHFR allows us to further understand the interaction between both the wild-type and mutated enzyme with the pyrimethamine analogues.

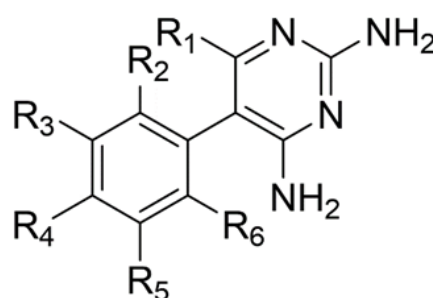


Figure 6: General structure of pyrimethamine analogues

Evidently, there is a clear need for a new and effective inhibitor of mutated DHFR (Muiruri et al., 2018), and this research aims to synthesise a novel analogue of pyrimethamine. A particular point of interest was the effect of replacing the chlorine atom with an iodine atom at the R4 position, namely the 4-iodopyrimethamine analogue (2) (Figure 7). Although approximately 50 analogues have been synthesised and tested, this specific analogue (2) has not yet been synthesised. The incorporation of the larger iodine atom into the structure has the potential to improve biological activity through enhanced binding interactions in the enzyme active site. Furthermore, since the carbon-iodine bond is more reactive than a carbon-chlorine bond, it can be used as a 'synthetic handle' for metal catalysed cross-coupling reactions such as the Suzuki or Nigishi coupling, streamlining the synthesis of a library of other analogues from a single starting compound (Biajoli, 2004). This ability to functionalise the R4 position with a carbon-carbon bond will create opportunities for future research, providing access to a vast array of more complicated analogues with varying structural features which could potentially increase binding affinity.

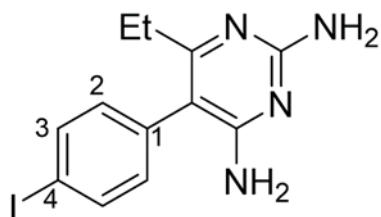


Figure 7: Proposed 4-iodopyrimethamine analogue (2)

The synthetic pathway developed by Sydney Grammar School students in 2016 for the synthesis of pyrimethamine will be the focus of the methodology (Figure 8) (SGS, 2016). In collaboration with the University of Sydney and the Breaking Good Project, an organisation that assists the public in conducting chemical research, these students were able to successfully synthesise pyrimethamine in their school laboratory (SGS, 2016). Having access to the same

resources provided by Breaking Good, this proposed methodology should be applicable to the synthesis of our proposed iodine analogue (2) from 4-iodophenylacetonitrile (3) in our school laboratory.

Scientific research question

Can the iodo-analogue of pyrimethamine (2) be synthesised from 4-iodophenylacetonitrile (3) in a school laboratory and be tested as an anti-malarial agent against *Plasmodium falciparum*?

Scientific hypothesis

That the iodo-analogue of pyrimethamine (2) can be synthesised from 4-iodophenylacetonitrile (3) and be tested as an anti-malarial agent against *Plasmodium falciparum*.

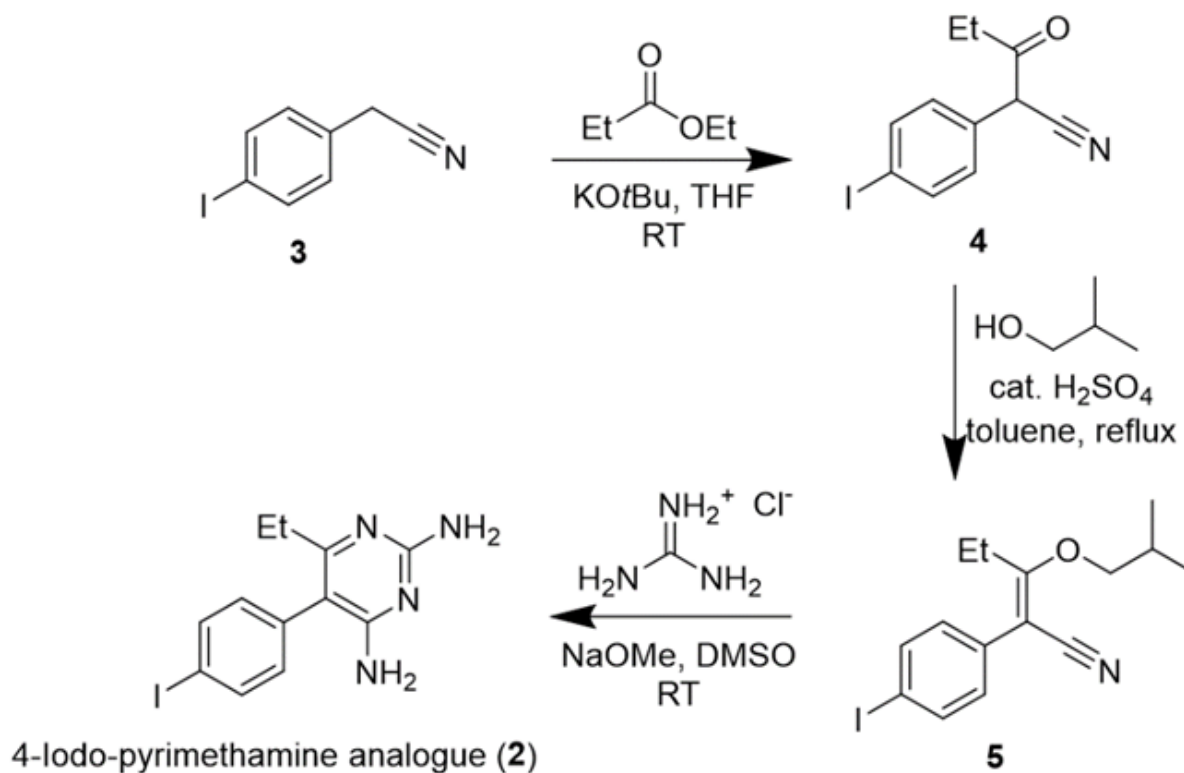


Figure 8: Proposed synthetic pathway for the synthesis of 4-iodopyrimethamine analogue (2)

Methodology

General experiment details

^1H and ^{13}C NMR spectra were recorded at 300 K using a Bruker Avance DRX400 NMR spectrometer. Residual acetone (δ 2.05) and chloroform (δ 7.26) were used as internal reference for ^1H NMR spectra. The data is reported as chemical shift (δH ppm), relative integral, multiplicity (s = singlet, d = doublet, t = triplet, q = quartet, m = multiplet) and assignment. Atom labels on structures are to illustrate ^1H NMR spectral assignments and do not necessarily correspond to the IUPAC names given. The solvent peak for chloroform (δ 77.0) was used as an internal reference for ^{13}C NMR spectra. Mass spectra were recorded by the Mass Spectrometry Unit of the School of Chemistry, The University of Sydney, Sydney. The molecular ion $[\text{M} + \text{H}^+]$ or $[\text{M} - \text{H}^+]$ is listed. Analytical thin layer chromatography was performed with Merck Kieselgel 60 F254 (0.2 mm) pre-coated aluminium sheets, and visualisation was achieved by inspection under UV light. Throughout the reaction process Thin Layer Chromatography (TLC) was conducted to gauge the progress of the reaction and determine the point of completion. TLC analysis was conducted with either 50:50 Dichloromethane (DCM):Hexane, 70:30 ethyl acetate : hexane, or pure ethyl acetate.

Step 1: Synthesis of 2-(4-iodophenyl)-3-oxopentanenitrile

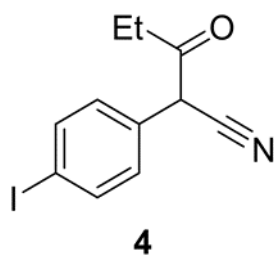


Figure 9: 2-(4-iodophenyl)-3-oxopentanenitrile (4)

4-iodophenylacetonitrile (7.00 g, 0.0462 mol, 1 equiv.), ethyl propionate (4.95 g, 0.0485 mol, 1.05 equiv.) and potassium tert-butoxide (10.4 g, 0.0924 mol, 2 equiv.) were combined in THF (60 mL) at room temperature, with stirring in a round bottom flask. The reaction mixture turned to a dark red and heated up rapidly. When the mixture appeared homogeneous (30 minutes) stirring was turned off. The reaction was sealed and left for 2 hours in a fume hood.

The reaction mixture was worked up by the addition of 1.0 M HCl (100 mL) to the reaction vessel. The acidified reaction mixture was transferred to a separating funnel and the aqueous layer was extracted with DCM (3 x 65 mL). The combined organic layer was washed with brine (100mL), dried with anhydrous sodium sulfate, filtered, and concentrated *in vacuo* to afford 2-(4-iodophenyl)-3-oxopentanenitrile (4) (8.92 g, 0.0298 mol, 65%) as a reddish oil. TLC was conducted with 50:50 DCM : hexane as the eluent. The crude 2-(4-iodophenyl)-3-oxopentanenitrile was used without purification in the second step of the synthesis.

Step 2: Synthesis of 2-(4-iodophenyl)-3-(2-methylpropoxy)-pent-2-enitrile

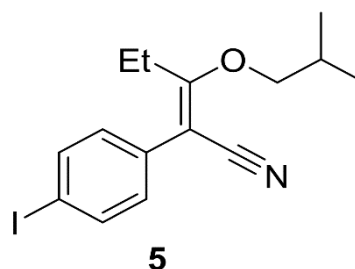


Figure 10: 2-(4-iodophenyl)-3-(2-methylpropoxy)-pent-2-enitrile (5)

2-(4-iodophenyl)-3-oxopentanenitrile (8.92 g, 0.0298 mol) was dissolved in a mixture of toluene (65.0 mL) and 2-methylpropan-1-ol (6.50 mL). 18M H_2SO_4 (1.00 mL) was added and the mixture was refluxed for 10 hours in a Dean Stark apparatus. The reaction mixture was poured onto a saturated sodium hydrogen carbonate in a separating funnel and the aqueous phase was extracted with DCM (3 x 50 mL). The combined organic extracts were dried over anhydrous sodium sulfate.

Addition of 2.5 mL of triethylamine to the reaction mix converted the unreacted starting material to its very polar triethylammonium enolate salt. Chromatography silica (25g) was added to the organic phase, which was made up to 200mL with dichloromethane and stirred for two hours. The organic phase was decanted and rinsed with 1M HCL (2 x 50 mL) and deionised water (50 mL) to remove all traces of triethylamine. The solvent was removed from the organic phase to yield 2-(4-iodophenyl)-3-(2-methylpropoxy)-pent-2-enitrile (6.02g, 0.0170 mol, 57%) as a red oil. This product was used in the next step of synthesis.

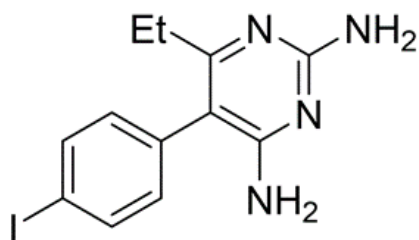
Step 3: Synthesis of 4-iodopyrimethamine analogue

Figure 11: 4-iodopyrimethamine analogue (2)

2-(iodophenyl)-3-(2-methylpropoxy)-pent-2-enitrile (6.02 g, 0.0170 mol) was dissolved in DMSO (45.0 mL). Guanidine hydrochloride (3.20 g, 0.0335 mol) was stirred into the solution followed by sodium methoxide powder (2.00 g, 0.0370 mmol). The solution became dark red in colour on addition of the sodium methoxide, which dissolved into the solution within an hour. No precipitation of sodium chloride was observed. The solution was allowed to stand at room temperature for 48 hours. The reaction mixture was poured onto water and extracted with DCM. The resultant solution was concentrated *in vacuo* to afford a red oily solid. The solid was then dissolved in 100% ethanol and left for 48 hours until crystals of the 4-iodopyrimethamine had formed.

Results

Step 1: Synthesis of 2-(4-iodophenyl)-3-oxopentanenitrile

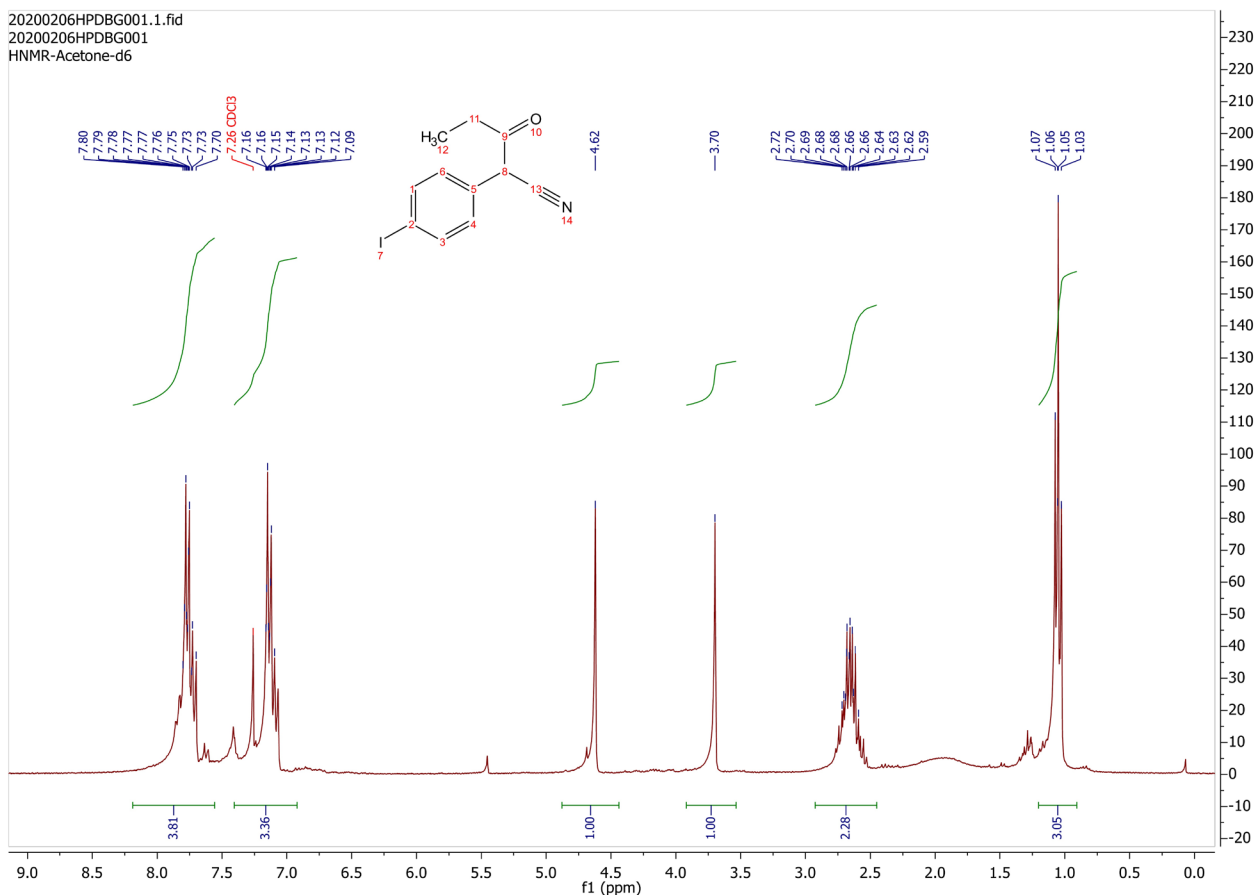


Figure 12: ¹H NMR spectra after step 1

¹H NMR (400MHz, (CD₃)₂CO) δ 7.80-7.70 (2H, m, H1), 7.16-7.09 (2H, m, H2), 4.62 (1H, s, H3), 2.72-2.59 (2H, m, CH₂), 1.05 (3H, t, CH₃); MS (+ESI) [M-H⁺] m/z = 297.46.

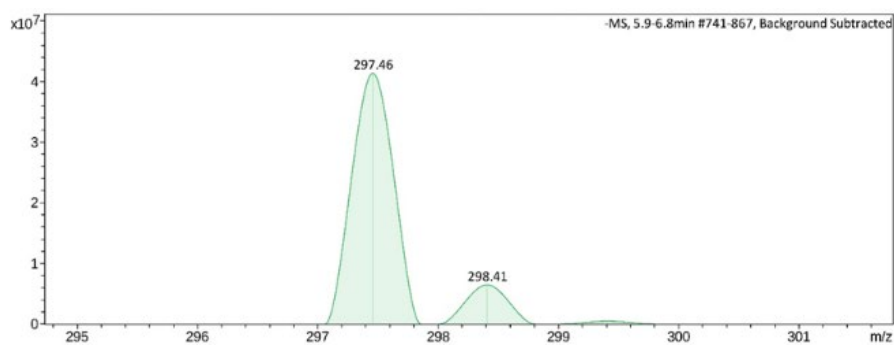


Figure 13: Mass spectra after step 1

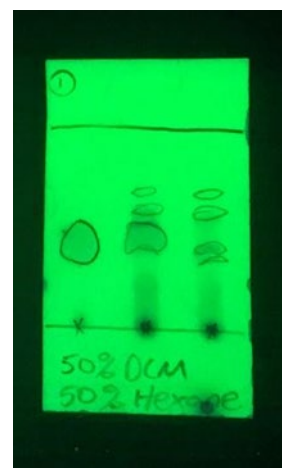


Figure 14: TLC after step 1

Step 2: Synthesis of 2-(4-iodophenyl)-3-(2-methylpropoxy)-pent-2-enitrile

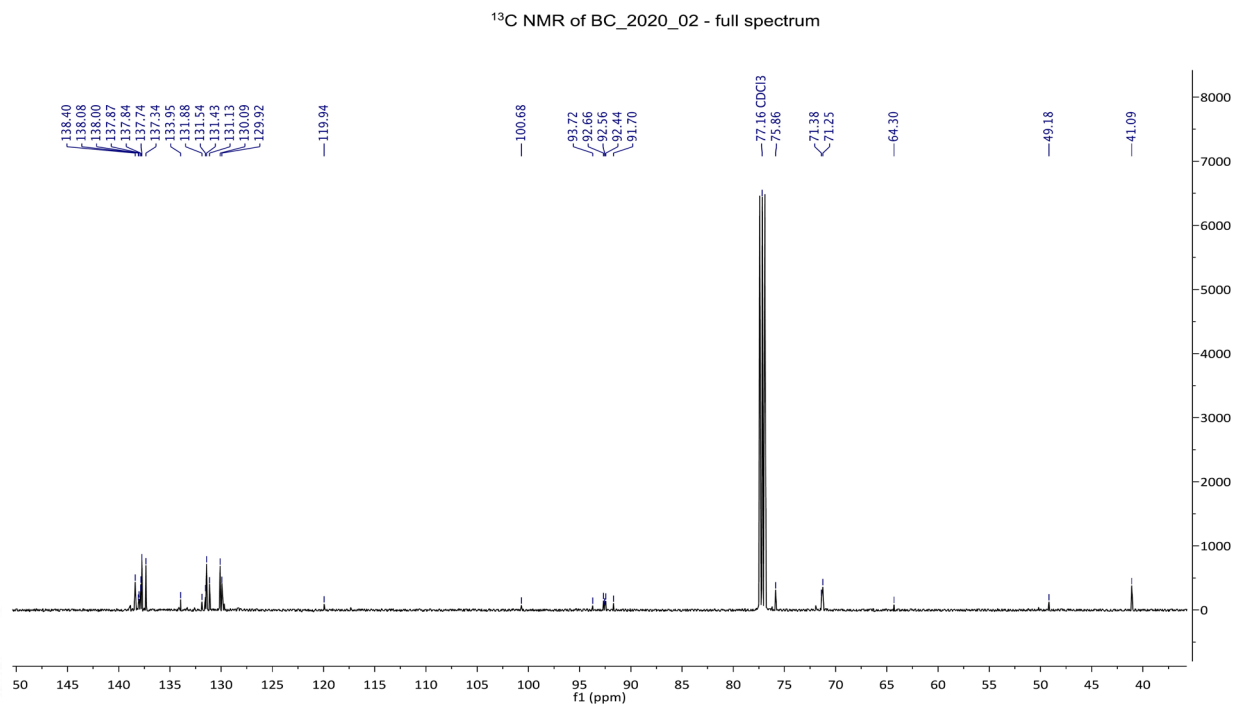


Figure 15: ¹³C NMR spectra after step 2

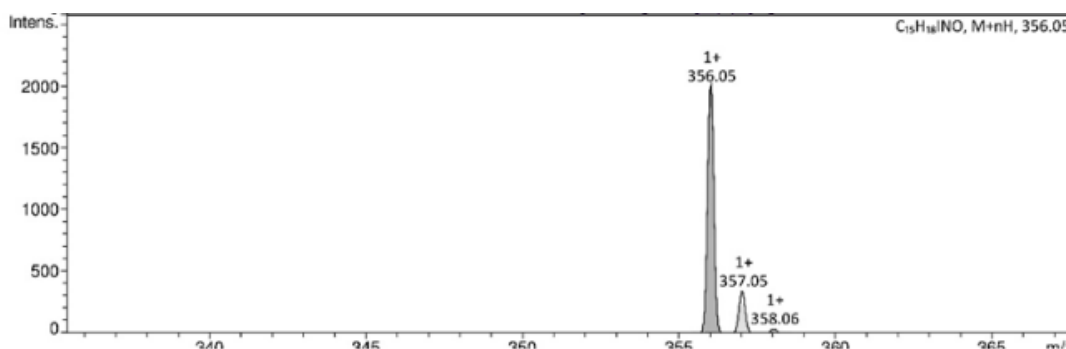


Figure 16: Mass spectra after step

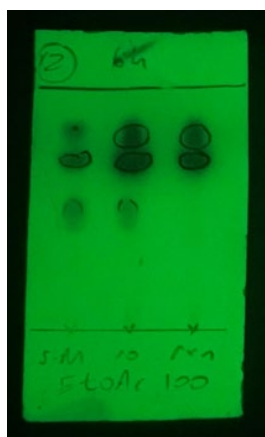


Figure 17: TLC before addition of Et₃N



Figure 18: TLC after addition of Et₃N

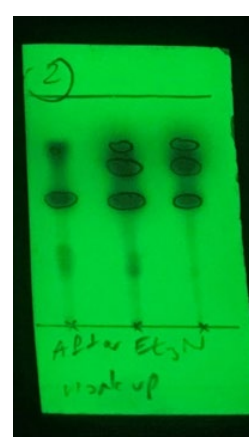
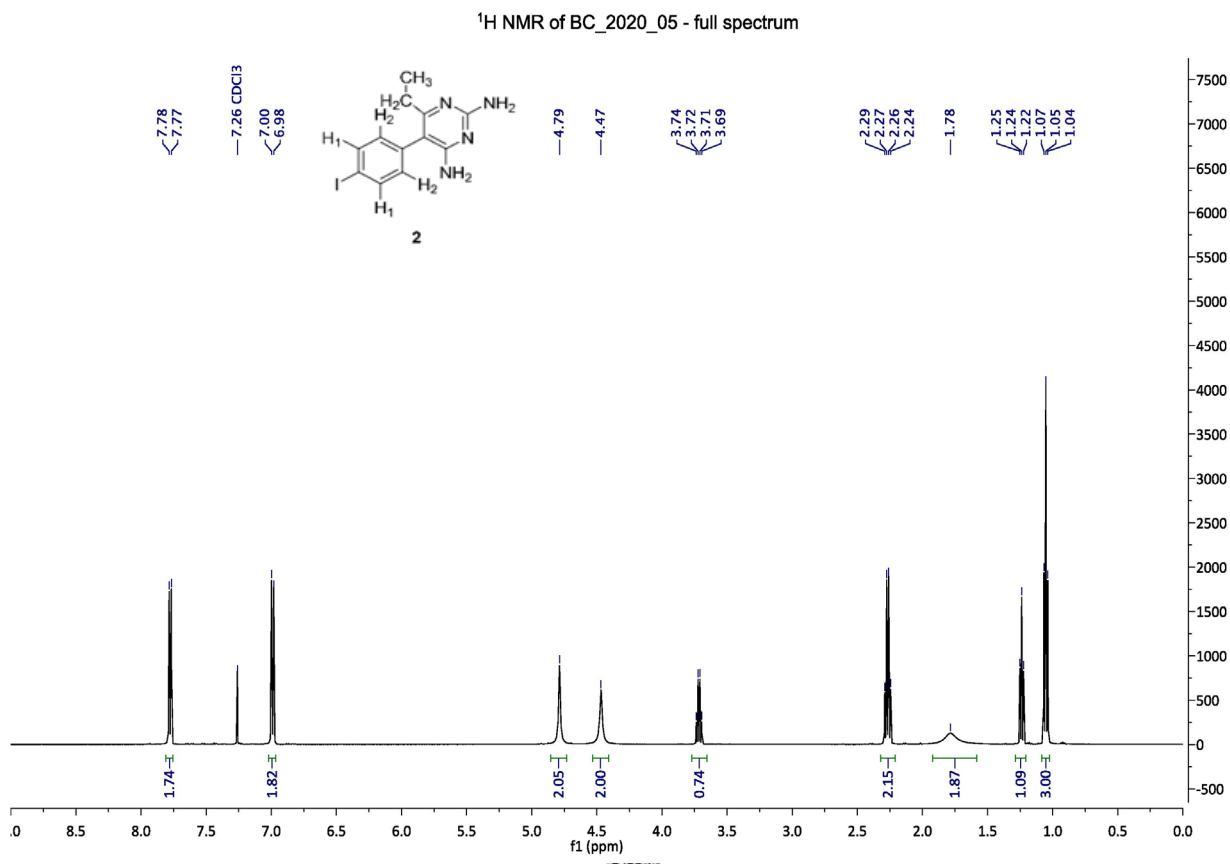


Figure 19: TLC after work up

Step 3: Synthesis of 4-iodopyrimethamine analogue


 Figure 20: ¹H NMR spectra after step 3

¹H NMR (400MHz, (CDCl₃) δ 7.78 (2H, d, **H1**), 6.99 (2H, d, **H2**), 4.79 (2H, br s, **NH₂**), 4.47 (2H, br s, **NH₂**), 2.27 (2H, q, **CH₂**), 1.05 (3H, t, **CH₃**); ¹³C NMR (100.6 MHz, CDCl₃) δ 168.7 (7 C-N), 162.0 (6 + 8 C-N), 138.6 (3 Ar-CH), 135.1 (4 Ar-C), 132.7 (2 Ar-CH), 107.4 (5 Ar-C), 93.7 (1 Ar-C), 28.3 (CH₂), 13.4 (CH₃); MS (+ESI) [M + H⁺] m/z = 341.03.

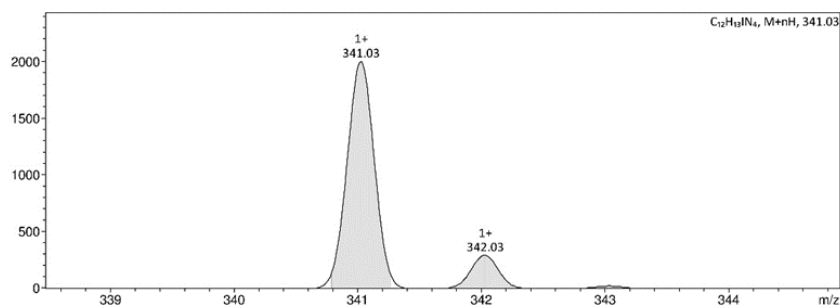


Figure 21: Mass spectra after step 3



Figure 22: TLC after step 3

Discussion

Step 1: Synthesis of 2-(4-iodophenyl)-3-oxopentanenitrile

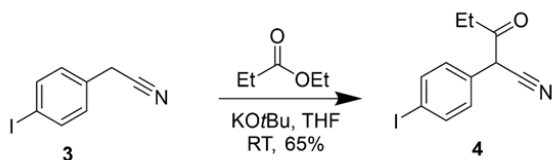


Figure 23: Reaction of 4-iodophenylacetonitrile (3) to form 2-(4-iodophenyl)-3-oxopentanenitrile (4)

Step 1 of the synthesis was performed to afford Compound 4 from a condensation reaction between 4-iodoacetonitrile (3) and ethyl propionate. More specifically, addition of the strong base potassium *tert*-butoxide caused deprotonation at the CH₂ group of Compound 3, and reaction with ethyl propionate led to the elimination of ethanol (Figure 24). The yield obtained for this step was 65%, which was significantly smaller than Sydney Grammar's 90% yield, likely due to a lack of reaction optimisation due to time constraints (SGS 2016). Furthermore, due to the high cost of Compound 3, only 7 grams of this starting compound was available for research. Thus, future trials should optimise reaction conditions such as temperature and reaction times as well as the isolation step to improve the yield and perform a scaled-up synthesis.

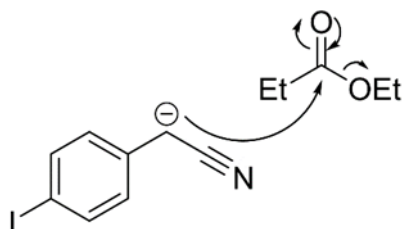


Figure 24: Mechanism of the reaction between 4-iodophenylacetonitrile and ethyl propionate

The appearance of polar baseline material on the TLC (Figure 14) corresponded to the formation of the more polar Compound 4. The ¹H NMR spectrum was very complex, likely due to a combination of enol and keto tautomers in equilibrium. The doublet between 7.80-7.70 ppm was assigned to the H1 aromatic protons and the doublet between 7.16-7.09 ppm was assigned to the H2 aromatic protons. This was as expected since hydrogen atoms on a benzene ring characteristically appear in the 7-8 ppm region. The H3 singlet was assigned to the signal further upfield at 4.62 ppm. This is due to the electron withdrawing nature of the nitrile group and carbon-

oxygen double bond causing a deshielding of the hydrogen atom in this environment. There was an impurity at approximately 3.7 ppm which may have been caused by residual solvent or unreacted starting material. The impurity could not be properly identified as it did not match any of the listed common trace impurities (Gottlieb et al., 1997). The multiplet signal between 2.72-2.59 ppm is indicative of the CH₂ on the ethyl group, which is typically a quartet but may have been complicated due to impurities or the appearance of the enol tautomer. Finally, a characteristic triplet splitting pattern at 1.05 ppm indicated the presence of the CH₃ on the ethyl group. Mass spectroscopy indicated a molecular mass of 297.46, corresponding to [M - H]⁺ for Compound 4. Unfortunately, due to time constraints, no ¹³C NMR was conducted. However, there was enough information provided by both ¹H NMR and mass spectroscopy to confirm the formation of Compound 4.

Step 2: Synthesis of 2-(4-iodophenyl)-3-(2-methylpropoxy)-pent-2-enitrile

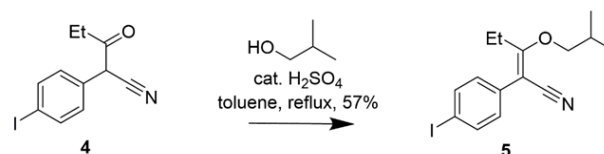


Figure 25: Reaction of 2-(4-iodophenyl)-3-oxopentanenitrile (4) to form 2-(4-iodophenyl)-3-(2-methylpropoxy)-pent-2-enitrile (5)

Step 2 of the synthesis was performed under reflux whereby a substitution reaction led to the formation of Compound 5 from Compound 4. A Dean Stark apparatus was used to remove water and drive the equilibrium reaction in the forward direction.

Initial TLC indicated the presence of some residual starting material (Figure 17). This was to be expected as Sydney Grammar also observed remaining starting material after their Dean-Stark reaction. Upon addition of triethylamine, the remaining starting material was converted to the triethylammonium enolate salt, corresponding to the polar baseline material observed in the second TLC (Figure 18). Addition of silica gel at this stage facilitated the removal of this salt from the reaction mixture. However, the third TLC after work up once again indicated the presence of starting material (Figure 19). This is most likely due to some silica gel appearing in the separating funnel after decantation. Re-protonation of the triethylammonium enolate salt stuck to

the silica gel would have occurred after addition of HCl, reforming the enol tautomer of Compound 4 (Figure 26). Future attempts to repeat this step should incorporate the use of a sintered funnel as an alternative to decanting in order to effectively isolate and remove all of the silica gel. This will improve the purity and yield of the reaction.

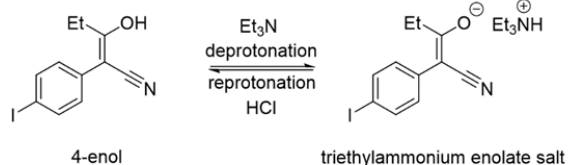


Figure 26: Mechanism of the reaction between 4-iodophenylacetone and ethyl propionate

These impurities led to a complex ^1H NMR that was difficult to analyse. However, new peaks in the ^{13}C NMR between 90-101 ppm provided evidence of the carbon-carbon double bond formed in Compound 5 (Figure 15). Other peaks between 70-80 ppm also indicated the carbon-oxygen bond signal also in Compound 5. More data is needed to confirm the presence of aromatic groups in the region 93.7-137 ppm. Overall, in combination with evidence provided by mass spectroscopy, where signals at 356.05 corresponded to $[\text{M} + \text{H}]^+$, it was confirmed that the desired compound was synthesised (Figure 16).

Step 3: Synthesis of 4-iodopyrimethamine analogue

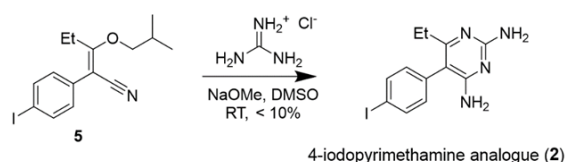


Figure 27: Reaction of 2-(4-iodophenyl)-3-(2-methylpropoxy)pent-2-enitrile (5) to form 4-iodopyrimethamine (2)

Step 3 of synthesis was initiated by the deprotonation of the guanidine ion by sodium methoxide. Following this, guanidine reacted at the nitrile carbon of Compound 5, and subsequent electron rearrangement and the elimination of 2-methylpropanol afforded the pyrimidine ring seen in Compound 2.

The appearance of polar baseline material in the TLC indicated the formation of the pyrimidine rings which contains polar NH_2 groups. In the ^1H NMR spectrum, doublet signals at 7.79 and 6.99 ppm were assigned to aromatic H1 and H2 hydrogen environments. The two characteristic broad singlets at 4.79 and 4.47 ppm were

indicative of the NH_2 groups. Signals at 3.71 and 1.24 ppm were caused by residual EtOH from recrystallisation. The splitting pattern of the quartet at 2.27 ppm was characteristic of the CH_2 from the ethyl group, and the splitting pattern of the triplet at 1.05 ppm was indicative of the CH_3 on the ethyl group (Figure 20). Mass spectroscopy signals at 341.03 also corresponded to $[\text{M} - \text{H}]^+$, therefore confirming the successful synthesis of 4-iodopyrimethamine (2) (Figure 21).

The yield for the third step of this synthesis was very low due to difficulties in precipitating out the desired compound. Compared to Sydney Grammar School's 31% yield and 3.67 grams of pyrimethamine, only a small mass of 4-iodopyrimethamine was able to be crystallised and isolated, despite using the same 100% EtOH solvent (SGS 2016). This is likely because 4-iodopyrimethamine analogue (2) had a higher degree of solubility compared to the original pyrimethamine compound (1). These difficulties contributed to a final mass of 4-iodopyrimethamine that was insufficient to properly conduct biological testing against *P. falciparum*. Reaction yields may have been improved by using vacuum filtration of mixtures to avoid unwanted loss of compound during filtration. Other optimisation will allow for biological testing to be conducted in the future.

Future Research

In addition to its potential as a new and more effective inhibitor of DHFR, the successful synthesis of the novel 4-iodopyrimethamine may have important applications in the development of other analogues. Since the synthetic pathway for preparation of 4-iodopyrimethamine (2) is simpler than the synthesis of other analogues reported in the literature, it could be used as a precursor molecule for cross coupling reactions to synthesise more complex analogues with different substituents at the R4 position (Yuthavong et al., 2004). This is due to iodine's effectiveness in serving as a leaving group in cross-coupling reactions to form a carbon-carbon bond (Biajoli, 2014). Therefore, even if the iodo-analogue itself is not particularly potent against mutant DHFR, it will create opportunities for future research to develop other molecules which may exhibit higher binding affinity and more effective inhibition against mutant DHFR. Future trials could investigate the effect of replacing the iodine atom with long carbon chains or aromatic groups at the R4 position.

Conclusion

The research conducted resulted in a successful synthesis of the novel compound 4-iodopyrimethamine (**2**) via the 2016 synthetic pathway developed by Sydney Grammar School (SGS, 2016). Structural conformation was carried out using mass spectrometry, ¹H NMR and ¹³C NMR to confirm the desired product was synthesised after each step. However, due to time constraints and low product yield, biological testing was unable to be conducted. Yield optimisation and testing of the iodo-analogue against *P. falciparum* could be completed in the future to provide biological data on its efficacy in combating malarial pathogens. The synthesis of the 4-iodopyrimethamine analogue (**2**) also allows for the possibility of investigating cross coupling reactions for the synthesis of a library of R4-substituted analogues and subsequent investigation of their enzyme binding activity.

Acknowledgements

I would like to thank Dr Terrett for her invaluable help and support with all aspects of the project. This research would not have been possible without her deep knowledge and patient explanations of organic chemistry. I would also like to acknowledge the Barker College Science Department for funding the purchase of our starting compound. Thanks also to collaborators of the Breaking Good Project at Sydney University, who kindly ran our samples through their NMR and Mass Spectroscopy machines.

References

- Ashley, E.A., Phyo, A.P. 2018. 'Drugs in Development for Malaria'. *Springer Open Choice*, vol. 78, no. 12, pp. 1-19.
- Biajoli, A. 2014. 'Recent Progress in the Use of Pd-Catalyzed C-C Cross-Coupling Reactions in the Synthesis of Pharmaceutical Compounds'. *Journal of the Brazilian Chemical Society*, vol. 25, no. 12, pp. 1-27.
- Birdsall, B., Tendler, B. and Arnold, P. 1990. 'NMR Studies of Multiple Conformations in Complexes of *Lactobacillus casei* Dihydrofolate Reductase with Analogues of Pyrimethamine'. *Biochemistry*, vol. 29, pp. 9660-9667.
- Boland, P. and World Health Organization. 2001. *Drug resistance in malaria*, Anti-Infective Drug Resistance Surveillance and Containment Team, viewed 25 June 2020, <https://www.who.int/csr/resources/publications/drugresist/malaria.pdf>.
- Endo, N., Yamana, T. and Eltahir, E. 2017. 'Impact of climate change on malaria in Africa'. *The Lancet*, vol. 389, no. 7, pp. 29-32.
- Falco, E., Goodwin, L. and Hitchings, G. 1951. '2: 4-Diaminopyrimidines - A New Series of Antimalarials', *Brit. J. Pharmacol*, vol. 6, pp. 185.
- Gottlieb, H.E., Kotlyar, V. and Nudelman, A. 1997. 'NMR Chemical Shifts of Trace Impurities: Common Laboratory Solvents, Organics, and Gases in Deuterated Solvents Relevant to the Organometallic Chemist'. *J. Org. Chem.* vol. 62.
- Imwong, M., Suwannasain, K. and Kunasol, C. 2017. 'The spread of artemisinin-resistant Plasmodium Falciparum in the greater Mekong subregion: a molecular epidemiology observational study'. *Lancet. Infect.*, vol. 17, pp. 491-491.
- Muiruri, P., Juma, D. and Ingasia, L. 2018. 'Selective sweeps and genetic lineages of Plasmodium falciparum multi-drug resistance (pfmdr1) gene in Kenya'. *Malaria Journal*, vol. 17, pp. 398-399.
- Nattee, C., Toochinda, P. and Lawtrakul, L. 2017. 'A novel prediction approach for antimalarial activities of Trimethoprim, Pyrimethamine, and Cycloguanil analogues using extremely randomized trees'. *Journal of Molecular Graphics and Modelling*, vol. 71, pp. 13-27.
- Oaks, S, Mitchell, V, Pearson, G and Carpenter, C 1991, *Malaria: Obstacles and Opportunities*, The National Academies Press, Washington, DC.
- Okombo, J. and Chibale, K. 2018. 'Recent updates in the discovery and development of novel antimalarial drug candidates'. *Med. Che. Comm.*, vol. 9, pp. 437-453.
- Sydney Grammar School Synthesis (Open Source malaria 2016, *Pyrimethamine Synthesis: Status at the end of 2016*, viewed 20 May 2020, http://malaria.ourexperiment.org/daraprim_synthesis/15813/Pyramethamine_synthesis_Status_at_the_end_of_2016.html.
- Talakpo, J., Skrllec, I. and Alebic, T. 2019. 'Malaria: The Past and the Present'. *Microorganisms*, vol. 7, no. 6, pp. 2-4.
- Tarnchompoo, B., Chitnumsub, P. and Jaruwat, A. 2018. 'Hybrid Inhibitors of Malarial Dihydrofolate Reductase with Dual Binding Modes That Can Forestall Resistance'. *ACS Med. Chem. Lett.*, vol. 9, pp. 1235-1240.
- Tarnchompoo, B., Sirichaiwat, C. & Phupong, W. 2018. 'Development of 2,4-Diaminopyrimidines as Antimalarials Based on Inhibitions of the S108N and C59R+S108N Mutants of Dihydrofolate Reductase from Pyrimethamine-Resistant Plasmodium Falciparum'. *Journal of Medical Chemistry*, vol. 45, pp. 1244-1252.
- Tropak, M., Zhang, J. & Yonekawa, S. 2015. 'Pyrimethamine Derivatives: Insight into Binding Mechanism and Improved Enhancement of Mutant β -N-acetylhexosaminidase Activity'. *Journal of Medical Chemistry*, vol. 58, pp. 4483-4493.
- World Malaria Report 2019*, 2019 World Health Organization, viewed 22 February 2020, <https://www.who.int/malaria/publications/world-malaria-report-2019/report/en/>.

Yuthavong, Y., Quarrell, R., Lowe, G. and Ponsinet, R. 2004. 'Inhibitors of Multiple Mutants of *Plasmodium falciparum* Dihydrofolate Reductase and Their Antimalarial Activities'. *J. Med. Chem.*, vol. 47, no. 3, pp. 673-680.

Storage temperature and its effect on the concentration of Lycopene extracted from tomatoes

Alexander de Montemas

Barker College

Tomatoes are an important dietary source of antioxidants. In particular, tomatoes contain a high concentration of the carotenoid compound, lycopene. Lycopene is a powerful antioxidant which has been the subject of many investigations. This report will describe an investigation into the effect of the storage temperature of tomatoes on the concentration of lycopene which can be extracted. The lycopene was extracted from tomato puree that had been incubated at different temperatures over a 24 hour period, using a solution of BHT:Hexane:Acetone. The lycopene solution was analysed using a PASCO colourimeter and the absorbance values were recorded at 500nm and concentrations calculated thereafter. The results showed no significant change in lycopene concentration as a result of heating however there were complications encountered in the experimental process.

Literature review

Lycopene (1), (Figure 1), ($C_{40}H_{56}$, molecular weight 536.85 g/mol) is a naturally occurring organic compound which gives fruits such as tomatoes and watermelon their bright red pigment. Lycopene is a long chain hydrocarbon molecule containing alternating single and double carbon-carbon bonds, referred to as a conjugated structure. This structural feature is common to all molecules in the carotenoid class of compounds, of which β -carotene is also a member (Figure 1).

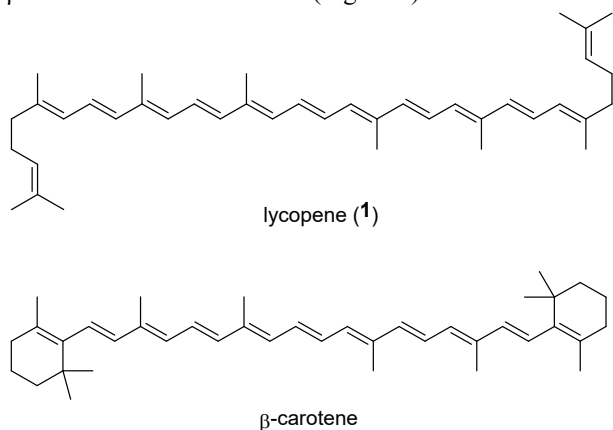


Figure 1: Chemical structures of lycopene (1) and β -carotene.

Lycopene is a potent antioxidant, which means that it has the ability to prevent oxidation from occurring as a result of the presence of free radicals. As defined by Cheeseman (1999), 'A free radical can be defined as any molecular species capable of independent existence that

contains an unpaired electron in an atomic orbital.' As free radicals can either donate or accept an electron, they are both oxidants and reductants, this makes them highly reactive. Free radicals are produced through normal metabolic processes or through external sources such as exposure to UV light, X-rays, cigarette smoke, air pollutants and industrial chemicals. Free radical formation occurs continuously in the cells as a result of both enzymatic and non-enzymatic reactions. Enzymatic reactions, which serve as a source of free radicals, include those involved in the respiratory chain, in phagocytosis and in prostaglandin synthesis (Roberts, 1999). When functioning normally, free radicals can help to fight off pathogens thus aiding in protecting the body from infection. Normally there is a balance in the body between antioxidants and free radicals, however if there is an imbalance in which there are excess free radicals it can cause oxidative stress. This is where the build-up of free radicals starts to react with fatty tissue, DNA, and proteins by causing chain reactions that can damage cells. Studies have shown a link between free radicals and diseases such as atherosclerosis, cancer, inflammatory joint disease, asthma, diabetes, senile dementia and degenerative eye disease (Ashok, 1999).

Normal cells will stop dividing when there is no more need for daughter cells, however cancer cells do not stop dividing as a result of a mutation that inhibits the termination of mitosis. This mutation can occur as a result of excess damage from free radicals. Due to its powerful antioxidant properties, Lycopene can react with

free radicals easily due to its conjugated structure, making it a very powerful antioxidant. Thereby reducing the number of free radicals it will reduce cancers that have formed as a result of radical damage.

Plants naturally produce a trans-isomer lycopene molecule (1), as shown in Figure 1. However, when exposed to light, lycopene will degrade by isomerising into various cis-isomers (Figure 2). These cis-isomers are more unstable than the trans-isomers and the chemical structure will degrade faster once in this structural form. Although cis-lycopene isomers are also potent antioxidants, their instability means that the antioxidant properties of the fruit start to decrease once the trans-lycopene begins to degrade into cis-isomers, making them less effective antioxidants.

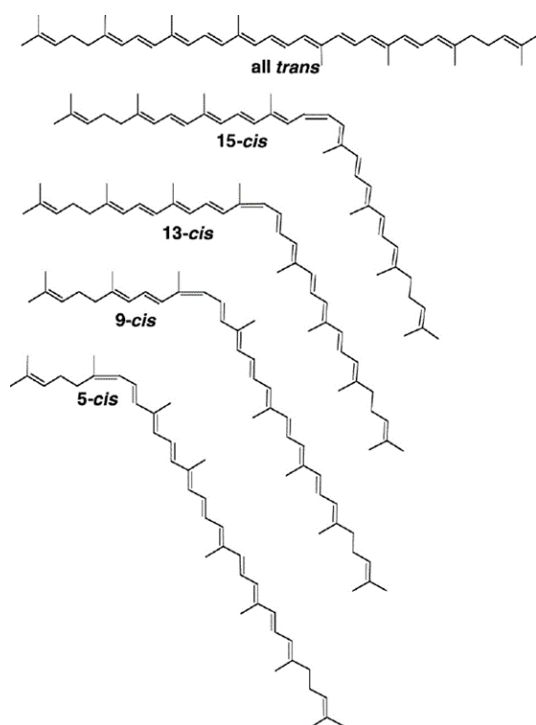


Figure 2: Various cis-isomers of lycopene. Source: Agarwal S (2000)

In western culture, 70% of dietary lycopene comes from tomatoes. Due to this fact and the potential antioxidant benefits that humans can gain from lycopene it is important to understand how to maximise the lycopene concentration in tomatoes before consumption. There have been previous studies reported that show a positive correlation between temperature and pressure and the concentration of lycopene. Studies such as those by M. I. Mohammed (2013).

There are various methods of extracting lycopene. Many of which are time consuming and tedious, this of course

was not possible in a school lab. All of them involve using harmful inorganic compounds to dissolve the lycopene, because lycopene is not soluble in water, hexane has to be used. The method that was chosen uses the lycopene extract in the colourimeter set to 500nm (Anthon & Barrett, 2007).

A colourimeter works by emitting a specific wavelength of light which passes through a solution containing a compound which can absorb the chosen wavelength of light. The sample will absorb a percentage of the light and what remains will be detected on the other side by the detector. According to the Beer Lambert law (Equation 1), the intensity of light absorbed by the sample is proportional to the concentration of the compound absorbing the light. Building on previous research, the optimal wavelength for lycopene to absorb is 503 nm.

$$A = \epsilon \times l \times c$$

(In which A = absorbance, ϵ = molar absorptivity, l = optical path length, c = concentration.)

Equation 1: The Beer Lambert Law

This study aims to investigate the effect of storage temperature in a household setting on the concentration of extracted lycopene, measured using colourimetry. Other reported studies in this area have focused on higher cooking temperatures and the effect of different pressures. To complement the research which has already been undertaken in this area, we will focus on lower temperatures which tomatoes are most likely to be exposed to in the home. Most households in the developed world will have access to freezers and refrigerators, and it is possible that these two different storage options could have an effect on the lycopene concentration in the whole tomatoes. In addition, higher temperatures will also be considered in an attempt to mimic the cooking temperatures that tomatoes may be exposed to. This will shed light on whether cooked tomatoes or uncooked tomatoes may have significant differences in the concentrations of extracted lycopene. There are studies that have shown a significant change in lycopene concentration due to various cooking times (Ajmera, 2006). This is particularly interesting as a simple change in storage temperature could facilitate an increase in lycopene concentration ingested by humans, hence enhancing the benefits we can gain from this powerful antioxidant.

Scientific research question

How does the storage temperature of tomatoes affect the concentration of lycopene extracted from the tissue of the tomato?

Scientific hypothesis

That increasing the storage temperature of the tomato will increase the concentration of lycopene extracted.

Methodology

Preparation of chemicals

A solvent mixture of 2:1:1 Hexane:BHT:acetone was used to extract lycopene from the tomato samples and was prepared as follows:

Butylated hydroxytoluene (BHT) (0.10g, 0.0454mol) was dissolved in absolute ethanol (200ml) and the resulting solution was protected from light. BHT in ethanol (100ml) was combined with acetone (100ml) and hexane (200ml) to produce the required solvent mixture for extraction.

Preparation of Tomatoes

The following procedure was carried out with the lights turned off and the blinds closed.

Procedure 1

5 tomatoes were cut into quarters and randomised. Four slices were taken at random and placed into five different groups corresponding to five different storage temperatures (the groups were: -18°C, 4°C, 25°C, 30°C, 60°C). Each tomato quarter was wrapped in plastic wrap followed by aluminium foil and tomatoes that were submerged in water (30°C and 60°C) were sealed in zip-lock bags. The samples were left to incubate at temperatures for 24 hours.

Procedure 2

6 large (≈100g) tomatoes were blended together in a Nutri-Bullet, until a uniform puree was formed. The tomato puree was divided into five separate 500ml glass Schott bottles, each of which was covered with aluminium foil in order to protect the samples from light. Each bottle was placed at a different temperature and left to incubate in the dark for 24 hours.

Extraction of Lycopene

Tomato puree¹ (0.6g) was weighed into a 20mL volumetric flask on an analytical balance resulting in four flasks per storage temperature. Each flask was filled to the 20mL mark with the hexane:BHT:acetone mixture using a glass pipette. Each flask was shaken and magnetic stirrer bars were added and the mixtures were stirred for 15 minutes. After this time, the flasks were filled to the top with distilled water and stirred for an additional 5 minutes. The flasks were shaken and allowed to stand until two distinct layers were visible.

Colourimetry

A PASCO colourimeter was used alongside SPARKvue data logging software. A sample of the hexane:BHT:acetone solvent mixture was placed into a clean quartz cuvette and used to calibrate the colourimeter at 500nm. The coloured organic layer from each volumetric flask was used to fill a clean and dry quartz cuvette and absorbance at 500 nm was recorded. The absorbance values of the samples were converted into mg/g tissue using the following equation:

$$\begin{aligned} \frac{A_{503}}{\text{kg tissue}} \times \frac{536.9\text{g}}{\text{mole}} \times \frac{1\text{L}}{10^3\text{mL}} \times \frac{10^3\text{mg}}{1\text{g}} \times \frac{10.0\text{mL}}{\text{kg tissue}} \\ = \frac{A_{503} \times 0.0312}{\text{kg tissue}} = \frac{A_{503} \times 31.2}{\text{g tissue}} \\ = \text{mg/g tissue} \end{aligned}$$

Equation 2: converts the raw absorbance values into mg per gram of tomato tissue using values discovered by Fish et al., (2002).

Results

Table 1: Absorbance values for each sample for procedure 1

T (°C)	#1	#2	#3
-18	0.588	0.555	0.535
4	0.435	0.423	0.545
25	0.517	0.560	0.523
30	0.520	0.506	0.506
60	0.486	0.696	0.600

¹ After Preparation procedure 1 was followed, each individual tomato quarter was allowed to warm or cool to room temperature, unwrapped and blended using a stick blender until a uniform puree was obtained.

Table 2: Concentration of lycopene in each sample for experimental procedure 1

T (°C)	Concentration (mg/g)		
	#1	#2	#3
-18	30.578	28.84	27.796
4	22.606	21.919	28.34
25	26.87	29.141	27.196
30	27.023	26.317	26.317
60	25.266	36.184	31.2

Table 3: ANOVA test results for concentrations under procedure 1

T (°C)	Mean (mg/g)	Standard deviation	Standard Error
-18	29.0713	1.4054	0.8114
4	24.2883	3.5256	2.0355
25	27.7357	1.2279	0.7089
30	26.5523	0.4076	0.2353
60	30.8833	5.4659	3.1557

P-value = 0.16472
 F-statistic value = 2.3775

Table 4: Absorbance values for each sample for procedure 2

T (°C)	#1	#2	#3	#4
-18	0.342	0.311	0.351	0.395
4	0.412	0.411	0.375	0.410
25	0.421	0.405	-	0.424
30	0.387	0.394	0.391	0.402
60	0.351	0.320	0.393	0.438

Table 5: Concentration of lycopene in each sample for experimental procedure 2.

T (°C)	Concentration (mg/m)			
	#1	#2	#3	#4
-18	17.3502	15.6756	17.8068	20.6432
4	21.3884	21.5154	19.4676	20.4345
25	21.2200	21.0250	-	21.5804
30	20.0239	19.7316	20.3659	20.7312
60	18.1012	16.5298	20.2003	21.5206

Table 6: Results for ANOVA test for procedure 2

T (°C)	Mean (mg/m)	Standard deviation	Standard Error
-18	17.8689	2.064	1.032
4	20.7015	0.9536	0.4768
25	21.2751	0.2818	0.1627
30	20.2132	0.4318	0.2159
60	19.088	2.2116	1.1058

P-value = 0.05059
 F-statistic value = 3.059952

Discussion

The two different experimental procedures for determining the concentration of lycopene in tomatoes

following incubation at varying temperatures showed quite different results. The first procedure, which involved individual tomato segments being pureed after incubation, indicated that the results were not reliable as the values were inconsistent for each incubation temperature. The standard deviation for the first procedure ranged between 0.4076 and 5.4659. These high values for σ indicate a large spread in the data points.

ANOVA statistical analysis (Table 3), indicated a p-value of 0.16472 for procedure 1. Hence, as $p >$ than the alpha value of 0.05, we cannot reject the null hypothesis (H_0 : That there is no statistically significant difference between the means for each group). This indicates that storage temperature has no significant effect on the concentration of lycopene which can be extracted from the tomatoes. However, we encountered various complications with this following this experimental method. Firstly, pureeing the individual tomato segments was difficult due to the small quantities of tomato. This meant that some of the skin was left intact and not included in the puree mixture. Additionally, the cuvette initially used for colourimetry started to dissolve when this came into contact with the hexane:BHT:acetone mixture. Due to this setback, the tomato puree samples were left at room temperature for about 2 hours while a more appropriate quartz cuvette was located. This could have counteracted any changes that occurred as a result of the storage temperatures alone. Lastly, the outer epidermis of the tomato contains the highest concentration of lycopene (Sakar 2012). The skin of the -18 and 60°C tomato samples were degraded to a much higher extent than the skin of the tomatoes incubated at the other temperatures. This may have made the lycopene more easily extractable when it was being blended, causing the concentration recorded through colourimetry to be inaccurate.

Following the second experimental procedure, the values in the second test were much more reliable as the method for pureeing the tomato sample was more consistent as seen in table 6. The data from the second procedure was more reliable in comparison with the data obtained from the first procedure in Table 3. In this case, the highest standard deviation value was only 2.2116, indicating less variation in the data for each temperature. This increased reliability has most likely come as a result of the change in experimental method, as this methodology provided more consistent puree and immediate analysis of the lycopene after extraction. There are several variables such as ripeness and exposure to light that were not able to be controlled, thus this could have affected the final results. The p-value for the second procedure was

0.05059 and since the p-value > alpha-value the null hypothesis cannot be rejected again in this case.

Although the results indicate that there was no direct correlation between the concentration of lycopene and the temperatures that were used for incubation this does not mean that temperature does not impact the concentration of lycopene in tomatoes. The lack of positive correlation could be attributed to the limited range of incubation temperatures. The aim was to imitate household temperatures and add to the already existing literature in this area, therefore only a few temperatures were considered. Previous studies have used temperatures that are much higher than what was used in this experiment but these temperatures were not practical for this project due to the incubation conditions available in a school laboratory, nor would they be able to be repeated in a domestic setting.

In addition, an additional source of error for this experiment came from using a colourimeter. In the non-polar extraction solution, other carotenoids and pigments such as chlorophyll and β -carotene may have been present. At 500nm these impurities would have absorbed some of the light, as seen in Figure 3.

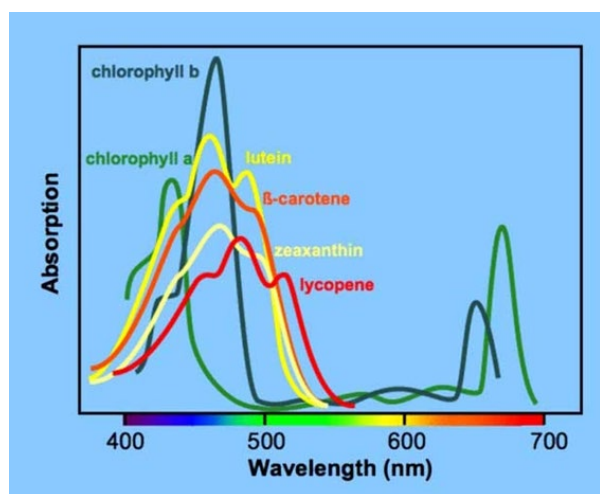


Figure 3: absorbance of pigments in tomatoes.
Source: Jeffery, 2009

The dominant carotenoid present other than lycopene is β -carotene. According to Anthon (2007), published values for the amount of β -carotene in red tomatoes, based on HPLC analysis, vary widely but in most cases are between 5% and 15% of the amount of lycopene (Anthon, 2007). Due to this discrepancy, the results may not be accurate. Further testing would need to be undertaken to determine the concentration of these other carotenoids in the extracted sample for example,

purification prior to colorimetric analysis may assist in this determination.

From the results of this study, there is no ideal temperature at which tomatoes should be stored. Regardless of the incubation temperature, tomatoes still contained comparable amounts of lycopene.

Future work

In order to achieve a definitive answer more research is needed. To add to this study, a greater range of temperatures would need to be analysed in an attempt to more broadly probe whether or not a correlation exists between temperature and lycopene concentration. The incubation time also needs to be taken into account, as this may also have an effect on the lycopene concentration. Furthermore, studies such as Sharma (2008) have shown that the pressure along with temperature has an impact on the concentration. Since the tomatoes are not the only food to contain lycopene studies of how temperature impacts lycopene concentration in other fruits such as water melon will be beneficial. The p-value in the second test was only 0.00059 above the alpha value. This indicates that the experiment was relatively close to being significant. If the second procedure were to be repeated it may produce a significant result.

Conclusion

This report has outlined a method for extracting lycopene from tomatoes stored at different temperatures and the subsequent colorimetric analysis. Concentrations were determined based on the absorbance values obtained. The results have shown that there was no effect on the concentration of lycopene due to a change in temperature in both experiment 1 and 2. Future work will involve investigation a larger range of temperatures as well as other lycopene containing fruits to gain more insight in this area.

Acknowledgements

I would like to thank Dr Terrett for her help and guidance in the preparation and execution of the experiment.

References

- Agarwal, S 2000, Structures of trans and cis isomers, Figure, *Tomato lycopene and its role in human health and chronic diseases*, CMAJ, Florida.
- Ajmera, S 2006, 'The Effects of Different Cooking Times and Temperatures on Tomato Sauce Lycopene Content', *Master of Family Consumer Science*, December, pp. 3-9.

Anthon, G & Barrett, DM 2007, 'Standardization of a Rapid Spectrophotometric Method for Lycopene Analysis', *Department of Food Science and Technology*, pp. 111-119.

Ashok BT, Ali R. The aging paradox: Free radical theory of aging. *Exp Gerontol.* 1999;34:293–303.

Cheeseman KH, Slater TF. An introduction to free radicals chemistry. *Br Med Bull.* 1993;49:481–93

Fish, WW, Perkins-Veazie, P & Collins, JK 2002, 'A Quantitative Assay for Lycopene That Utilizes Reduced Volumes of Organic Solvents', *Journal of Food Composition and Analysis*, vol. 15, pp. 309-316.

Jeffery, SW 2009, Some Spectral Characteristics of Chlorophyll, Graph, *The Biological Bulletin*, The University of Chicago, Chicago.

Mohammed, M & Malami, D 2013, 'Effect of Heat Treatment on the lycopene Content of Tomato Puree', *ChemSearch*, no. 2276 - 707X, June, pp. 18-20.

Roberts LJ, Liu T, Stern A., The isoprostanes: Novel prostaglandin-like products of the free radical catalyzed peroxidation of arachidonic acid. *J Biomed Sci.* 1999;6:226–35

Sakar, S, Chatterjee, S & Medina, N 2012, 'Touring the Tomato: A Suite of Chemistry Laboratory Experiments', *Journal of Chemical Education*, pp. 368-371.

Sharma, R, Pal Singh Oberoi, D & Sogi, D 2008, 'Thermal Degradation Kinetics of Pigments and Visual Colour in Watermelon Juice', *International Journal of Food Properties*, pp. 439-448.

Synthesis of Pyrimethamine and statistical analysis of product formed, assessing reliability of Sydney Grammar’s published Method (2016)

Jasmine Sims

Barker College

Pyrimethamine’s lifesaving qualities makes it an essential drug for the treatment of diseases like malaria and toxoplasmosis. This report outlines the attempted synthesis of pyrimethamine following a three-step process developed by Sydney Grammar School in 2016. The first step of this synthesis was successfully achieved to produce 2-(4-chlorophenyl)-3-oxopentanenitrile, attesting to the reliability of this synthetic step and the simplistic nature of the synthesis of this drug.

Literature review

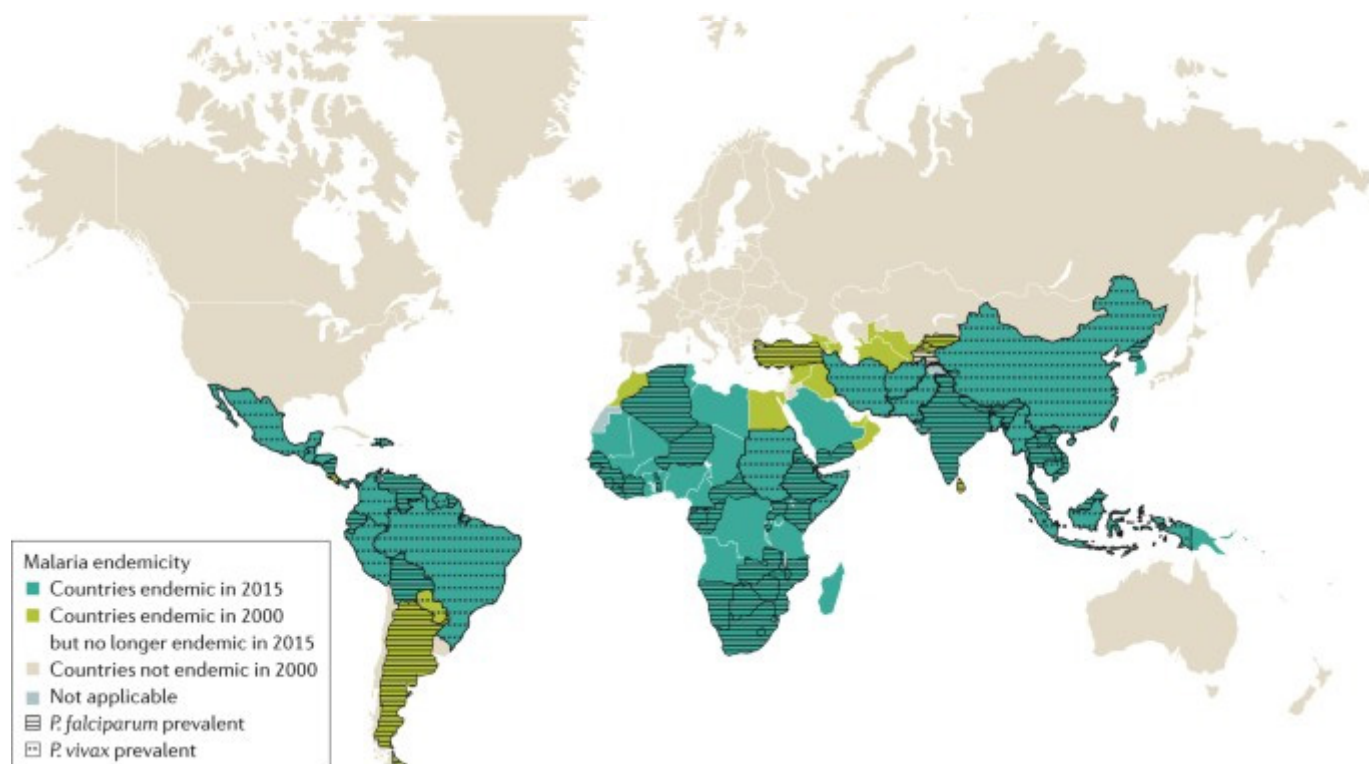
Malaria

Malaria is an infectious disease caused by five different species of *plasmodium*, predominantly *plasmodium falciparum*. Malaria is a disease transmitted between people through a female mosquito vector.

Initial symptoms of malaria can present with varying severity in people, labelled as uncomplicated or severe. Uncomplicated symptoms can be as simple as a fever, aches and chills, while in more severe cases malaria can be a life-threatening disease as once *P. falciparum* invades the red blood cells the disease can cause severe

humans. Although Malaria is deadly, it is a treatable disease with the use of treatment drugs.

Malaria caused by *P. falciparum* is highly prevalent in third world countries (Figure 1). Figure 1 indicates that the majority of cases are in Africa, Asia and South America. *Plasmodium falciparum* is found predominantly in tropical areas as the gametocytes require 10-18 days at temperatures above 21 degrees Celsius to mature into the infectious plasmodium (Muiruri, 2018). As a result, malaria is the leading cause of death in third world countries, killing more than 3,000 African children below the age of 5 every day (Boland, 2001). According to the World Health Organisation



countries – 10 in Sub-Saharan Africa plus India – accounted for around 70% of malaria cases and deaths globally. In 2018 there were an estimated 228 million cases of malaria, accompanied by approximately 405,000 deaths, whereby children under the age of 5 accounted for 67% of these deaths. Malaria's fast paced global infection highlights a prevalent need for effective and affordable treatments, accessible worldwide and in particular, in third world countries (Boland, 2001).

Treatment for malaria varies depending on which plasmodium has caused the disease. For *P. falciparum*, the most likely candidate, successful treatments include the use of quinine analogues like Chloroquine and Quinine sulphate (Nattee, 2016). However, one drug that has been particularly successful in the past has been Pyrimethamine.

Pyrimethamine (Daraprim)

Previously, an effective treatment for *P. falciparum* malaria has been the drug Pyrimethamine (Figure 2). This anti-malarial drug, sold under the brand name Daraprim, was first synthesised in 1951 and was successfully used to treat *P. falciparum* malaria up until recently where the drug was no longer effective in treating drug resistant strains of *P. falciparum* (Nattee, 2016). Pyrimethamine is also used to treat many other diseases caused by parasitic infections such as Toxoplasmosis and Cytoisporiasis. In addition, it has also been successfully used as a second line treatment for both pneumonia and HIV. Given the usefulness of this drug for the treatment of not just malaria but several other diseases, both its accessibility and price have become an important focus in recent years.

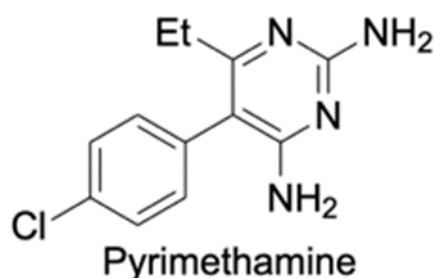


Figure 2. Chemical structure of pyrimethamine (Daraprim).

Inaccessibility of the drug

With the importance of pyrimethamine in the treatment of various parasitic diseases and as a gateway into the development of potential lifesaving drug analogues for the treatment of malaria, accessibility of the drug is highly important for those who need it world-wide. In

2015, the CEO of Turing Pharmaceuticals, Martin Shkreli, purchased the pyrimethamine drug patent, from CorePharma. Impax Laboratorie, and significantly increased the commercial sale price (Pollark, 2015).

At this time, pyrimethamine increased in price from \$13.50 per pill to \$750 (Pollark, 2015). Although Shkreli is no longer the CEO of this company, the price still remains at over \$750 per pill. Drug prices are "easy to raise and harder to lower, particularly if there's no competition," says Nicholson Price, an assistant professor at the University of Michigan Law School (Luthra, 2020). With the proven ability of this drug to help millions of people world-wide these pharmaceutical company business pricing strategies are problematic, as the majority of people affected by such diseases are in developing third world countries and are not able to afford this.

As well as this, the absurd price is stunting the amount of research that can and should be done on the development of analogues that have potential to be highly effective in treating previously drug resistant strains of malaria.

The Breaking Good Project

The Breaking Good project is a project led by Associate Professor Alice Motion at the University of Sydney where high school students have the opportunity to contribute to real drug development research in an effort to try and bring to light common issues regarding drug pricing where the cost does not reflect the effort associated with the drug synthesis.

In 2016 as part of the Breaking Good project, students at Sydney Grammar School were successful in synthesising pyrimethamine in their school lab on a large scale (10 g), very clearly highlighting that the high cost of this drug is unethical and unnecessary. They developed a new synthesis of pyrimethamine, using cheap, easily accessible starting materials which are safe for high school chemistry students to use (Sydney Grammar School, 2016).

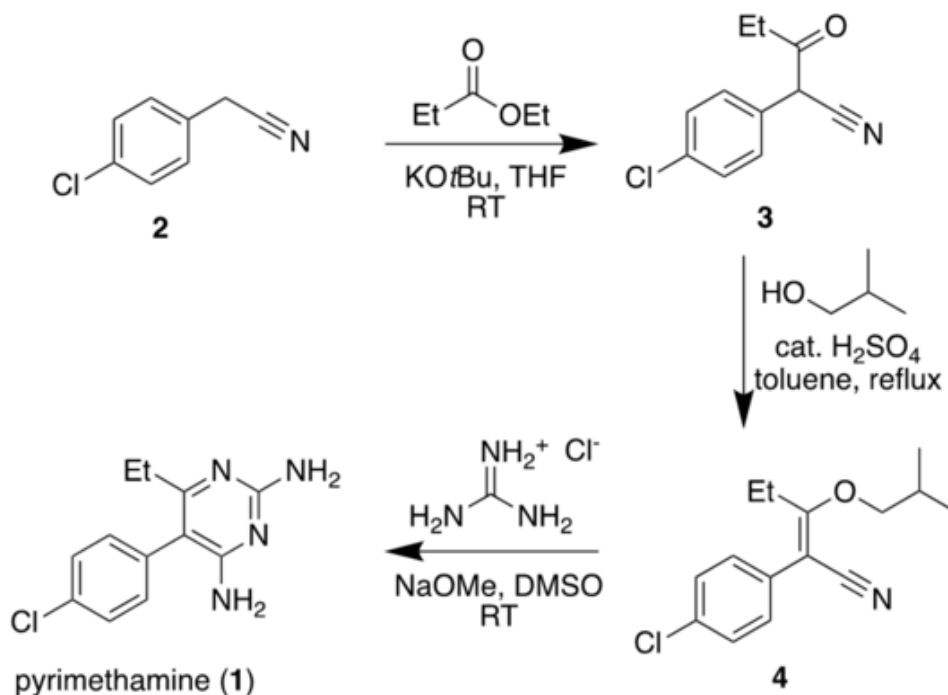


Figure 3. Three step synthesis used by Sydney Grammar (2016).

As this synthesis was only carried out once and in only one school lab, my project will focus on testing the reliability of this synthetic procedure by following the method used by Sydney Grammar. In doing this, we aim to reproduce their synthetic procedure and compare the yield obtained for each step. This will allow us to probe the strength of each step of this procedure in a different school laboratory setting to make conclusions about the usefulness of this synthesis in a broader context.

The procedure that Sydney Grammar has published to be a three-step synthesis seen in figure 3 is exactly as published in order to create a controlled replicate of their synthetic pathway and test reliability.

Scientific research question

Will following Sydney Grammar School's method for the synthesis of pyrimethamine be reproducible with a comparable yield in a different school laboratory setting?

Scientific hypothesis

That pyrimethamine can be synthesised with a comparable yield at Barker College following the Sydney Grammar School method.

Methodology

General experimental details

^1H NMR spectra was recorded at 300 K using a Bruker Avance DRX400 NMR spectrometer. Residual chloroform (δ 7.26) was used as an internal reference for ^1H NMR spectra. The data is reported as chemical shift (δ ppm), relative integral, multiplicity (s = singlet, d = doublet, t = triplet, q = quartet, m = multiplet), coupling constant (J Hz), and assignment. Atom labels on structures are to illustrate ^1H NMR spectral assignments and do not necessarily correspond to the IUPAC names given.

Mass spectra were recorded by the Mass Analysis Facility at the School of Chemistry, The University of Sydney. Mass data is reported for the molecular ion.

Experimental Procedure for the synthesis of 2-(4-chlorophenyl)-3-oxopentanenitrile (3):

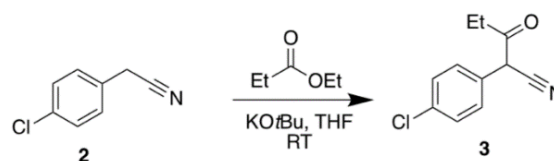


Figure 4: First step synthetic pathway

4-chlorophenylacetonitrile (8g, 1.03 mmol, 1 equiv.), ethyl propionate (80ml, 0.876mmol, 1.1 equiv.) and potassium tert-butoxide (12.44g, 2.58 mmol, 2.5 equiv.) were combined in THF (80 mL) at room temperature, with stirring in a round bottom flask. The reaction mixture turned to a dark red and heated up rapidly. When the mixture appeared homogenous (30 minutes) stirring was turned off. The reaction was sealed and left for 5 hours in a fume hood.

The reaction mixture was worked up by the addition of 1.0 M HCl (15 mL) to the reaction vessel. The acidified reaction mixture was transferred to a separating funnel and the aqueous layer was extracted with DCM (3 x 20 mL). The combined organic layer was washed with brine and dried with anhydrous sodium sulfate, filtered and concentrated *in vacuo* to afford a red oil. TLC analysis was conducted with 10:1 hexane: DCM as the eluent. TLC analysis indicated that the majority of the starting material had reacted.

Results

NMR analysis of the crude sample of compound **3** was undertaken with ^1H NMR and ^{13}C NMR to confirm the chemical structure as well as information regarding the sample's purity.

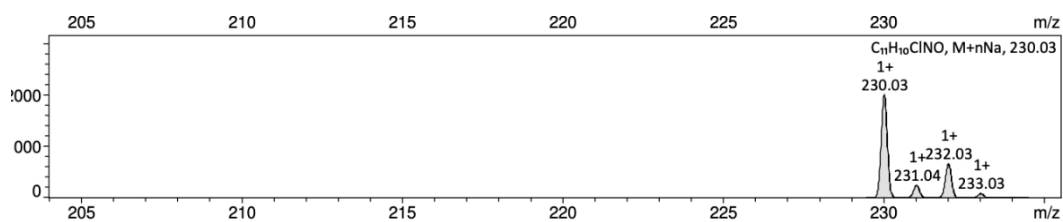


Figure 5. molecular ion plus sodium

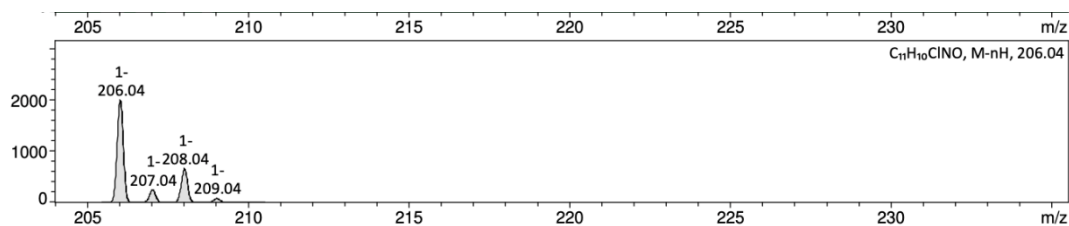


Figure 6. molecular ion minus hydrogen

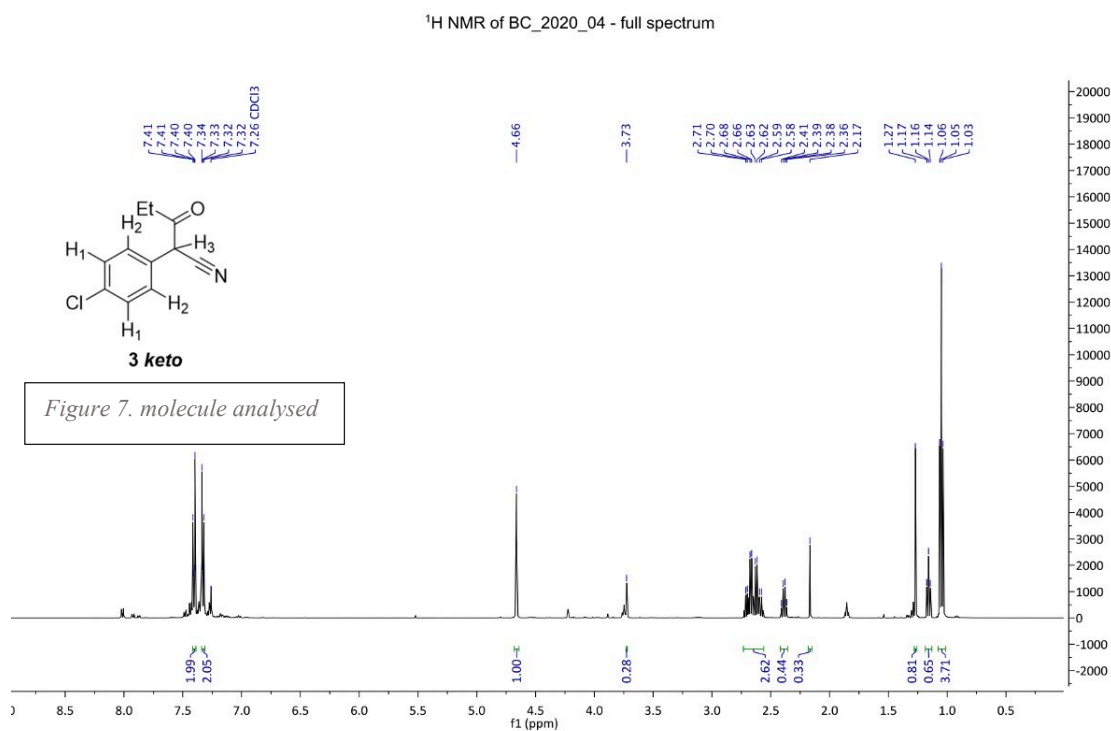


Figure 8. ¹H NMR Spectra (Barker College step one)

¹H NMR (400 MHz, CDCl₃) d 7.41 (2H, d, H₁), 7.32 (2H, d, H₂), 4.66 (1H, s, H₃), 2.71-2.58 (2H, m, CH₂), 1.05 (3H, t, CH₃);

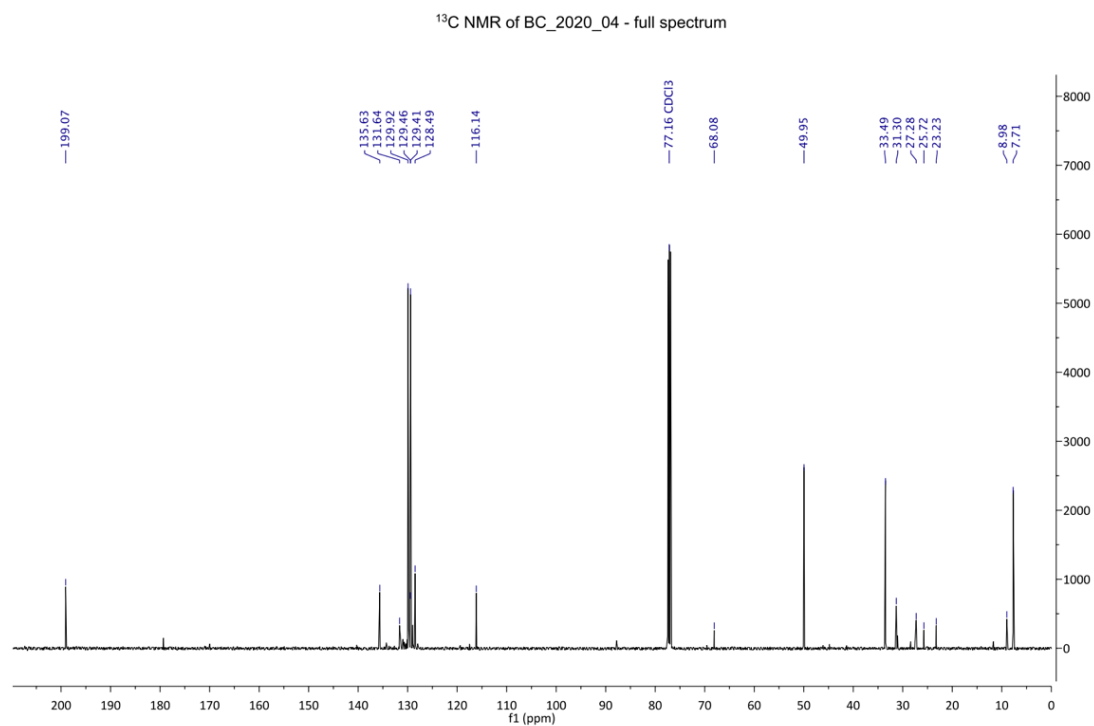


Figure 9. ¹³C NMR spectra (Barker College step 1)

¹³C NMR (100.6 MHz, CDCl₃) d 199.1 (C=O), 135.6 (C), 129.9 (CH), 129.4 (CH), 128.5 (C), 116.1 (C), 50.0 (CH), 33.5 (CH₂), 7.71 (CH₃); MS (+ESI) [M + Na⁺] m/z = 230.03.

Discussion

The synthesis of 2-(4-chlorophenyl)-3-oxopentanenitrile was undertaken following the first step in the synthesis of pyrimethamine reported by Sydney Grammar School seen in figure 4. Limiting factors such as time constraints and access to analytical services meant only the first step of the synthesis was completed. It was concluded by both ^1H NMR and ^{13}C NMR Mass spectrometry that the desired product was synthesised.

NMR Analysis

The successful synthesis of 2-(4-chlorophenyl)-3-oxopentanenitrile (**3**) (Figure 7) is shown through the comparison of both ^1H NMR and ^{13}C NMR spectra in Figures 8-9. The peaks in both spectra are very similar indicating the presence of the compound 2-(4-chlorophenyl)-3-oxopentanenitrile (**3**).

Closer analysis of the ^1H NMR spectra (Figure 8) indicates that the signal at 7.41ppm can be attributed to H1 chemical environment seen in Figure 8. The H2 chemical environment can be attributed to the signal at 7.32ppm. Between the range of 7.0 – 8.0ppm, signals belonging to aromatic hydrogen environments are generally found, which matches out assignment of H1 and H2. The signal at 4.66ppm belongs to the H3 environment. As well as this seen in the ^{13}C NMR figure 9 signals at 1.05ppm depicts the CH3 part of the ethy group and at 2.71ppm shows the CH2 area. With all of these present in the ^1H NMR and ^{13}C NMR spectrums, it confirms the production of 2-(4-chlorophenyl)-3-oxopentanenitrile (**3**).

While the ^1H NMR data shows a few impurities, it is evidently very similar to that of Sydney Grammar proving the reliability of their method. Impurities are seen at 3.76 and 1.85ppm indicating residue of solvent THF and at 1.27ppm there is *tert* butanol. These impurities are due to the lack of high vacuum apparatus in the Barker College school laboratory, meaning that there was some residual solvent remaining before NMR analysis. Additionally, although not observed in the Sydney Grammar ^1H NMR spectrum, the presence of both the 3 keto and 3 enol tautomers could have accounted for some of the additional complexity seen in the ^1H NMR spectrum, this equilibrium can be seen in figure 10. This may have arisen due to different temperatures of slight variations in the NMR solvent used to dissolve the sample.

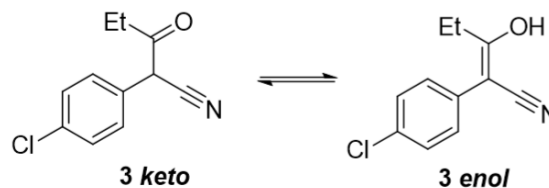


Figure 10: equilibrium between the two tautomers of compound 3

Through a comparison of Barker College labs NMR data with the analysed NMR sample data from step one of Sydney Grammars synthesis in figure 11 and 12, allows conclusion that step one was successful in synthesis of 2-(4-chlorophenyl)-3-oxopentanenitrile.

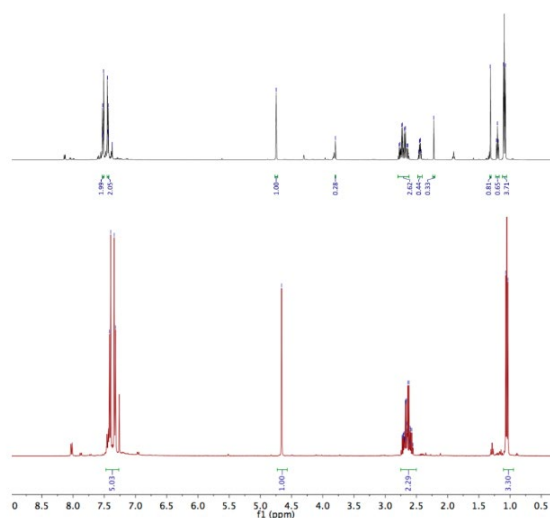


Figure 11. comparison of ^1H NMR

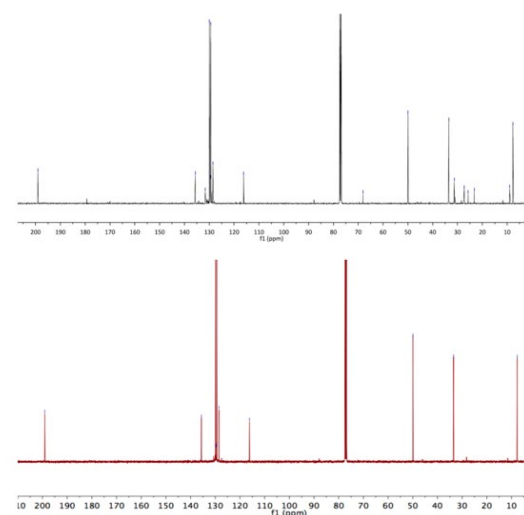


Figure 12. Comparison of ^{13}C NMR

Both of the spectrums represent that 2-(4-chlorophenyl)-3-oxopentanenitrile (**3**) was formed as

peaks align exactly with the samples from step one synthesised by Sydney Grammar. In figure 11 (^1H NMR) the Hydrogen presence at similar locations (matching peaks) and within figure 12 (^{13}C NMR) the similarity of peaks indicates the same ethyl groups.

Further proof of production of 2-(4-chlorophenyl)-3-oxopentanenitrile (**3**) is from the Mass spectrometry data (Figures 7 and 8). A molecular ion plus sodium peak was detected confirming the identity of the product synthesised ($207 + 23 = 230$).

The yield of product synthesised in the Barker College lab was 98% while the yield at Sydney Grammar lab was 90%. Indicating that both first step synthesis in producing pyrimethamine are successful and reliable.

Limiting factors

The completion of all three steps for the synthesis of Pyrimethamine was hindered by a range of factors, such as limited access to analytical technology. This meant that the ending compound was not completely pure. As well as this time pressure from stay at home order meant that less access time to the laboratory was available to complete further steps 2 and 3 fully completing the synthesis of pyrimethamine.

Future research

As the successful yield of product formed from completing step one of synthesis the continuation of steps two and three could have been completed. In the future additional steps of completion and assessing the yield and NMR results would denote a more accurate representation of the Sydney Grammar method for synthesising the completed drug Pyrimethamine.

From shedding light on the success of this simple method, it could help achieve a wider availability of the drug not only for treating diseases, but for more laboratory study into effective analogues of Pyrimethamine that could make life saving strides in treating malaria.

Conclusion

The completion of the first step in the synthesis of pyrimethamine was successful in producing 2-(4-chlorophenyl)-3-oxopentanenitrile. The process was confirmed to have a yield of 98% and the compound was analysed through both ^1H NMR and ^{13}C NMR confirming that the step was successful.

The presence of the desired compound after the first step of the synthesis of Pyrimethamine relates to the hypothesis that pyrimethamine could be synthesised with a comparable yield of 98% at Barker College and 90% at Sydney Grammar, following the Sydney Grammar School's published method. However, the reliability of Sydney Grammar's method can only be derived from the yield determined from the first step 2-(4-chlorophenyl)-3-oxopentanenitrile. As the first step for synthesis of pyrimethamine and compound was made in high yield and achieved in two school laboratories both Sydney Grammar and Barker College, by high school students it can attest to the simplicity of producing the drug and successfully denotes the absurd price and inaccessibility of the drug.

Acknowledgement

I would like to thank Dr Terrett for her valuable chemistry knowledge and input throughout my entire project as well as her guidance through the synthesis and preparation of chemistry equipment.

References

- Ashley, E. (2018). *Drugs in Development for Malaria*. Yangon, Myanmar: Nuffield Department of Medicine.
- Boland, P. (2001). *Drug resistance in malaria*. USA: World health organisation.
- Daraprim Synthesis. (2016). Sydney: Sydney Grammar school. [Accessed 1 May. 2020].
- Dunlop, G., 2016. Martin Shkreli: Australian boys recreate life-saving drug. *BBC news*, [online] Available at: <<https://www.bbc.com/news/world-australia-38153254>> [Accessed 11 May 2020].
- ed, J. (2004). *Target Guided Synthesis of 5-Benzyl-2,4-diaminopyrimidines: Their Antimalarial Activities and Binding Affinities to Wild Type and Mutant Dihydrofolate Reductases from Plasmodium falciparum*. Sydney: Sydney University.
- Luthra, S. (2020). *Martin Shkreli is in prison, but pyrimethamine's price is still high*. [online] Pharmacist.com. Available at: <https://www.pharmacist.com/article/martin-shkreli-prison-pyrimethamines-price-still-high>.
- Muiruri, P, Juma, D & Ingasia, L 2018, 'Selective sweeps and genetic lineages of Plasmodium falciparum multi-drug resistance (pfdmr1) gene in Kenya', *Malaria Journal*, vol. 17, p. 398.
- Natee, C. (2016). *A novel prediction approach for antimalarial activities of Trimethoprim, Pyrimethamine, and Cycloguanil analogues using extremely randomized trees*. Thailand: Sirindhorn International Institute of Technology, Thammasat University, Thailand.

Okombo, J, Chibale K. Recent updates in the discovery and development of novel antimalarial drug candidates. *Med. Che. Ccomm.* 2018, 9, 437-453.

Phillips, M. (2017). *Malaria*. Texas: Nature reviews, Department of biochemistry, university of Texas.

Pollark, A., 2015. Drug Goes From \$13.50 a Tablet to \$750, Overnight. *New York Times*, [online] Available at: <https://www.nytimes.com/2015/09/21/business/a-huge-overnight-increase-in-a-drugs-price-raises-protests.html>.

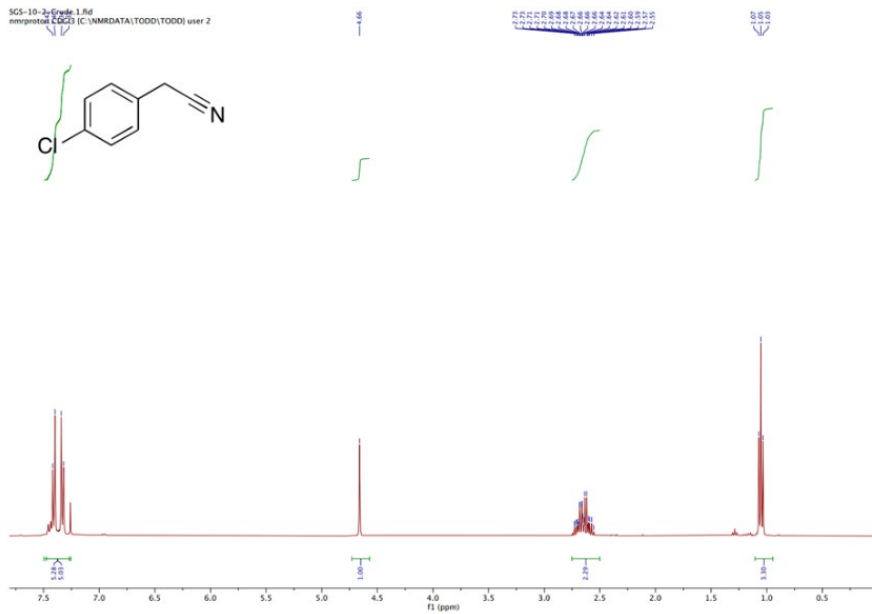
Unknown author, World Health Organisation 2018, *World Malaria Report 2018*,

<<https://www.who.int/malaria/publications/world-malaria-report-2018/report/en/>>. [Accessed 10 May. 2020].

Weiss, D. (2019). *Mapping the global prevalence, incidence, and mortality of Plasmodium falciparum, 2000–17: a spatial and temporal modelling study*. UK: Health Information and Discovery, University of Oxford, Oxford, UK.

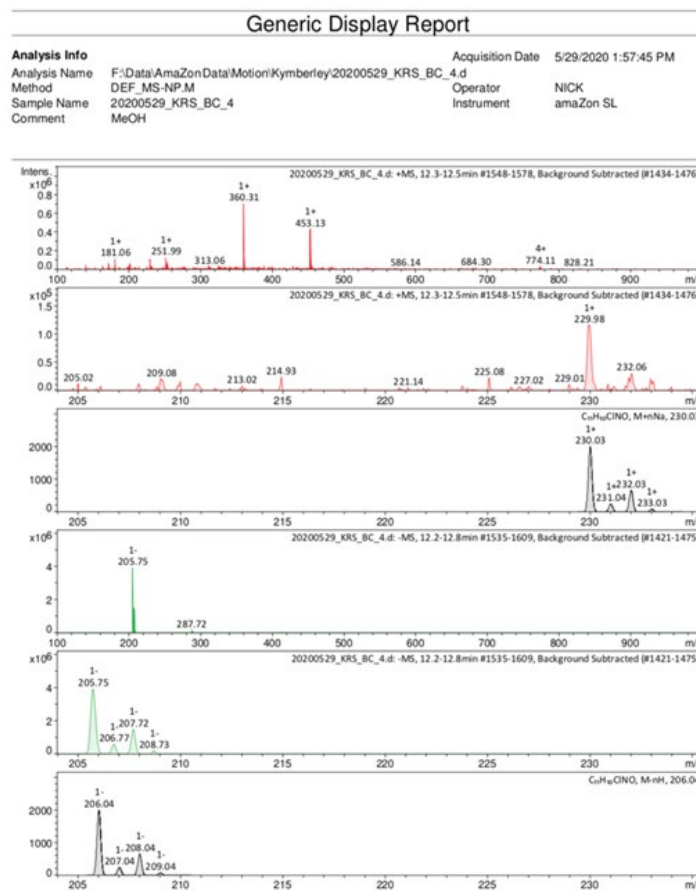
Appendix 1

¹H NMR Spectra (Sydney Grammar step one)



Appendix 2

Generic display report of 2-(4-chlorophenyl)-3-oxopentanenitrile (3)





Biology & Environmental Science

Biology is the study of living things, astounding in the breadth of opportunities it offers for student investigation. From human biomechanics to agricultural production, our students have explored questions from across the spectrum of the discipline.

We are tremendously proud of the efforts of our students that undertook research in the domains of Biology and Environmental Science. Yana's project on the relative abundance of microplastics in the digestive tract of imported Vietnamese prawns and Australian farmed prawns was both topical and informative and we feel certain that it will be a springboard for future projects. Likewise, Jacob's work on microplastics in the water and beaches of Lizard Island was fascinating. We were particularly thrilled to see Jacob obtain permission to collect data on the Barker Lizard Island trip and then to use these samples for his research. Cormac's work on the antimicrobial properties of manuka honey was a really well conceived project that presented an opportunity to interrogate the claims about the superiority of manuka honey. In undertaking his research, Cormac developed laboratory skills not often used in the traditional school laboratory.

Jed's work on cyanobacteria was unfortunately interrupted by the shutdown of our laboratories. Prior to this, Jed had managed to successfully culture the notoriously tricky *Anabaena* which was a triumph in its own right. He was then able to shift his research to consider the impact of salinity and temperature fluctuations on the stress responses of the *Anabaena*. It was very exciting to watch Laura Redman build on the work of a previous Barker student and explore the potential for *Casuarina* xylem to successfully filter *E. Coli* from a water sample. Laura's report demonstrated the significance of her findings for water security in developing countries.

In our second year of teaching Science Extension we have been carefully diversifying the equipment in our laboratories to support students to undertake research projects of considerable breadth and depth. We commend these students for their efforts, and their work to your reading.

Escherichia Coli Filtration using Casuarina Xylem: The potential of Casuarina species to filter E. coli from water

Laura Redman

Barker College

This report investigates the efficacy of using the vascular structures of *Casuarina* as a method of filtration of biological contaminants from water. A filter was constructed using stem cuttings from *Casuarina cunninghamiana* and *Casuarina glauca* specimens. A fixed volume of nutrient broth containing *E. coli* (K-12) was passed through each filter and the resulting filtrate was inoculated on a Petrifilm plate and incubated at 37.5 degrees for 24 hours. The Petrifilm was then photographed and the number of coliform forming units (CFUs) was counted to determine the efficacy of the filter. The results demonstrated that both species used were significantly effective at removing *E. coli*. This is an important indicator for the potential of using angiosperms as biological filters and presents potential opportunities for real world application.

Literature review

Casuarina is a genus of Australian angiosperms that is quite unique. It is from the *Casuarinaceae* family, which is comprised of over 90 species and are either dioecious or monoecious trees or shrubs (Wilson, 1989). *Casuarina* have clustered roots and nitrogen fixing bacteria called *Frankia sp* in their root nodules, providing them with helpful adaptations to infertile soils, especially those low in nutrients like phosphorus and nitrogen (Dörken, 2017).

Gymnosperms are plants that reproduce via exposed seeds, often on cone like leaves whereas angiosperms have seeds that are enclosed in mature ovaries, often forming fruits (Gerald, 2015). The angiosperm, *Casuarina cunninghamiana* is a river she-oak native to Australia, with applications primarily in agroforestry and use as fodder. Its growth rate is around 10 cm per month (Orwa, 2009) meaning it is a plentiful and easily replaceable resource. The family *Casuarinaceae*, 'is unique amongst the angiosperms and is assigned to an order of its own, the *Casuarinales*' (Beadle, 1981). *Casuarina glauca* is a close relation to *Casuarina cunninghamiana*. The slight differences between the two include *Casuarina glauca* having slightly larger cones and more leaf-teeth (12-16) as well as generally more subglaucous colored and coarser foliage (Castle, 2008).

Casuarina is, 'native to the Andaman Islands (India) and seacoasts from southern Bangladesh, Myanmar (formerly Burma), Thailand, and Malaysia to subtropical Australia, Melanesia, Micronesia, the Philippines and Polynesia'

(Parotta, 1993). Beyond that, the genus has been introduced worldwide in the subtropical and tropic zone, preferring drier and more barren environments (Warrier, 2010). Largely due to the work of the Australia Tree Seed Centre in the 1980s, the genus can now be found in over 103 countries after seedlots were dispatched globally (Potgieter, 2014). This can be seen in Figure 1. In some places where it has been introduced, notably South Africa and USA it has become invasive. In Kenya, *Casuarina cunninghamiana* is used as a living fencing technique around rural farms and is a renewable timber product due to its rapid growth.

Third world countries are especially susceptible to issues relating to safe drinking water, notably Kenya which faces a widespread problem with rural water contamination. 24% of the population of Sub-Saharan Africa was found to have access to safely managed handwashing facilities, safely managed sanitation and safely managed drinking water in 2015 (WHO/UNICEF, 2017), despite there being great variability among countries (Figure 2). In urban Kenya, water kiosks are available and sell water for around US\$0.03 for a 20-liter jerry can (UNDP, 2011) and make up approximately 23% of water vendors (UN, 2019). Its implementation in such cities as Mombasa has helped improve water access, up from 50% of the population receiving water 2-3 days a week previously (Economic and Social Rights Centre, 2016). Currently, 41% of Kenyans rely on unimproved water sources and 71% use unimproved sanitation solutions (Water.org, 2020) with many having to source

water themselves. This means that the rate of exposure to various waterborne diseases is high as much of the water at the pumps, and the basins and containers it is collected in is contaminated. Most of the objects used are simply any vessel that could be found, often meaning they were previously used for fertilizer, wastes or oil.

Such water is then drunk almost immediately by those collecting it, with little measures in place to attempt to sanitize it. This is caused by two main issues; lack of education and a lack of access to resources to do so. Education in Africa or the lack thereof is a widespread issue as more than two in five adults are still illiterate (Beegle et al., 2016) and the quality of any schooling is often low. Additionally, the only resources available to attempt to clean any water is often only a simple boiling method, however many people will opt to use their limited energy available for other concerns such as cooking food. Thus, there exists a significant need for a cheap and easily implemented way to make water safe to drink.

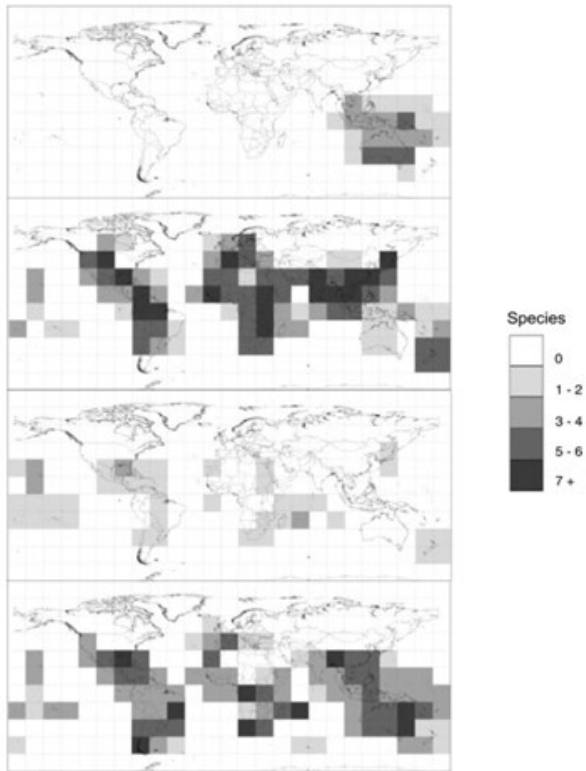


Figure 1: Worldwide Casuarina Distribution by Species Prevalence

Source: Potgieter, Richardson & Wilson, 2014

Escherichia coli (*E. coli*) is a common contaminant of drinking water and is readily available for laboratory experimentation. It is a coliform bacterium comprised of many different strains, with many harmless ones often found in the intestine of warm-blooded animals. When carried through water systems, harmful strains can have significantly adverse effects such as abdominal cramps, diarrhea, nausea and death. For this investigation, *E. coli* K-12, was chosen as the biological contaminant to be filtered. The K-12 and related strains of *E. coli* have been genetically modified and are widely used in scientific studies as they are only able to survive in cultures under very specific conditions, meaning survival in the human gut is not possible (Carr, 2014).

Previous research has suggested that plant vascular structures may be used to filter water (Chalmers, 2019). Using dye pigments, Chalmers (2019) demonstrated ‘that the gymnosperm filters were significantly more effective at filtering out the dye from the water than the

- Surface water
- Unimproved
- Limited
- Basic
- Safely managed

- Open defecation
- Unimproved
- Limited
- Basic
- Safely managed

*Insufficient data to estimate safely managed services.

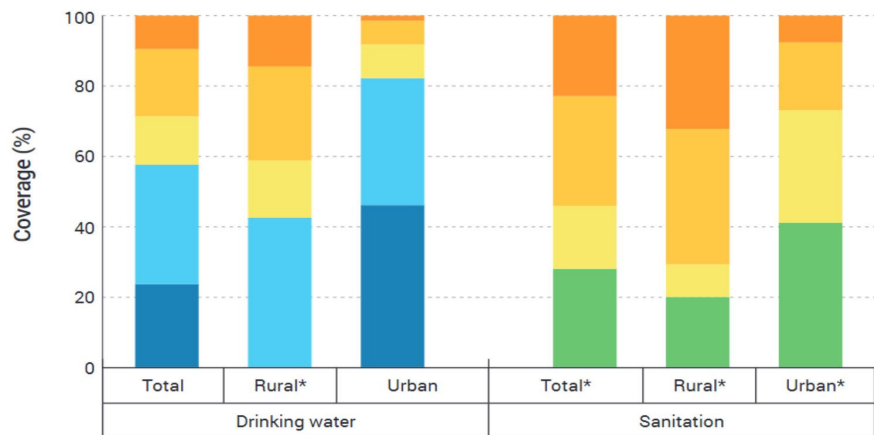


Figure 2: Drinking Water and Sanitation Coverage in Sub-Saharan Africa, 2015

Source: WHO/UNICEF, n.d.

angiosperm filters,' (Chalmers, 2019). Previous research using the white pine, *Pinus strobus*, used dye as a proxy for biological contaminants and, 'measured flow rates of about 0.05mL/s using only ~1cm² filter [and] correspond to a flow rate of over 4L/day,' which is greater than the necessary amount needed to meet any one person's required daily water intake (Boutilier et al., 2014). The same study also found that the related rejection rate of bacteria was at least 99.9%, however this was only in relation to looking at a species of gymnosperm.

Despite being an angiosperm, the structure of *Casuarina* vascular bundles suggests a potential for using species within the genus as biological filters for contaminated water. Previous research has suggested gymnosperms to be more effective as a filter for contaminated water than angiosperms (Chalmers, 2019). This finding is attributed to the difference in xylem morphology between angiosperms and gymnosperms. This difference can be attributed to the distinct foliage of *Casuarinas*, even to that of other angiosperms, which have long needle-like articulate photosynthetic branchlets (Price, 2007), on which have small scale-like leaves that are organized into whorls. This feature is important as it means that the species are well adapted to arid and semi-arid climates as a result. The spiral shape of the plant means there is less surface area exposed to the air and therefore less water loss, beneficial to the plant in essential processes such as photosynthesis.

Scientific research question

To what extent can the vascular structures of *Casuarina* be used to filter bacterial contamination from water?

Scientific hypothesis

Casuarina stems will be effective in filtering some bacteria from a water sample contaminated with *E. Coli* (K-12).

Methodology

10mL of *E. coli* (K-12 Strain) was purchased from Southern Biological. Sterile technique was used to transfer the sample into a 125mL flask of a commercially prepared sterile nutrified broth which was then cultured for 48 hours at 37°C. To avoid the use of agar plates, Petrifilm sleeves for *E. Coli* were purchased and stored in the laboratory according to manufacturer's instructions. As a control, 3 Petrifilm sleeves were immediately inoculated with 1mL at 37 degrees for 48 hours and then photographed.

In the weeks prior to the experiment, reconnaissance was undertaken to find suitable local specimens of *Casuarina cunninghamiana* and *Casuarina glauca*. In order to meet the criteria for inclusion in the research, specimens must be safely accessible and on public land, with accessible stem material of diameter 5-7mm. The trees were identified by the distinct foliage of *Casuarinas* with long needle-like articulate photosynthetic branchlets (Price, 2007), on which have small scale-like leaves that are organized into whorls. The *Casuarina glauca* was identified as around the stem it has 10-12 teeth on it that are light brown to grey in colour. *Casuarina cunninghamiana* was identified in a similar way as it has 6-10 upright teeth that are light brown to grey tips (Castle, 2007). The chosen specimens can be seen in Figure 3-6.



Figure 3: Tree 1- *C. Glauca* Figure 4: Tree 2- *C. Glauca*



Figure 5: Tree 3- *C. Cunninghamiana* Figure 6: Tree 4- *C. Cunninghamiana*

Two stem sections from four tree specimens were taken 3 hours prior to experiment and kept submerged in water to prevent either end of the xylem from drying out. The branches were assessed using calipers to ensure that all were the same diameter and then cut with secateurs. Back in the laboratory, the stems were shaved using a scalpel and trimmed to a uniform length. The trimming ensured

uniformity but also exposed a fresh face of xylem immediately prior to the experiment. An apparatus was then constructed using PVC tubing attached to the top of the branch. The PVC was softened in boiling (sterile) water and then forced over the stem to create a tight-fitting sleeve. The purpose of the PVC sleeve was to act as a reservoir for the culture before it passed through the filter. 2mL of broth was then added to the top of the 8 tubes using a calibrated pipettor. The apparatus can be seen in Figure 7. The stem cuttings and their sleeves were replaced in test tubes in a rack and the broth passed under gravity through the stem and into the vial beneath. After 12 hours, the filtrate was fully recovered in a test tube. Two Petrifilm sleeves were then inoculated with 1mL each of filtrate from each sample so that each sample had two plates created (Figure 8). The plates were then incubated at 37 degrees for 24 hours.



Figure 7: Demonstration of Broth added to Sample



Figure 8: Petrifilm Plates inoculated with Filtrate

After 24 hours, each plate was observed and photographed. The photographs were used to count the number of coliform forming units (CFUs) on each plate and the data was recorded in a table. Each plate was counted twice to ensure the reliability of the data. In subsequent days, ideally the plates would have been counted again to see if there was a maximum growth of colonies that could be observed on each plate, however the laboratory had to be shut down due to COVID-19 restrictions and thus this check was unable to be performed.

When counting the plates, all photos taken were observed on an A4 sheet, with the left and right sides of the circular Petrifilm taken to the sides of the page, ensuring that each result was observed at the same size. From here, a judgement was then made on all observable coliforms, as to make it easier to determine a counting protocol. It was sometimes difficult to determine the differences between air bubbles and colonies. Keeping each observation of a given Petrifilm at the same resolution, a judgment was able to be more easily made in counting coliforms and when a colony was counted at an acceptable size was more easily determined also.

Results

Tables 1-3 shows the plate counts collected from samples of filtered *E. coli* from tree samples and a control. Table 2 shows the average and standard deviations of this data. A t-test based on this did not show a statistically significant difference between the mean number of spots for the *Casuarina glauca* and *Casuarina cunninghamiana* trees ($t=0.929$, $p=0.373$). The results indicate that both the varieties of *Casuarina* saw a large reduction in the counts of bacteria versus the control used. This is consistent with the hypothesis as the filter can clearly be proven to be effective. This is consistent with the previous research findings that xylem structures are significantly effective at filtration (Chalmers 2019). As seen in Table 4, the average counts on plates were 10.4 for *Casuarina glauca* samples and 6 for *Casuarina cunninghamiana*, compared to greater than 100 on control plates. The standard deviation of results was also calculated and a comparison of the two species as well as the control can be seen in Figure 9.

Table 1: *C. Glauca* Plate Counts

Plate number	Count (cfu)
1a	0
1b	20
2a	16
2b	0
3a	2
3b	25
4a	15
4b	5

Table 2: *Cunninghamiana* Plate Counts

Plate number	Count (cfu)
5a	A
5b	3
6a	5
6b	10
7a	11
7b	1
8a	B
8b	B

Table 3: Control Plate Counts

Plate number	Count (cfu)
0a	>100
0b	>100

Table 4: Standard Deviation and Averages of Results

	Glauca	Cunninghamiana	Control
Average	10.375	6.000	100
StDev	9.812	4.359	

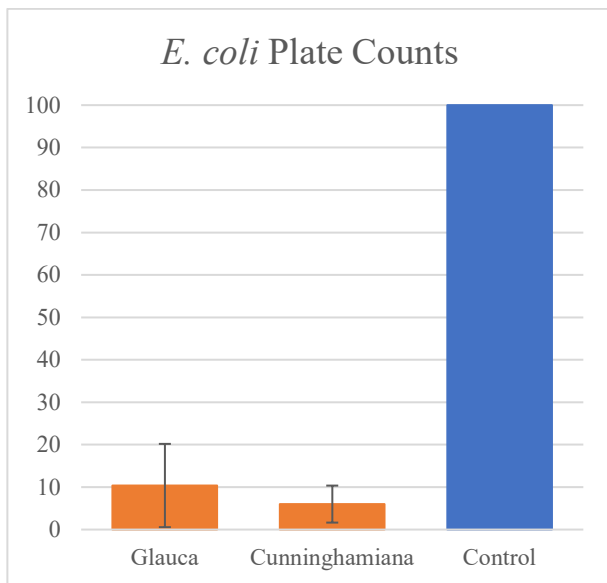


Figure 9: *E. coli* Plate Counts

The results need to be treated cautiously because there were several limitations to the experiment. The sample size of the plants tested was relatively small and some samples experienced issues. Notably, one branch did not filter the *E. coli* at all (Box B, Table 2). This could be attributed to structurally the branch being dried out or the xylem vessels being blocked. Additionally, one branch showed counts of over 100 (Box A, Table 1) which could be attributed to the apparatus used having issues with unfiltered *E. coli* potentially leaking through. Both of these results were treated as outliers and were thus not included in the final results. Additionally, the plates were only viewed after 24 hours due to issues with the involuntary COVID-19 shutdown of the laboratory and could have showed different or greater counts if potentially viewed at 48 hours or even later.

Other methods that could be taken from this experiment could look at filtering the same species using a dye pigment instead of *E. coli*. Whilst the results did show effective filtration using angiosperms, getting a reliable count of the bacteria was difficult and thus using a dye pigment could lead to more reliable and accurately counted results. Additionally, use of a larger sample size as well as observations of results for a longer period of time could give a greater and more accurate result.

Discussion

This experiment has demonstrated the efficacy of *Casuarina* as a filter. Both *Casuarina cunninghamiana* and *Casuarina glauca* species were effective in removing bacteria from the water because the CFU counts in all cases were significantly lower than the control. The considerable difference between the counts found on the plates after the application of the filter demonstrate its effectiveness at filtering *E. coli* when compared to that on control plates.

While the filtrate still exceeds the WHO drinking water guideline of ‘undetectable’ or <1 CFU on an incubated plate (WHO, 1997), this result is still valuable. Whilst unable to fully eliminate the presence of *E. coli* in a sample, the significant reduction in its prevalence could still be of great use. With potential in developing countries for a biological filter to be implemented and the inability in some cases to access any other sterilisation techniques, an almost 80% reduction in the prevalence of *E. coli* over a long span of time greatly reduces the chance of illness occurring as a result of it entering a person’s system. Additionally, the ease at which such a filter can be established holds promise in communities wherein education rates create a necessity for easily understood systems.

Several methods were employed to ensure there was no cross contamination with the bacteria in order to ensure that it was only the *E. coli* that was being tested on for its efficacy through the filter.

Before placing the plastic tubing around the branch, it was placed in boiling water, not only to make it looser to fit around the branch, but also to ensure any potential bacteria on the tubing was sterilised. Additionally, the tube and the branch spotted was suspended in the tube with tape, placed around the outside of the plastic tube to ensure it didn't catch the branch (as seen in Figure 10). This ensures that the branch did not come in contact with the filtrate or the tubing it was collected in to ensure no other bacteria was introduced. Additionally, the collection tube for the filtrate was autoclaved so that it was sterilised before and a micropipette machine was used with different tips each time when moving the nutrient broth into the top of the plastic tubing and after when the filtrate was transferred from the collection tube onto the Petrifilm plates. Also, all bench space and apparatus used were routinely wiped with ethanol and a Bunsen flame was kept on, creating a convection cell, which ensured no aerial contamination.



Figure 10: Apparatus for Filtration

The research found in this report was heavily influenced by Chalmers (2019) and his report, 'Filtering water using plant xylem'. His research concluded that when comparing using filters from angiosperm and gymnosperm samples, using dye as a proxy for biological contaminants, 'the filtering capability of the gymnosperm filters are significantly greater than for angiosperm filters.' However, whilst gymnosperm effectiveness was significantly higher, that was not to necessarily say that angiosperms were ineffective, as the use of angiosperm filters were still proven to be

somewhat effective. This is important as angiosperms make up approximately 80% of global plant types (Sperry 2003) and thus if an effective filter could be found using one or several species within it, the application of a biological filter could be much more widespread. Thus, using the angiosperm, *Casuarina* was an effective build on this idea as the almost hybrid nature of it made it a suitable choice for a potentially effective angiosperm.

A drawback of such a filter is that the rate at which it is able to pass a sample through is quite slow, taking almost 24 hours during the experimental component of this research. Further research should look into developing a more accessible filter to work towards one that could be actually used and implemented in a real-life scenario.

An increase in the number of replicates should also be used in future research to build on these discoveries. Whilst the findings of this experiment were still able to demonstrate a clear reduction in the number of *E. coli* coliforms when the use of a biological filter was implemented, further replications of such results would increase this conclusion's validity. In such a small dataset, there was an 18.75% occurrence of outliers, with filters that failed to even filter the broth and a Petrifilm plate that showed a considerably greater count of coliforms and thus was not counted in the final results.

Due to this, the amount of actually usable results was lessened and thus there was a lower validity to the dataset. Future direction for research should look at greater replication of results so that the reliability of the actual filter can be found. In practice, this means looking at how many times the actual branch sample used is effective, including an investigation into whether the xylem vessels themselves could get blocked with *E. coli* and render the filter ineffective as a result. Had COVID-19 restrictions not led to laboratory shutdown, this may have been able to be further explored.

Along with further replication of results, the Petrifilm plates in future experiments should be allowed to incubate for longer periods of time. Due to the restrictions during the height of lockdowns as a result of COVID-19, there were limitations on the experimental process in relation to time. All counts of the plates were taken 24 hours after being inoculated and were unable to be counted in successive times after this due to restrictions. Further research should take counts of the plates also at 48, 72 and 96 hours in order to determine whether the sample would hit a maximum amount of contamination wherein no more coliforms would be able to be produced. In doing so, a more accurate data set

could be created as the contaminated rate (the amount of time in which coliforms take to form on a plate) after being passed through a branch may differ to that of a pure *E. coli* broth. A slower rate does not necessarily infer a safer sample in terms of water quality as any instance of harmful bacteria is problematic.

Conclusion

There has been significant potential found in the use of plant xylem as a means of filtration for biological contaminants. This experiment investigated the effectiveness of the *Casuarina* genus, specifically two species, *Casuarina cunninghamiana* and *Casuarina glauca*, in filtering a biological contaminant, *E. coli*, from a sample of water. Filters made of branch samples and PVC tubing were constructed and nutrient broth containing *E. coli* was passed through them. The resulting filtrates were then incubated on a Petrifilm plate, with the number of coliforms on them determining the efficacy of each filtrate. There was not a statistically significant difference between the mean counts of *Casuarina glauca* and *Casuarina cunninghamiana* samples. The results indicated a significant reduction in the counts of bacteria on plates that had been incubated with filtrate from any of the sample against the nutrient broth itself, thus supporting the initial hypothesis.

This result addressed the original research question as it showed that the vascular structures of *Casuarina* can be used to filter bacterial contamination leading to the acceptance of the hypothesis that the stems would be effective filters. There is need for further research in several areas including the extension of the time allowed and number of replicates used for the experiment to progress and an investigation into the development of an easily usable filter. The success of such xylem filters has the potential for widespread use in developing countries where *Casuarina* is widely distributed however greater research is needed in the meantime.

Acknowledgements

I would like to thank Dr Gates and Dr Hill for their assistance in the completion of my project. For Dr Hill for his help with statistical analysis and notably to Dr Gates for her extensive help and support throughout all stages of the report.

References

Beadle N.C.W. (1981) *The Vegetation of Australia*. Cambridge Univ. Press, Cambridge, 690pp.

Beegle, K., Christiaensen, L., Dabalen, A. and Gaddis, I. 2016. *Poverty in a Rising Africa*. Washington, DC, The World Bank. openknowledge.worldbank.org/bitstream/handle/10986/22575/9781464807237.pdf?sequence=10&isAllowed=y.

Boutilier, M.S., Lee, J., Chambers, V., Venkatesh, V. and Karnik, R., 2014. Water filtration using plant xylem. *PLoS one*, 9(2), p.e89934.

Carr, S., 2014. *E Coli K12*. [online] Mun.ca. Available at: https://www.mun.ca/biology/scarr/CG_wimp.html#:~:text=The%20K12%20and%20related%20strains,all%20in%20the%20human%20gut.&text=coli%2C%20which%20would%20indicate%20possible,human%20or%20animal%20fecal%20material.

Castle, W.S., 2008. *Field guide to identify the common Casuarina (Australian pine) species in Florida*. University of Florida, IFAS Extension.

Castle, W.S., 2008. *Field guide to identify the common Casuarina (Australian pine) species in Florida*. University of Florida, IFAS Extension.

Chalmers, H. (2019). Filtering Water using Plant Xylem. *Scientific Research in School*, 1, pp.31-38.

Dörken, Veit & Parsons, Robert. (2017). Morpho-anatomical studies on the leaf reduction in *Casuarina*: the ecology of xeromorphy. *Trees*. 31. 10.1007/s00468-017-1535-5.

Economic and Social Rights Centre. 2016. *State of Water and Sanitation Service Provision Performance in Mombasa County. Community Score Card*. Nairobi, Economic and Social Rights Centre (Hakijamii). www.hakijamii.com/wp-content/uploads/2016/05/Final-Community-Report-Card-Report.pdf.

Gerald, M, Gerald, G, 2015, *The Biology Book: From the origin of life to epigenetics, 250 milestones in the history of biology*, Sterling, New York, NY.

Orwa C, A Mutua, Kindt R, Jamnadass R, S Anthony. 2009 *Agroforestry Database: a tree reference and selection guide version 4.0* <http://www.worldagroforestry.org/sites/treedbs/treedatabases.asp>.

Parrotta, A. 1993. 'Casuarina equisetifolia'. *Casuarina, Australian Pine*. pp1.

Potgieter, Luke & Richardson, David & Wilson, John. (2014). *Casuarina: Biogeography and ecology of an important tree genus in a changing world*. *Biological Invasions*. pp. 10530-013-0613.

Price, R. and Wildeboer, D. (2007). *Casuarina glauca*. *Biotechnology in Agriculture and Forestry*, 60, pp.433-434.

Price, R. and Wildeboer, D. (2017). *E. coli as an Indicator of Contamination and Health Risk in Environmental Waters*. *Recent Advances on Physiology, Pathogenesis and Biotechnological Applications*.

Sperry, J. S. 'Evolution of water transport and xylem structure'. *Int J Plant Sci* 2003, vol. 164, pp. 115-127.

UNDP. 2011. Small-Scale Water Providers in Kenya: Pioneers or Predators? New York, UNDP. [www.undp.org/content/dam/undp/library/Poverty%20Reduction/Inclusive%20development/Kenya%20paper\(web\).pdf](http://www.undp.org/content/dam/undp/library/Poverty%20Reduction/Inclusive%20development/Kenya%20paper(web).pdf).

United Nations (2019) World Water Development Report 2019. *UN Water*.

Warrier, K. 2010. 'Improving Productivity of Casuarina through Clonal Forestry'. Institute of Forest Genetics and Tree Breeding Coimbatore. pp. 22.

Water.org. (2020). *Kenya's Water Crisis - Kenya's Water In 2019* | *Water.org*. [online] Available at: <https://water.org/our-impact/kenya/>.

WHO/UNICEF. 2017. Safely Managed Drinking Water – Thematic Report on Drinking Water 2017. Geneva, WHO. <https://data.unicef.org/wp-content/uploads/2017/03/safely-managed-drinking-water-JMP-2017-1.pdf>.

Wilson, K.L. & Johnson, L.A.S. (1989). Casuarinaceae. In 'Flora of Australia.' Vol. 3, (Australian Government Publishing Service: Canberra.), pp. 100-174, 190-202.

World Health Organisation (WHO). 1997. 'Guidelines for drinking-water quality.' Surveillance and control of community supplies. Vol. 3, no. 2, pp.

Comparison of the antimicrobial properties of manuka honey vs store bought honey as an antimicrobial agent

Cormac Sutherland

Barker College

Honey is well researched and known for its antimicrobial properties but more specifically manuka honey is known to be more effective against bacteria than normal honey. This experiment is to test this observation by using two differing honeys and measuring the growth of a gram-positive bacteria and a gram-negative bacteria as they develop across an agar plate. To test the hypothesis, each agar plate has 6 sections, one control, three antibiotic and two different types of honey. The result of this experiment was that the manuka honey showed a greater area of inhibition than the regular honey. The manuka honey was equally effective across both types of bacteria but less effective than the regular antibiotics. In conclusion this experiment showed that manuka honey had a far better antibiotic effect than store bought honey.

Literature review

Honey has been used and documented throughout history for medicinal purposes for example, 'honey was used by the Egyptians in many different medical remedies' (Al-Jabri, 2005). It was also described as a key element in a wound salve most likely being utilized for its antibacterial properties to help prevent and heal infected wounds. Honey was also widely utilised by the ancient Greeks who often used honey as a remedy for gout as well as certain nervous disorders. The Greek scientist Hippocrates prescribed a diet which involved favouring honey given as oxymel which was vinegar and honey for pain, hydromel which was water and honey for thirst. Hippocrates also utilized honey for many other medical operations including wound healing and as a treatment for coughs and sore throats. Manuka honey today is used for many similar medical purposes. It is listed with the Australian Therapeutic Goods Administration for similar uses including wound healing pain relief inflammation relief treatment of cough, smoothing the skin and as an antioxidant (Australian Government Therapeutic Goods Association, n.d.).

It has been discovered that the antimicrobial properties of the honey does not originate from the bees that produce the honey but instead the antimicrobial properties originate from the flowers that the bees use collect their nectar to make their honey (Alvarez-Suarez et al., 2014).

Manuka honey and regular honey have both been described to consist of carbohydrates, minerals, proteins, fatty acids, phenolic and flavonoid compounds (Mavric et al., 2008).

While there are many varieties of honey, only a few types of honey are known for their high antimicrobial properties. Two examples which have been studied in great detail are manuka honey which is produced by the bee (*Apis mellifera*) and gets its name from the flowers of the manuka tree as well as Malaysian Tualang honey which is another multifloral honey. Malaysian Tualang is produced by the bee (*Apis dorsata*) and gets its name by building hives on the branches of tall Tualang trees. (Johnston et al., 2018). Manuka honey has also been described as having high levels of Methylglyoxal (MGO). Atrott et al describes the correlation between MGO and antibacterial activity. A grading system for manuka honey was established by the UMF honey association in New Zealand. This system correlates a Unique Manuka Factor (UMF) with levels of MGO (see Figure 1). However, the relationship between UMF rating, MGO levels and antibacterial effect is not well understood. (Johnson et al., 2018)

Bacteria are universally classified based on Gram staining as either a positive or negative. These responses are connected to the wall thickness and composition of the cell wall of bacteria. It is also widely observed that gram-positive and gram-negative bacteria have

developed different mechanisms of antibiotic resistance. (Johnson et al., 2018). *E. coli* is an example of gram-negative bacteria and *B. subtilis* is an example of gram-positive bacteria.

MGO	UMF EQUIVALENT
MGO 83+	5+
MGO 100+	6+
MGO 250+	10+
MGO 400+	13+
MGO 550+	16+
MGO 700+	18+
MGO 850+	20+
MGO 1000+	22+

Figure 1: Comparison between Methylglyoxal (MGO) levels and Unique manuka Factor (UMF).

Source: Manuka Honey Organic, n.d.

It is also known that different types of manuka honey seem to have differencing effects on gram-negative bacteria and gram-positive bacteria. However, unlike normal antibiotics it is unknown if bacteria are able to become resistant to honey. For the purposes of this experiment *E. coli* is the gram-negative bacteria used and *B. subtilis* is the gram-positive bacteria used because they were bacteria that I had easy access to get my hands on.

Recently a comparison of the effects of manuka honey compared to a generic multifloral honey on wound healing was published in the Australian Veterinary Journal. The study concluded that wounds treated with manuka honey healed faster than those treated with generic honey. However, in this study there was no bacterial infection mentioned. The question remains, is manuka honey a more effective antimicrobial than generic honey (Tsang et al., 2017)?

Scientific hypothesis

The hypothesis of this experiment is that there will be a significant difference in the zone of inhibitions of the normal store-bought honey compared to the zone of inhibition for the manuka honey.

Methodology

The materials that my experiment required are listed below:

20 Nutrient Agar Plates, 20 Sterile Pipettes, 20 Disposable Spreaders, 50 Penicillin Discs, 50 Ampicillin Discs, 50 Chloramphenicol Discs, 50 Blank Discs Forceps, 70% Alcohol, honey and manuka honey. As well as the two differing bacteria the *E. coli* gram-negative and the *B. subtilis* gram-positive

Method

First the workplace was sterilized with a solution of 70% alcohol and a Bunsen burner was used near to where the experiment was taking place in an attempt to use the updraught of the flame to keep potential contaminants away from my materials. Then the agar plates were divided into 6 sections and label P (penicillin), A (ampicillin), C (Chloramphenicol), B (control disc), H (honey) and MH (Manuka honey). Then the petri dishes were also labelled based on which bacteria they were going to be inoculated with *E. coli* or *B. subtilis* however there were only 50 base discs and 40 of them were used to make the honey and manuka honey discs, so only half the plates had a control disc. Then using a previously sterilised pipette about 0.5mL of the bacterial broth was placed onto one of my plates with the correctly labelled bacteria plate then repeated this process until all plates were inoculated. Note: glass spread was used to spread the bacteria so it had to be sterilised before each use. The petri dishes were then left for 10min before the disc were added to the plates to give the bacteria a chance to grow. 20 blank discs were laced with honey and another 20 with manuka honey. Then the different discs were placed into the middle of their assigned segment using forceps. making sure to flame the forceps between each disc. Then the agar plates were placed in an incubator at 37°C for around 24 hours. Then after the 24h period the zone of inhibition was measured marking down the diameter of the zone and was recorded into a results table.

Results

After the experiment the results were first placed into a table as well as pictures taken of the petri dishes. Figure 1 is one of the pictures of the petri dishes. Specifically it is a photo of one of the *B. subtilis*. It shows properly how the petri dishes were split into the 6 sections as well as showing the bacteria growth on the plates.

Table 1 has the raw data taken from the test showing the measurements of the zones of inhibition as well as the averages across the different discs.



Figure 2: *B. subtilis* petri dish

Table 1: Diameter of the zone of inhibition for agar plates inoculated with *b. subtilis*. Key: P (penicillin), A (ampicillin), C (Chloramphenicol), H (honey), MH (Manuka honey).

<i>B. subtilis</i>	Zone of inhibition diameter (cm)				
	P	A	C	H	MH
1	1.6	3.0	2.5	0.0	0.5
2	1.7	2.3	3.0	0.0	0.6
3	2.0	3.0	2.2	0.0	0.4
4	3.0	3.0	3.0	0.0	0.6
5	3.0	3.0	3.0	0.0	0.5
6	1.6	3.0	3.0	0.0	0.6
7	1.6	3.0	2.2	0.0	0.4
8	1.7	3.0	3.0	0.0	0.5
9	1.9	3.0	2.5	0.0	0.5
10	3.0	3.0	3.0	0.0	0.6
Average	2.11	2.93	2.74	0.00	0.52

Table 2: Diameter of the zone of inhibition for agar plates inoculated with *E. coli*. Key: P (penicillin), A (ampicillin), C (Chloramphenicol), H (honey), MH (manuka honey).

<i>E. coli</i>	Zone of inhibition diameter (cm)				
	P	A	C	H	MH
1	0.0	1.5	0.0	0.0	0.6
2	0.0	1.6	2.0	0.0	0.4
3	0.0	1.7	1.9	0.0	0.5
4	0.0	1.6	2.0	0.0	0.0
5	0.0	1.7	2.0	0.0	0.5
6	0.0	1.6	1.7	0.0	0.5
7	0.0	1.8	2.3	0.0	1.0
8	0.0	1.7	1.5	0.0	0.6
9	0.0	1.6	1.2	0.0	0.5
10	0.0	1.7	1.8	0.0	0.5
Average	0.00	1.65	1.64	0.00	0.51

Table 1 and 2 show the measurements of the diameter of the zone of inhibition in cm. If the zones were too large to be measured accurately (often they would extend into other segments), they were given a pre-determined maximum value of 3.0cm.

Figure 3 and figure 4 are graphs of the averages of the zones of inhibition to illustrate the differences in the zones visually. Figure 3 is the graph of *B. subtilis*' average. Figure 4 is the graph of *E. coli*'s average.

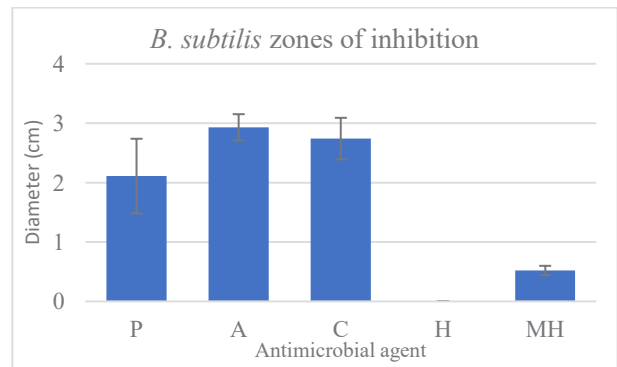


Figure 3: Average diameter of zone of inhibition for each antimicrobial agent (*B. subtilis*).

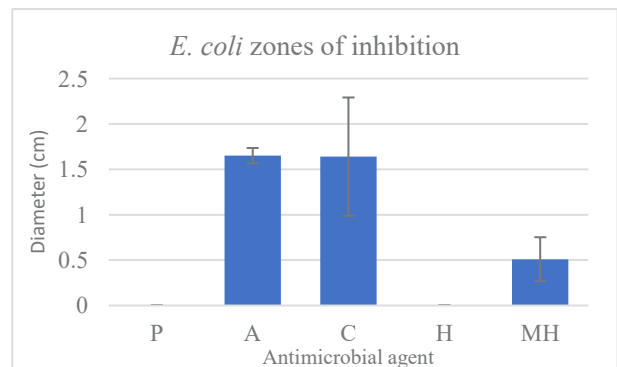


Figure 4: Average diameter of zone of inhibition for each antimicrobial agent (*E. coli*).

Figure 3 shows the zone of inhibition of the disc against *B. subtilis* showing Penicillin to have an average zone of 2.1cm, ampicillin to have an average of 2.9cm, Chloramphenicol having an average of 2.7, and manuka honey having an average of 0.52cm. While Figure 4 shows the zone of inhibition of the disc against the *E. coli* showing ampicillin having an average of 1.65cm, Chloramphenicol having an average of 1.64cm, and manuka honey having an average of 0.51cm.

Table 3 and table 4 are the results after the data from table 1 was placed through an online one-way ANOVA with post-hoc Tukey HSD Test Calculator and they show if

the results across the zones of inhibition were significantly different or not.

Table 3: Post hoc tests for the one-way ANOVA testing antimicrobial agents against *B. subtilis*.

Treatments pair	Tukey HSD		Inference
	Q statistic	p-value	
P vs A	7.67	0.00101	** p<0.01
P vs C	5.89	0.00126	** p<0.01
P vs H	19.72	0.00101	** p<0.01
P vs MH	14.86	0.00101	** p<0.01
A vs C	1.78	0.69512	insignificant
A vs H	27.39	0.00101	** p<0.01
A vs MH	22.53	0.00101	** p<0.01
C vs H	25.61	0.00101	** p<0.01
C vs MH	20.75	0.00101	** p<0.01
H vs MH	4.86	0.01065	* p<0.05

Table 4: Post hoc tests for the one-way ANOVA testing antimicrobial agents against *E. coli*.

Treatments pair	Tukey HSD		Inference
	Q statistic	p-value	
P vs A	16.65	0.00101	** p<0.01
P vs C	16.55	0.00101	** p<0.01
P vs H	0.00	0.89999	insignificant
P vs MH	5.15	0.00601	** p<0.01
A vs C	0.10	0.89999	insignificant
A vs H	16.65	0.00101	** p<0.01
A vs MH	11.51	0.00101	** p<0.01
C vs H	16.55	0.00101	** p<0.01
C vs MH	11.40	0.00101	** p<0.01
H vs MH	5.15	0.00601	** p<0.01

Discussion

Based on the results we can see a clear difference in the effectiveness of the manuka honey vs the store-bought honey. First in the case of Table 1 we can see that the store-bought honey did nothing to stop the growth of the bacteria forming no zone of inhibition in both *E. coli* and *B. subtilis* while the manuka honey had a very consistent zone of inhibition of around 0.5 across both bacteria. We also see from the preformed ANOVA test in Figures 5 and 6 that there is a significant difference between the manuka honey and the store-bought honey with the P value being less than 0.05 supports the original hypothesis of this experiment.

Another interesting point to gain from the graphs in Figure 3 and 4 is that even though the *E. coli* was generally more resistant than the *B. subtilis* with the

antibiotics having much smaller zones of inhibition on the *E. coli* agar plates but the manuka honey’s zone of inhibition didn’t change from bacteria to bacteria having the same effect on both of them.

One of the more concerning and interesting things we can gather from the results but more specifically from Figure 2 is that the non-manuka honey actually helped the bacteria to develop with the area around the bacteria being a deep yellow showing that the bacteria were using the normal honey as a food source causing the opposite of what we wanted the honey to do. Now the main thing to gather from that is to try to figure what that means. One of the possibilities is that it’s possible that normal honey like manuka honey has antimicrobial properties but in the process of being treated to sell in the supermarket those antibacterial properties were lost. But what this does show is that manuka honey from a pharmacy is definitely better than honey bought in a super market when it comes to fighting a bacterial infection.

However, these results should be taken with a grain of salt for many differing reasons. One of which is that the UMF rating of the manuka honey that I used was 15+, which isn’t nearly the highest value, meaning that it is probable that if I had used a stronger manuka honey the results could have been very different. Similarly, one of the things that I would be really interested to find out if I was able to do this experiment again is to use fresh regular honey from the honey hive rather than buying the honey from a store and see if that produces a differing result than the one I got from doing the experiment with the store-bought honey.

Another one of the main issues with this experiment is how easily it can be affected by sources of error. The main source of error in this experiment was because of the layout of the petri dishes, it was possible for the zone of inhibitions to spread out into other areas causing the two zones to join as one; this can be seen in some of the images. To counter this I decided that if the zones would reach out into other zones I would write it down as a maximum value which I later decided to label as 3.0cm. Another main source of error that effected the experiment were possible problems with the method which could have happened at any stage of the experiment. The most extreme of which was that in the *E. coli* discs some of the penicillin discs fell off when placed in the incubator. While this had little effect on the *E. coli* because it was already resistant to penicillin, it shows that it was possible for other discs to fall off ruining the results. This

could explain some of the results specifically in the E coli Table where there are some antibiotic discs that should have affected the bacteria instead gave no zone of inhibition.

The final possible source of error that could have occurred during the experiment is that there were spots on some of the disc that had no bacteria grow on them. This could be the result of the method of spreading the bacteria onto the agar plates with me possibly missing a spot or it could be a place where I accidentally dropped one of the antibiotic discs while trying to put them on the plate. The main problem with this is that it's possible that this had an effect on the zones of inhibition possibly making some zones appear larger than they were causing the results to possibly be inaccurate.

If I was to improve on this experiment I would want to focus on having more types of honey rather than just the manuka honey and the store-bought honey. It would be better to do the experiment again using fresh honey as well as store-bought honey of differing brands to see if that had an effect on the outcome of the experiment.

Conclusion

This experiment clearly shows that in the case of this experiment, the manuka honey used was far better as an antibacterial medication than the store-bought honey from the supermarket. It also shows that the effectiveness of the manuka honey vs. the store-bought honey is significantly different as the results from the ANOVA test showed. This research also shows the potential importance of manuka honey for medicinal antibacterial purposes be that for wound treating like the Egyptians used regular honey for, or even according to the background research it's possibilities for burn wound treatment. This shows that it is possible that the reason that manuka honey's high levels of antibacterial activity, in comparison to the store-bought non-manuka honey could be due to the special UMF rating which is correspondent to higher phenolic and methylglyoxal content. However, this does not definitely show or prove in any way that normal honey is not possibly useful also as an antimicrobial source and most definitely more research should be done to improve this experiment and change it into an experiment that can show if normal honey is also useful as an antimicrobial when it has not first been treated.

In conclusion the results of the experiment show that the manuka honey had an obvious effect on the growth of the

bacteria causing it to have a zone of inhibition while the store-bought honey also had an obvious effect on the growth of the bacteria around it, which was causing the bacteria to grow stronger around it. This shows that if humans desperately needed to find another way to combat bacterial infections certainly manuka honey is a better option than using store-bought honey, however using traditional antibiotics is preferable than using either honey.

Acknowledgements

I would like to thank Dr Gates for helping me come up with this research task, helping me to finalise my method and helping me collect my data. I would also like to thank Dr Hill for helping me understand how to analyse and understand the data I had collected.

References

- Adams CJ, Manley-Harris M, Molan PC. The origin of methylglyoxal in New Zealand manuka (*Leptospermum scoparium*) honey. *Carbohydr Res.* 2009.
- Administration, A.G.D. of H.T.G. (n.d.). Search the TGA website. [online] Therapeutic Goods Administration (TGA). Available at: http://search.tga.gov.au/s/search.html?collection=tga-artg&profile=record&meta_i=338214.
- Al-Jabri AA. Honey, milk and antibiotics. *Afr J Biotechnol.* 2005.
- Alvarez-Suarez J, Gasparrini M, Forbes-Hernández T, et al. The composition and biological activity of honey: a focus on manuka honey. *Foods.* 2014.
- Atrott J, Henle T. Methylglyoxal in manuka honey—correlation with antibacterial properties. *Czech J Food Sci.* 2009
- Johnston, M., McBride, M., Dahiya, D., Owusu-Apenten, R., & Nigam, P. S. (2018). Antibacterial activity of manuka honey and it's components: An overview. *AIMS microbiology*, 4(4), 655.
- Manukahoneyorganic.com. n.d. What Is UMF?. [online] Available at: <<https://www.Manukahoneyorganic.com/what-is-umf/>> [Accessed 21 July 2020].
- Mavric E, Wittmann S, Barth G, et al. Identification and quantification of methylglyoxal as the dominant antibacterial constituent of manuka (*Leptospermum scoparium*) honeys from New Zealand. *Mol Nutr Food Res.* 2008.
- Tsang, A., Dart, A., Sole-Guitart, A., Dart, C., Perkins, N. and Jeffcott, L. (2017). Comparison of the effects of topical application of UMF20 and UMF5 manuka honey with a generic multifloral honey on wound healing variables in an uncontaminated surgical equine distal limb wound model. *Australian Veterinary Journal*, 95(9), pp.333–337.

An investigation of the concentration of microplastics in the beaches of Lizard Island

Jacob Kalnins

Barker College

Microplastics are a contentious and topical issue in contemporary environmental science. Due to the public interest, there has been a rush to approximate the total number/volume of microplastics in different settings around the globe. Existing research on microplastics seeks to establish a baseline for future research and facilitate a more organized global response. This report looks at the beaches of Lizard Island Australia and analyses how microplastics are distributed along the shoreline. Four sites were sampled along each of six transect lines to determine that microplastics decline in abundance from the water to the shore. Microplastics were strained out of sand samples, collected and counted using a light microscope. The data demonstrated that the concentrations of microplastics in the beaches of Lizard Island were higher in water at the shoreline, gradually decreasing in concentration as you move toward land.

Literature review

Plastics are very common and persist in the environment long after they have been discarded. It was in the 1950's that the mass production of plastics began. Now their presence in the environment has become a global issue.

This issue causes many problems in the natural environment from inhibiting growth of plants to killing animals through the consumption of this indigestible material. Much has been heard of the impact of intact plastic items such as straws and single-use bags but plastics degrade instead of decomposing, they remain in the environment getting worn down and broken into smaller pieces but still they remain. This plastic residue is known as microplastics and it comes in all shapes and sizes.

Each year approximately 400 million tonnes of new plastics are created globally. These plastics are then used around the world in many places. The plastics are used in a range of items such as single use food wrapping to long term bitumen. All these different plastics have their own life cycles as products but when they are used up, they remain around for thousands of years. These plastics are left in landfill and when blown away they add to the global microplastic count as they begin to break down

(Windsor et al., 2019). Plastics fuel the human tendency to use and then dispose.

Currently the amount of mismanaged plastic waste in the world is estimated to be between 60 to 100 mega tonnes. This number is projected to increase to 155 to 265 mega tonnes by the year 2060. A majority of this waste, 91%, is transported via water bodies larger than 100 square kilometres. This suggests that rivers are major pathways for the transportation of mismanaged waste to the ocean (Lebreton & Andrady, 2019).

Microplastics come from two sources. They either degrade from plastic objects or are produced from overspill in the production of large plastic items. Fibre reinforced plastic products such as chairs microplastics are employed in the fabrication process. For example, Monoblock chairs are one of the most common type of plastic furniture around the globe and are currently being mass produced. Each Monoblock chairs weighs approximately 1 kilogram and is made from 16121 individual microplastic pieces weighing 0.0062 grams each, melted together.

Microplastics are seen commonly in wastewater treatment plants (Estahbanati & Fahrenfeld, 2016) as they travel through the sewage lines. Some of the most common sources of these are household washing

machines and driers (Seigfried et al., 2017). These devices produce microplastics every time they wash or dry cloths as the modern cloths are made up of plastic fibres that are all gradually torn apart. This process of degradation is sped up in the high speeds of the washing machine and driers as they churn the cloths pulling off many microplastics.

The tracking of microplastics has led to the oceans (Estahbanati & Fahrenfeld, 2016; Kooi et al., 2018; Kroeze et al., 2016) as billions of microplastics flow into them through rivers around the world. This has led to studies focusing on the effects of microplastics on ocean and beach life. Current studies have shown no ill effects on the ocean life yet but have shown high concentration of microplastics on beaches. Due to microplastics being a relatively new focus in the scientific community there have been many recent studies on the concentrations of microplastics in beaches around the world. This has helped given an approximation of the amount of microplastics that there are within the oceans and has allowed the scientific community to map out the highest concentrations of microplastics. This allows the scientific community to create a global image of the microplastic densities.

Microplastics can cause harmful effects to the many environments they traverse as they can be vectors for hazardous chemicals (Verla et al., 2019). This chemical pollution can involve hydrophobic organic contaminates and heavy metals. These pollutants can affect the food chain, soil, air and water of the environments they are a part of and can negatively affect human health. These contaminated microplastics originate in industrialized areas and spread out from there.

Microplastics when exposed under solar light irradiation have been shown to produce contaminants (Zhu et al., 2019). Microplastics such as polystyrene and phenol-formaldehyde are shown to produce environmentally persistent free radicals. These contaminants are shown to be significantly toxic towards organisms.

Microplastics are a new part of this world and due to this there is still intensive research into them as any long-term issues are yet to be established. An adult human has been noted to consume as much as 50,000 microplastics each year. As yet no adverse effects have been noted. The microplastics have so far been found unharmed to animals as they pass cleanly through the digestive tract unlike larger plastics, which kill by blocking the digestive

tract. There are still many things we do not know about the long-term effects of microplastics within our environment as such. It is right that this area of research should be of interest to the scientific community.

Scientific research question

The research questions this experiment intends to answer is what the concentrations of the microplastics of Lizard Island beaches is and do the concentrations vary as you move up the shoreline.

Scientific hypothesis

My scientific hypothesis for the density of microplastics in the beaches of Lizard Island is that the samples further away from the shoreline will have less microplastics in them compared to those closer to the shoreline.

Methodology

Due to Lizard Island being a National Park, obtaining permission to acquire samples was needed before any sample could be taken. This involved talking to the head researcher at the Lizard Island research facility and discussing whether permission could be obtained.

The sampling strategy used for this project is to take 4 separate samples from each of the 6 beaches visited (See Figures 1 and 2). The first sample is water taken from the water's edge. The second sample is taken off the sand from 1 metre from the shoreline, then from 2 and 3 metres (See Figure 3).



Figure 1: One of the beaches sampled

Samples were collected in small plastic containers and labelled according to the beach and distance from the water (Figure 4).



Figure 2: Lizard Island map with locations of beaches sampled
After: Google Maps

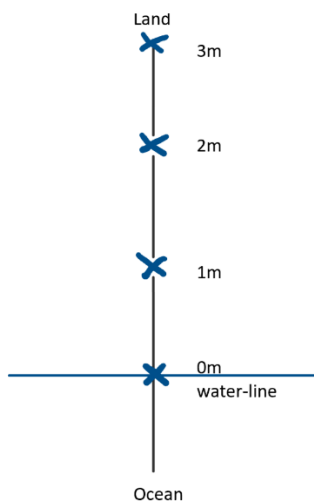


Figure 3 Transect line demonstrating location of sampling.

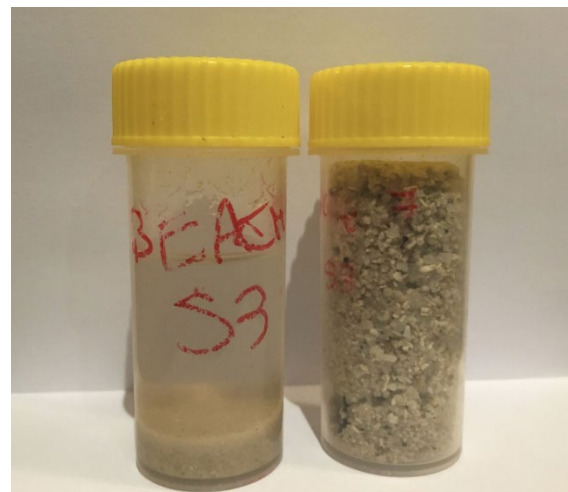


Figure 4: Samples collected from Lizard Island

Initially the ferro fluid method was used to extract the microplastics from the water. This method involved putting oil into the water which bonded with the microplastics. Then you placed in magnetite into the water as it would then bond with the oil. Due to the magnetite’s magnetic properties you can pull this fluid out of the water using a magnet bringing the plastics with it. This method while successful at removing the microplastics from the water didn’t help in counting the microplastics which was the intended goal of the experiment, so the method was scrapped and replaced with the current one (Fierra, 2019).

The experiment had two separate methods; one was used to turn the sand samples into water samples allowing all the samples to be the same type and the second was used to count the amount of microplastics within the water samples.

The method for extracting microplastics from sand into water samples started by placing 30 grams of sand into a beaker which was then filled with saline water until there was an excess of 10 millilitres of water sitting on top of the sand. The solution was then churned and left to sit for 15 minutes after which the water layer was extracted from the beaker creating a new water sample. This process was repeated for all the sand samples.

The method for finding microplastics in the water started by pouring the water samples into a see-through container which was then placed under a light microscope. The samples were then slowly looked through and all microplastics were recorded. This was then repeated for all the samples.

Results

The results of this test are shown in (Table 1) and show the amount of microplastics found in each sample, where they are located from the shore and which beach they are from. The results are also averaged along the distance from the shoreline. These results gathered for this experiment shown in (Table 1) when used within an ANOVA test (Table 2) that there is a significant result from the ANOVA performed on the microplastic counts of all sample types. The results are also averaged across the beaches which shows an estimate of the amount of microplastics per 30 grams of sand for each beach (Table 3). Figure 1 shows the transect lines used in all location on Lizard Island. Figure 3 shows the beaches the samples are gathered from.

Table 1: Count of microplastics recorded from each sample

Beach	Distance from water (m)			Water
	3	2	1	
1	2	3	4	5
2	1	2	2	4
3	2	3	2	3
4	2	2	3	4
5	1	4	3	5
6	1	3	2	4
Mean	1.5	2.8	2.7	4.2
Std dev	0.5	0.8	0.8	0.8

Table 2: Results of ANOVA test, the f-ratio value is 13.62434. The p-value is 0.000045. The result is significant at $p < 0.05$

Source	SS	df	MS
Between treatments	21.4583	3	7.1528
Within treatments	10.5	20	0.525
Total	31.9583	23	

Table 3: Approximate average microplastics for a 30g of sand

Beach	Average microplastics count for 30g of sand
1	3.50
2	2.25
3	2.50
4	2.75
5	3.25
6	2.50

Discussion

The issue of microplastics is a new focus within the scientific community as they have spread throughout the globe. The focus of this experiment was to test the beaches of Lizard Island and evaluate the concentrations of the microplastics within the different beaches of the island as well as their locations on the beach itself.

These samples were then converted into water samples using the first method. The results provided from the second method when analysed showed that this concentration of microplastics leads to a rejection of the null hypothesis as the resulting P values from the ANOVA test shown in (Table 2) was 0.000045 which is less than 0.05. This rejection of the null hypothesis results in an acceptance of the hypothesis being correct as there is a significant difference between the samples 3 metres from the water’s edge and those from the water itself. I

also performed a t-test on the results between 3 metres and 1 metre away from the water and 3 metres away from the water and the water itself both of which resulted in rejections of the null hypothesis and accepting the hypothesis with P values of 0.015656 this shows that with just a comparison of two of the four distances you can see that the hypothesis was correct.

The data was used to create an approximation of the amount of microplastics within 30 grams of sand for each of the beaches (Table 3). This gives an idea of the total amount of microplastics present on the beaches.

The method used was quite simplistic and was able to be used as the sample size was small. The review on measuring microplastic methods done by Mai et al., (2018) was helpful in the creation of this method as Mai outlined the ways to properly identify the microplastics within the different common sources as a standardisation. Their report stated that 'visual sorting should be combined with chemical composition analysis'. This would allow the ability to identify which types of microplastics are the key issue, allowing tracing of their source. As my intent was just to measure the amount of microplastics rather than their types the chemical processing wasn't needed.

This approximation is where the biggest limitation of the experiment is as only one sample was tested from each location at each beach, leading to the experiment itself being unreliable since each data point could be an outlier. This limitation in gathering data was due to the limit of the number of samples we were permitted to take as the Island itself is a national park we had to get a scientific research permit which only allowed for a few samples to be taken. For future experiments of a similar manner it would be best to take many more samples as the more taken from each location, the more accurate the experiment will be.

Another limitation that was a part of this experiment was the process documented the amount of microplastics within the samples. The documentation process for the samples was looking under a microscope and counting the few microplastics in the water samples. This can lead to missing or recounting previously documented plastics as they could have been moved around within the sample as they were being recorded.

Other scientific studies such as (Simeonova & Chuturkova, 2019) have also investigated the

microplastic concentration of the Bulgarian coast of the Black Sea. This study is similar to this as it is intended to document the amount of microplastics within an area so that further research can be made, and actions taken if deemed necessary.

The study done by (Kroeze et al., 2016) was another example of documenting the concentrations of microplastics within aquatic environments as Kroeze investigated the surface water concentrations of pollutants. Pollutants include microplastics, so getting an understanding of the way they are documented helped understand how to document microplastics and the goals of doing so. Looking into these concentrations Kroeze was able to create a global model of the concentrations of surface level pollutants. This was done to give an approximation of the level of severity of polluted areas allowing for areas of high concentration to be found and dealt with.

Future research into the microplastic concentrations in the beaches of Lizard Island can look toward comparing the concentrations of microplastics from Lizard Island and of other islands off the shore of Queensland's coast. This study will give a broader idea of the microplastic levels within the islands of the Great Barrier Reef.

Conclusion

The experiment that was conducted has analysed the recorded data from the samples taken at Lizard Island and has used them to create approximations of the concentrations of microplastics at different levels along the beaches and the approximation of microplastics within 30 grams of sand within each beach. These approximations have given an image to the pollution of microplastics within the Island and allowed a recording of this data to be used in further studies within the topic. The microplastic concentrations within the Island is currently considered as a pollutant but the microplastics are still an unknown in terms of their effects. These results will allow scientist to be able to make informed decisions about the environment of Lizard Island's beaches for future studies.

Acknowledgements

I would like to thank Dr Gates for her assistance in the process of writing the report as well as helping with the initial idea processing. I would also like to thank Lainie and Samuel Kalnins as they assisted in finding relevant papers and referencing them.

References

- Estahbanati, S. and Fahrenfeld, N.L. 2016. Influence of wastewater treatment plant discharges on microplastic concentrations in surface water. *Chemosphere*, 162, pp.277-284. doi: 10.1016/j.chemosphere.2016.07.083.
- Fierra F. 2019. An investigation into the removal of microplastics from water using ferrofluids. (n.d.). Retrieved February 9, 2020, from <https://www.googlesciencefair.com/projects/2018/2c3f6207b15f46cb4bb66a56095bd6d901ccfa42e7e51600c766df7856590c4e#beginning>.
- Kooi, M., Besseling, E., Kroeze, C., Van Wezel, A.P. and Koelmans, A.A., 2018. Modeling the fate and transport of plastic debris in freshwaters: review and guidance. In *Freshwater microplastics* (pp. 125-152). Springer, Cham.
- Kroeze, C., Gabbert, S., Hofstra, N., Koelmans, A.A., Li, A., Löhr, A., Ludwig, F., Stokal, M., Verburg, C., Vermeulen, L. and van Vliet, M.T. 2016. Global modelling of surface water quality: a multi-pollutant approach. *Current Opinion in Environmental Sustainability*, 23, pp.35-45.
- Lebreton, L. and Andrady, A., 2019. Future scenarios of global plastic waste generation and disposal. *Palgrave Communications*, 5(1), pp.1-11.
- Mai, L., Bao, L.J., Shi, L., Wong, C.S. and Zeng, E.Y. 2018. A review of methods for measuring microplastics in aquatic environments. *Environmental Science and Pollution Research*, 25(12), pp.11319-11332. <https://link.springer.com/article/10.1007/s11356-018-1692-0>.
- Siegfried, M., Koelmans, A.A., Besseling, E. and Kroeze, C., 2017. Export of microplastics from land to sea. A modelling approach. *Water Research*, 127, pp.249-257.
- Simeonova, A. and Chuturkova, R. 2019. Marine litter accumulation along the Bulgarian Black Sea coast: categories and predominance. *Waste Management*, 84, pp.182-193. doi: 10.1016/j.wasman.2018.11.001.
- Verla, A.W., Enyoh, C.E., Verla, E.N. and Nwarnorh, K.O. 2019. Microplastic-toxic chemical interaction: a review study on quantified levels, mechanism and implication. *SN Applied Sciences*, 1(11), p.1400. doi: 10.1007/s42452-019-1352-0.
- Windsor, F.M., Durance, I., Horton, A.A., Thompson, R.C., Tyler, C.R. and Ormerod, S.J., 2019. A catchment-scale perspective of plastic pollution. *Global change biology*, 25(4), pp.1207-1221.
- Zhu, K., Jia, H., Zhao, S., Xia, T., Guo, X., Wang, T. and Zhu, L. 2019. Formation of environmentally persistent free radicals on microplastics under light irradiation. *Environmental Science & Technology*, 53(14), pp.8177-8186. doi: 10.1021/acs.est.9b01474.

Microplastics in the Gastrointestinal Tract of Prawns from Vietnam compared to Australia

Yana McTeigue

Barker College

Microplastic contamination in seafoods has become a huge issue for marine life and human health. Microplastics are small particles of plastic smaller than 5mm which can be formed by the degradation of larger plastic or can be purposely manufactured to a small size. Microplastics themselves have not yet been known to cause harm to the human body, however microplastics can absorb heavy metals and toxins which can be released into the body causing illness. A method of quantitative analysis was employed with a sample which contained the gastrointestinal contents of Vannamei prawns from Vietnam and Tiger prawns from Australia. These samples were put under a microscope and displayed that there was significantly more microplastics in the Vietnamese prawn sample. Vietnam has about 730,000 tonnes of plastic enter their oceans compared to Australia with approximately 130,000 tonnes. A t-test was used as a form of statistical analysis to compare and display that there was significantly more microplastics found in the samples of Vietnamese prawns.

Literature review

Microplastics are small plastic pieces less than 5mm long which can be harmful to marine and aquatic organisms (NOAA, 2012). Microplastics are the most abundant items of plastic debris in the marine environment and will inevitably increase as large plastic items ultimately get degraded into millions of microplastic pieces (Law and Thompson, 2014). Microbeads are intentionally made microplastics that pass unchanged through the water ways and into the ocean (NOAA, 2012). Aquatic life and birds can mistake microplastics for food. In 2015, the US banned the use of microbeads (NOAA, 2012). Microplastics are not a recent problem, but there is still so much unknown about them.

Plastic pollution has negative effects on the ocean and wildlife health. High income countries generate more plastic waste per person, however the management of this waste varies with high income countries having better waste management and middle to lower income countries with poor waste management (Plastic Ethics, 2019; Ritchie & Roser, 2018; VnExpress International, 2019). It is estimated that 20% of the plastic waste in oceans come from marine waste (e.g. fishing nets, ropes, lines, etc.) (Barboza et al., 2018; Andrady, 2011). Microplastics are a particular concern to the environment due to their small size which a range of organisms can

ingest from which physical and toxicological harm may arise (Law & Thompson, 2014; Wright et al., 2013). Ingestion can cause chronic illness in marine life due to microplastic build up in cells and tissues (Sharma & Chatterjee, 2017). Potential hazards of human ingestion include alteration of chromosomes which can lead to infertility, obesity and cancer (Sharma & Chatterjee, 2017).

It is unclear about how microplastics can affect human health. Microplastics were found in faecal samples in a study of how humans inadvertently consume plastic (National Geographic, 2018; Akhbarizadeh et al., 2019). A study in the journal environmental Science and Technology says it's possible that humans may be consuming from 39,000 to 52,000 microplastic particles per year (Gibbins, 2019). With additional estimated to the amount of inhaled microplastics, that equates to more than 74,000 particles.

Since microplastics are associated with chemicals from manufacturing, there is a concern surrounding the physical and chemical toxicity absorbed by microplastics (Carbery et al., 2018). Microplastics contain an average of 4% of additives and the plastic can also absorb contaminants which can be either of organic or inorganic nature. Toxicity and toxicokinetic data are lacking for microplastics for a human risk assessment (EFSA, 2016).

Evidence regarding microplastic toxicity and epidemiology is emerging, as well as further research as to its potential implications on human health (Smith et al., 2018).

Multiple studies have investigated microplastic contamination in shrimp or prawns as examples of edible aquatic crustaceans.

In a recent study, Hossain et al. (2020) examined the microplastic content in the gastrointestinal tract of brown prawns and tiger prawns from the shallow and offshore waters of the Northern Bay of Bengal, Bangladesh. There was a total of 33 (tiger prawns) and 39 (brown prawns) microplastics found out of 10 tiger prawns and 20 tiger prawn. The types of microplastics most dominant were filament and fibres. The results of this investigation display microplastic contamination in seafood in Bangladesh.

Scientists have found thousands of microplastic particles in prawns from the deepest part of the ocean, the Mariana Trench (Griggs, 2019). Griggs (2019) found circular beads, fibres and other pieces of microplastics in every sample. Prawns are filter feeds, which suggests that the amount of microplastics in the gastrointestinal tract and stomach contents will reflect the abundance of microplastic pollution from their origin.

In order to measure microplastics contamination of shrimp, Green-Gavrielidis (2019) describes how researchers mixed a solution of microfibrils and microbeads which were dyed with a fluorescence and mixed with shrimp food and placed it with shrimp. After the food had been consumed, they extracted the fish and saw the microplastics through the flesh as Dutch shrimp are translucent. The shrimp would pass on the microplastics small enough for the digestive system, the larger microplastics were regurgitated.

Scientific research question

Do Australian grown prawns contain less microplastics in their gastrointestinal tract than Vannamei prawns imported from Vietnam?

Scientific hypothesis

That Vannamei prawns from Vietnam will contain more microplastics in their gastrointestinal tract than tiger prawns from Australia.

Methodology

Two 1kg parcels of prawns were purchased from Coles supermarket. One packet contained cooked Australian farmed prawns and the other contained cooked Vietnamese prawns. From these samples, 12 prawns were selected of approximately uniform size as a controlled variable. The prawns were peeled and the gastrointestinal tract was dissected out and laid on a cutting board. Then 1cm was measured and cut from the end from the end of the tract and placed into a vial. This was repeated four times for 1 vial and three more vials were made. This process was then repeated to create two more vials from each prawn parcel.

Using a 100ml measuring cylinder, 20mls of 30% hydrogen peroxide was measured and then added into each vial. The vials were then put into the incubator at 40 degrees Celsius and left for 72 hours. After 72 hours, the samples were taken from the incubator and 20mls of saline solution was added into each sample with a 20ml pipette. This was then left for five days with the vial caps ‘half-screwed’ on to prevent gas build-up.

A 1ml pipette was used to extract a drop of water which was placed on a slide and a cover slip was placed over it. The slide was placed under a microscope at 100X and three random field of view were discovered and the amount of microplastics were counted in each and recorded.

These steps were repeated for the other prawn country of origin.

Results

Table 1: Count of microplastics for Australian prawns for each field of view (FOV)

Slide	Count FOV 1	Count FOV 2	Count FOV 3	Average
1	4	2	3	3
2	4	2	3	3
3	2	2	1	1.7
Average				2.6

Table 2: Count of microplastics for Vietnamese prawns for each field of view (FOV)

Slide	Count FOV 1	Count FOV 2	Count FOV 3	Average
1	10	5	11	8.7
2	6	3	5	4.7
3	2	3	3	2.7
Average				5.3

Each result was obtained by looking three random fields of view under a microscope at 100X. The microplastics were counted if they were fibrous, round or fragmented.

In the Australian Tiger prawns, the total average of microplastics was calculated to be 2.555 per 100X field of view.

In the Vietnamese Vanemi prawns, the total average of microplastics was calculated to be 5.33333 per 100X field of view.

In both slides, a limitation of observing the microplastics were the many bubbles trapped under the cover slip and the smudges on the cover slip. To minimise limitations, coverslips were cleaned as best possible and cover slip was placed gently to minimise bubbles.

Statistical analysis of results

A t test was used to compare the means of treatment 1 (Australian tiger prawns) and treatment 2 (Vietnamese Vannamei prawns). The null hypothesis is that there is no significant difference between the amount of microplastics in prawns from Vietnam compared to Australia. The alternative hypothesis is that there is a significant difference between the amount of microplastics in prawns from Vietnam compared to Australia. The statistical test for these results would be a two-tailed t-test. In this case, the alpha value chosen was 0.1 or 10% as there is minimal consequence of attaining a false positive.

Table 3: Two-tailed t-test.

Value Type	Determined Value
Alpha Value	0.100
T-statistic	1.542
P-Value	0.099
A	0.1

Discussion

Microplastics are small particles of plastic that are smaller than 5mm. There are two types of microplastics; primary and secondary. Primary microplastics are microplastics that have been manufactured to be a small size, whereas secondary microplastics are plastics which have been broken down into small pieces. During this investigation, the microplastics mostly consisted of fibres and fragments.

To find the amount of microplastics, three fields of view were randomly selected in each slide, with three replicants. These samples field of views were seen at 100X. In the Tiger prawns there was an average of 2.6

microplastics in a 100X field of view. In the Vannamei prawns there was an average of 5.3 microplastics in a 100X field of view. Therefore, the hypothesis that Vannamei prawns from Vietnam will contain more microplastics in their gastrointestinal tract than tiger prawns from Australia is accepted.

A statistical analysis of the results was conducted and it was found that the p-value was less than the alpha value which means that the null hypothesis (that there was not a significant difference between the amount of microplastics in Australian prawns compared to Vietnamese prawns) was rejected. This mean that the alternative hypothesis could be accepted which stated that there was a significant difference between the amount of microplastics in Australia compared to Vietnam.

Approximately 130,000 tonnes of plastic enter Australia's oceans each year, whereas approximately 730,000 tonnes of plastic enter Vietnam's oceans each year. This explains why there were more microplastics in the Vannamei prawns than the tiger prawns. Figure 1 shows that Vietnam is fourth in the world for the most plastic pollution.

The hypothesis that Vannamei prawns from Vietnam will contain more microplastics in their gastrointestinal tract than prawns from Australia was tested by this experiment. The experiment extracted contents of the gastrointestinal tract and was processed to be able to observe the abundance of microplastics under a microscope.

A difficulty encountered while performing the experiment was counting the amount of microplastics in a field of view. A guideline was followed that only round, broken or fibrous pieces were counted. An initial experiment of using Nile red dye was first attempted, however the Nile red's fluorescence could not be seen without UV lenses on the microscope. Therefore, the method had to be altered to suit the resources provided.

A limitation of this experiment is that there were not the same prawn types in both countries so with prawn could digest differently than the other, however the most similar prawns were chosen for the experiment.

The results obtained were not consistent as there was a random selection of searched area. However, there was consistency with the Australian prawns having less

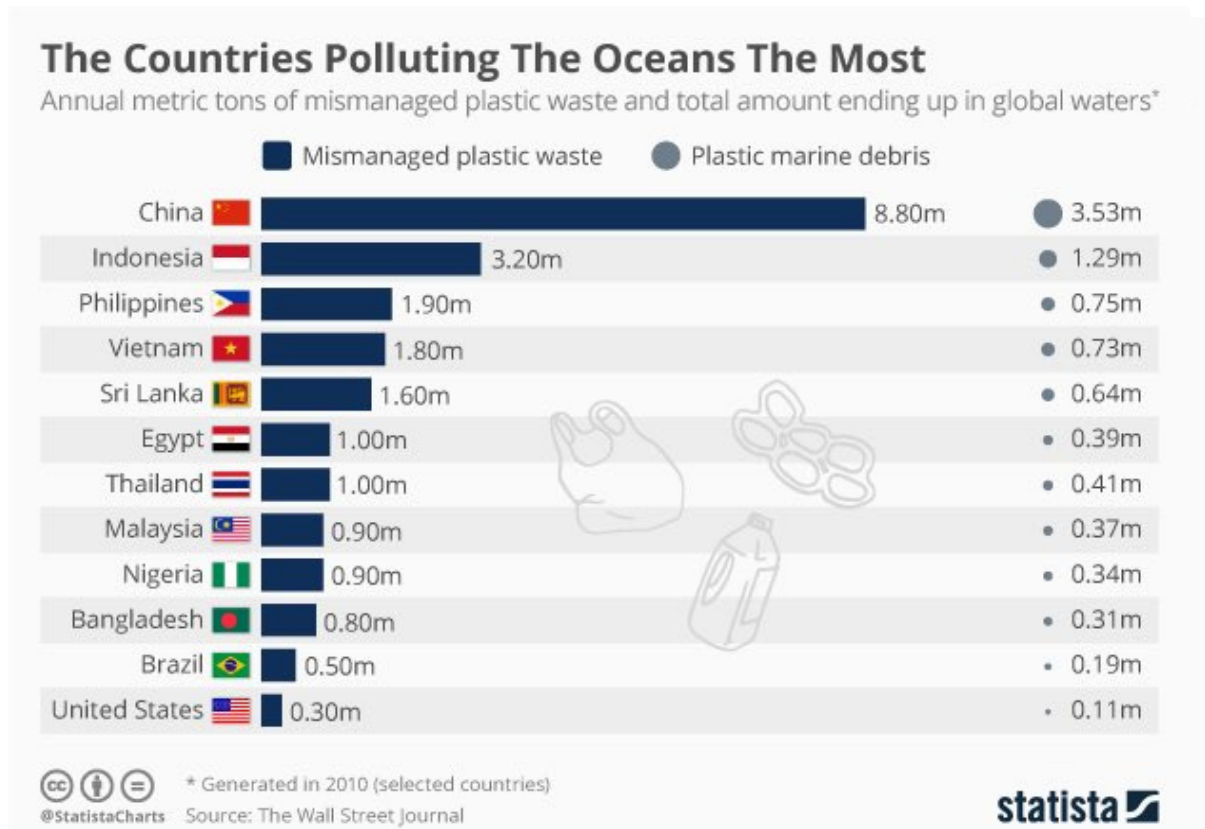


Figure 1: Graph comparing plastic pollution from various countries including Vietnam and surrounding nations. Source: Plastic ethics, 2019

microplastics than the Vannamei prawns. The results were reliable as we conducted a double-blind trial, this is where the experimenter did not know which prawn was which species. This allowed for reduced bias. These results are reliable as there were three sample replicants.

To improve the experimental design, a digital plastic identification machine would provide a more accurate reading of the sample and would be able to use the whole sample rather than a drop of the solution. Or a microscope with UV lenses would be useful to be able to identify microplastics using the ‘Nile Red’ dye.

For future scientific research, ideas should be explored for ways to eradicate plastic and microplastics from the ocean as it is harming wild life and humans as the microplastics can make its way into meals.

Conclusion

This investigation explored a comparison between the microplastic content of Australian Tiger prawns and Vietnamese Vanemi prawns. A statistical analysis of a t-test was used to show that there was significantly more microplastics found in the Vietnamese prawns than the Australian prawns. Therefore, the alternative hypothesis was accepted and the null hypothesis was rejected. This

evidence suggests that there is a significant amount of plastic pollution in the oceans off Vietnam. This is concerning as microplastics can cause harm to animals and humans. In further research, more countries should be compared to the microplastic content in Australia’s prawns. As well as creating ways to eliminate/reduce the amount of microplastics in the ocean.

Acknowledgements

Thank you to Dr Gates for supporting me throughout the project. Thank you for sharing ideas, giving up your time and guiding the research. Thank you to Dr Hill and Dr Terrett for assisting in answering questions through the process.

References

Akhbarizadeh, R., Moore, F. and Keshavarzi, B. (2019). Investigating microplastics bioaccumulation and biomagnification in seafood from the Persian Gulf: a threat to human health? Food Additives & Contaminants: Part A, 36(11), pp.1696–1708.

Andrady, A.L. (2011). Microplastics in the marine environment. Marine Pollution Bulletin, 62(8), pp.1596–1605.

- Barboza, L.G.A., Dick Vethaak, A., Lavorante, B.R.B.O., Lundebye, A.-K. and Guilhermino, L. (2018). Marine microplastic debris: An emerging issue for food security, food safety and human health. *Marine Pollution Bulletin*, 133, pp.336–348.
- Carbery, M., O'Connor, W. and Palanisami, T. (2018). Trophic transfer of microplastics and mixed contaminants in the marine food web and implications for human health. *Environment International*, 115, pp.400–409.
- Gibbens, S. (2019). You eat thousands of bits of plastic every year. [online] Nationalgeographic.com. Available at: <https://www.nationalgeographic.com/environment/2019/06/you-eat-thousands-of-bits-of-plastic-every-year/>.
- Green-Gavrielidis, L. (2019). Surviving in the age of microplastics: the tale of a curious shrimp. [online] envirobites. Available at: <https://envirobites.org/2019/09/13/surviving-in-the-age-of-microplastics-the-tale-of-a-curious-shrimp/> [Accessed 2 Jul. 2020].
- Griggs, M.B. (2019). Hunting for microplastics in your seafood. [online] The Verge. Available at: <https://www.theverge.com/2019/10/22/20925449/microplastic-s-seafood-shrimp-trial-and-error-verge-science> [Accessed 2 Jul. 2020].
- Hossain, M.S., Rahman, M.S., Uddin, M.N., Sharifuzzaman, S.M., Chowdhury, S.R., Sarker, S. and Nawaz Chowdhury, M.S. (2020). Microplastic contamination in Penaeid shrimp from the Northern Bay of Bengal. *Chemosphere*, [online] 238, p.124688.
- Law, K.L. and Thompson, R.C. (2014). Microplastics in the seas. *Science*, [online] 345(6193), pp.144–145. Available at: <http://science.sciencemag.org/content/345/6193/144>.
- National Geographic. (2018). We Know Plastic Is Harming Marine Life. What About Us? [online] Available at: <https://www.nationalgeographic.com/magazine/2018/06/plastic-planet-health-pollution-waste-microplastics/#:~:text=Experiments%20show%20that%20microplastics%20damage>.
- Presence of microplastics and nanoplastics in food, with particular focus on seafood. (2016). *EFSA Journal*, [online] 14(6).
- Ritchie, H. and Roser, M. (2018). Plastic Pollution. [online] Our World in Data. Available at: <https://ourworldindata.org/plastic-pollution>.
- Sharma, S. and Chatterjee, S. (2017). Microplastic pollution, a threat to marine ecosystem and human health: a short review. *Environmental Science and Pollution Research*, [online] 24(27), pp.21530–21547.
- Smith, M., Love, D.C., Rochman, C.M. and Neff, R.A. (2018). Microplastics in Seafood and the Implications for Human Health. *Current Environmental Health Reports*, [online] 5(3), pp.375–386.
- Socscistatitics.com. (2019). *T-Test Calculator for 2 Independent Means*. [online] Available at: <https://www.socscistatitics.com/tests/studentttest/default2.aspx>.
- The countries polluting the oceans the most with plastic waste — Plastic Ethics (2019). *Plastic Ethics*. [online] Plastic Ethics. Available at: <https://www.plasticethics.com/home/2019/3/17/the-countries-polluting-the-oceans-the-most-with-plastic-waste>.
- US (2012). What are microplastics? [online] Noaa.gov. Available at: <https://oceanservice.noaa.gov/facts/microplastics.html>.
- VnExpress (n.d.). Vietnam plastic waste problem goes from bad to worse - VnExpress International (2019). [online] VnExpress International – Latest news, business, travel and analysis from Vietnam. Available at: <https://e.vnexpress.net/news/news/vietnam-plastic-waste-problem-goes-from-bad-to-worse-3978124.html#:~:text=Vietnam%20annually%20produces%201.8%20million> [Accessed 2 Jul. 2020].
- Wright, S.L., Thompson, R.C. and Galloway, T.S. (2013). The physical impacts of microplastics on marine organisms: A review. *Environmental Pollution*, 178, pp.483–492.

The effect of temperature and salinity on the growth of *Anabaena*

Jed Tomlinson

Barker College

Eutrophication is a natural environmental process caused by rapid increases in nutrients in water ways causing algal blooms which smother, poison and kill plants and animals. In Australia, species of cyanobacteria, commonly known as ‘blue green algae’, are often responsible for these environmentally devastating events. This experiment intended to explore the impact of salinity and temperature on the growth of a filamentous cyanobacteria, *Anabaena*. However, the COVID-19 shutdown interrupted the culturing phase of the *Anabaena* which meant that the *Anabaena* suffered environmental stress (through lack of nutrients and/or evaporation) and developed akinetes, a natural adaptation to environmental stress. As a result, this experiment tested the impact of variations in ambient temperature and salinity on the akinete form of *Anabaena*. It was shown that temperature and salinity had no visible effect on the number of akinetes in the sample.

Literature Review

Cyanobacteria are a variety of algae in the family Cyanobacteriaceae (Komárek, 2014) more commonly referred to as ‘blue green algae’. While algae are unicellular photosynthetic organisms cyanobacteria are multi-cellular forming large cooperative colonies (Rachita, 2014). *Anabaena* are a common genus of cyanobacteria which belong to the order Nostocales. They have a simple body plan requiring little more than water, carbon dioxide, some inorganic substances and light to survive and proliferate (Mur, Skulberg & Utkilen, 1999).

Anabaena form long chain like filaments along which cells perform various functions. They include heterocysts which fix nitrogen which can be used to produce proteins and DNA (Haselkorn, 1978) and akinetes which enter a state of suspended animation allowing them to survive adverse conditions for a number of months or years (Sukenik et al., 2013). These abilities have allowed cyanobacteria to persist in most environments for over 2.45 billion years (Rasmussen et al., 2008). These filamentous structures and specialized cells can be seen in Figure 1.

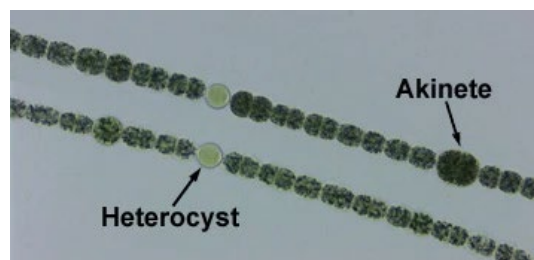


Figure 1: *Notocales* filament
Source: Soilage, 2020

This ability to survive in a wide range of environments, ecosystems and conditions has made cyanobacteria one of the most successful organisms in Earth's history. They proliferate in most fresh waterways and coastlines across the world (Mur, Skulberg & Utkilen, 1999) including those in Australia. However, cyanobacteria are notorious, not for their ability to survive in most aquatic environments, but instead for the negative impacts they have on the environment.

Eutrophication is the rapid multiplication of algae as a result of increased nutrients. This may be caused by natural events or seasonal change, natural disasters (storms, drought etc.) or by human causes such as industrial or agricultural runoff and other human pollutants (Carpenter et al., 1998).

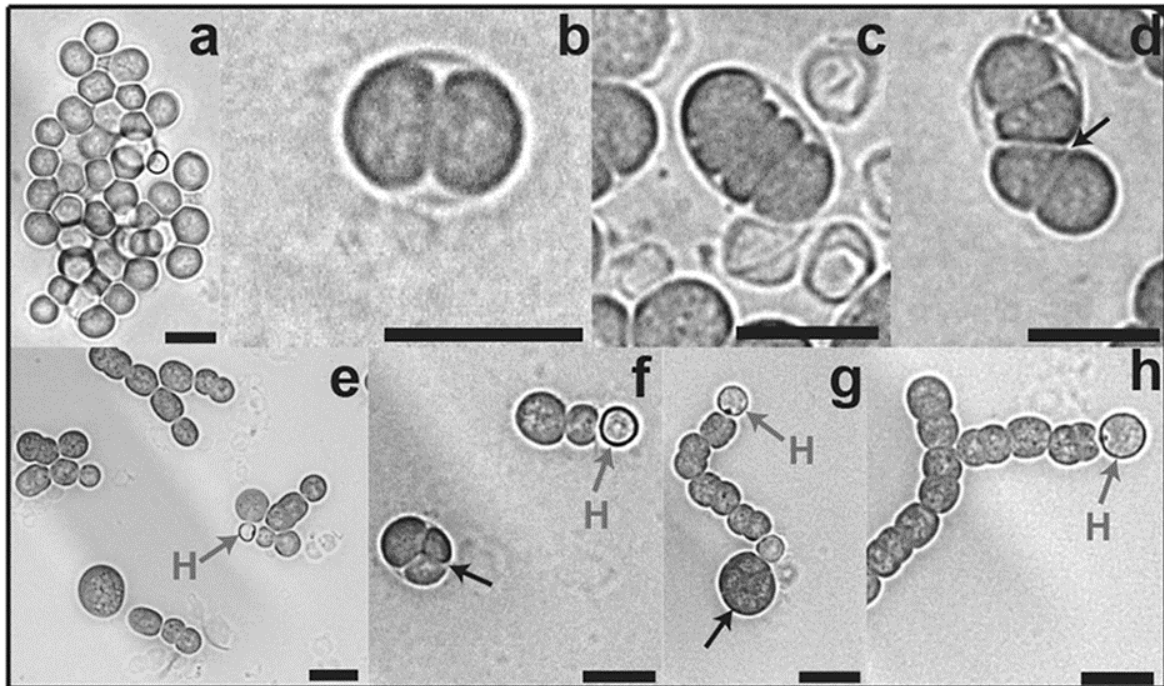


Figure 2: Multiplication of *Anabaena* from akinetes
Source: Perez et al., 2018

Cyanobacteria are one of the organisms commonly involved in eutrophication events. They can release deadly toxins into the water which kill animals, other microbes and plant life (Sivonen & Jones, 1999) as well as blocking out sunlight killing aquatic plants and using up oxygen in the water. These cause chain reactions to occur, a collapse in the food web and a loss of biodiversity in the local aquatic and terrestrial environment (Pretty et al., 2003).

Eutrophication has been known to occur due to rapid changes in salinity and temperature such as in 2019 when extreme weather and low water flow caused a eutrophication event that killed tens of thousands of native fish in the Murray Darling basin (Anne, 2019). This has been intensified due to climate change (Suikkanen et al., 2013), human activity such as irrigation, damming, dry land salinity, farm runoff, human pollution and deforestation (Goss, 2003).

Predicting eutrophication events has become increasingly important in Australia. More data is required on the conditions under which eutrophication occurs and salinity and temperature are two of the variables likely to be important. Therefore, this research aims to explore whether an increase in temperature allows cyanobacteria to better tolerate high salinities. In doing so it is hoped that more accurate predictions for eutrophication events may be made and more ways of managing such ecological disasters may be developed.

Goss (2003) describes Australian water ways such as the Murray Darling as varying greatly in temperature and salinity levels across the year and even in different parts of the river. Temperatures can vary across the year from a 9°C to 25°C, salinity can at times even exceed those found in the ocean (33-35ppt). Environmental flows are an ideal method to mitigate and prevent eutrophication in rivers (Glenn, 2017) as they flush away nutrients, dilute water (preventing buildup of salt) and introduce new oxygen.

Predictions of eutrophication events has become increasingly important in Australia especially for the Murray Darling as it supplies a great deal of water across South Eastern Australia. Too many environmental flows can, however, reduce the amount of water for human activities, too few can lead to eutrophication, which will spoil the river water and damaging the local environment.

It is well documented that increases in nutrients, more specifically potassium, is the major cause of eutrophication due to its importance in photosynthesis (Checchetto et al., 2012) and its ability to "re-awaken" dormant akinetes (Suikkanen et al., 2013). However, to produce more accurate predictions we need more data on the impact of temperature and salinity of cyanobacteria growth. Glenn (2007) explored the salt tolerance of typical cyanobacteria in reservoirs however, the research did not consider how temperature may affect cyanobacteria's salt tolerance. Figure 2 shows the

process by which Nostocales ‘re-awaken’ from their dormant akinetes.

This research aims to fill this gap of knowledge to enable a deeper understanding about the role of temperature and salinity in the growth of *Anabaena*. This could lead to further research enabling more accurate predictions and counter measures against cyanobacteria eutrophication. *Anabaena* are notoriously difficult to grow under laboratory conditions due to their strict growth conditions so the study will rely heavily on Castenholz’s (1988) methods for culturing cyanobacteria in order to produce ideal samples for laboratory experimentation.

Scientific research question

What effect does temperature have on the growth and proliferation of cyanobacteria at different salinities?

Scientific hypothesis

The number of filaments of *Anabaena* will decline in response to increasing ambient temperature and increased salinity.

Methodology

Growing out *Anabaena* culture:

Two 6ml vials of *Anabaena* sp. were purchased from Southern Biological and stored in a refrigerator as per manufacturer’s instructions. Two 200ml flasks of culture media specifically prepared for the *Anabaena* sp. were purchased from the same supplier.

When laboratory work commenced, the vials were brought to room temperature in a fume cupboard. The lip of the vials was sterilised using the flame of a Bunsen burner and both samples were decanted into an autoclaved conical flask containing 400ml the culture medium. Care was taken to follow aseptic technique. In order to prevent contamination of samples from an outside source gloves were worn and all surfaces within the fume cabinet were generously disinfected with alcohol. A gas flame in the fume cupboard provided a convection draft to further prevent contamination.

Once the culture was prepared, it was moved from the fume cupboard to a stirring incubator. The top of the conical flask was covered with a sterile filter paper to prevent contamination as it was brought out of the fume cabinet into a 25°C incubating hood with a shaking table. The table was set at 180rpm and a UVA+UVB grow light was positioned overhead and set on automatic timer to deliver 12 hours light and 12 hours darkness as can be

seen in Figure 3. The cyanobacteria were left to grow for 14 days.

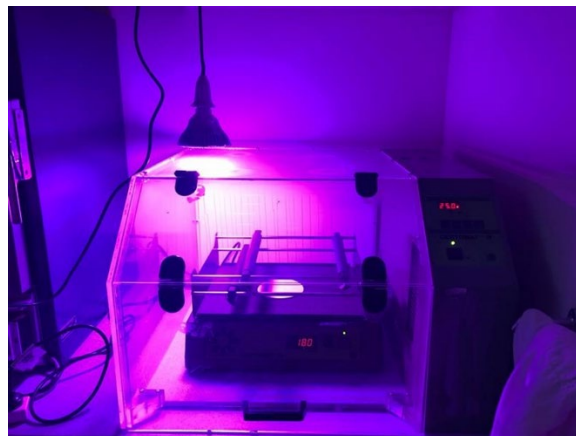


Figure 3: Incubation setup used during the experiment

During this 14-day period, the national Covid-19 shutdown occurred which meant that the school was closed and access to the laboratory space was prevented for a 6-week period. When school reopened, the *Anabaena* had visibly cultured the media (it was bright green) but the volume in the flask had evaporated by approximately half. This meant that there was insufficient volume for the experiment that was originally designed.

Furthermore, microscopic examination revealed that the *Anabaena* had consumed the food reserves in the media and had started to form individual spherical structures. These were later identified from photographs in various journal articles to be akinetes (Perez et al., 2018). Very few filaments were observed in the sample. At this point the experimental design was modified to work with a much reduced volume of sample.

Testing the effects of temperature/salinity on the growth of *Anabaena* culture:

Nine vials were filled with 5mL of *Anabaena* culture along with 5mL each of distilled water. They were divided into groups of 3 A, B and C. The labelling protocol that was used on the vials is described in Table 1.

Table 1: Locations of recorded groups on table

Salinity (ppt)	20°C	25°C	35°C
50.0	A	B	C
5.0	D	E	F
0.5	G	H	I
0.0	J	K	L

CG: 21.25

A brine solution was prepared according to the following method. 250mL of distilled water was heated on a magnetic stirring heat plate in an autoclaved Schott bottle until it began to boil. Salt was then dissolved in the heated mixture until the solution had been completely saturated. This was determined when the solution cooled, and a small amount of salt deposited on the bottom of the Schott bottle forming a brine of approximately 50 ppt. The brine was stored at room temperature.

5mL of the brine was added to nine more vials they were then filled with the 5mL of *Anabaena* culture. The vials were divided into groups of 3 D, E and F. 5mL of the brine was diluted with 95mL of distilled water forming a new solution of brine of concentration 5 ppt. 5mL of the diluted brine was added to 9 vials they were then filled with the 5mL of *Anabaena* culture. The vials were divided into groups of 3 G, H and I. 5mL of the diluted brine was diluted by a further 45mL of distilled water forming a new solution of brine of concentration 0.5 ppt. 5mL of the newly diluted brine was added to 9 vials they were then filled with the 5mL of *Anabaena* culture. The vials were divided into groups of 3 J, K and L.

Groups A, D, G and J were placed in an open plastic box. The box was placed in a 20°C well-lit room and left. Groups CG, B, E, H and K were placed in an open plastic box. The box was placed in a 25°C well-lit incubator and left. Groups C, F, I and L were placed in an open plastic box. The box was placed in a 35°C well-lit incubator and left.

Three vials capable of holding 15mL of liquid were filled with 10mL of undiluted *Anabaena* culture using a calibrated sterile pipettor and were labelled CG. These acted as a control group for the experiment.

After several days the vials were removed from the incubators (and room), examined under a light microscope and photographed (see Appendix 1). Cyanobacteria were counted using a 0.1 mm by 0.1 mm quadrat. Four quadrats were counted for each sample and an average was calculated. These values were recorded in a table and the average cyanobacteria counts to 2 decimal places for each group determined. The cyanobacteria were counted within four randomly selected quadrat squares of 0.1 mm by 0.1 mm.

Results

On observation of the sample, no filamentous strands of *Anabaena* were observed. It was determined from literature that the observed structures were akinetes. Therefore, the results reflect counts of the number of

akinetes that were present in each quadrat. Results of the experiment can be seen in Table 2.

The control group (CG) had an average value of 21.25. According to the data increases in temperature have no impact on the growth of the *Anabaena* with the results observed being random across all salinities. The growth of *Anabaena* ranged between 8 and 13. The results followed no obvious trends with the exception of column 35°C where increased salinity negatively influenced the growth of *Anabaena*.

Increases in salinity had no obvious impact on the number of akinetes other than in the aforementioned column 35°C. Columns 20°C and 25°C fell between 8 to 10 apart from the 5 ppt where both columns had greater numbers of *Anabaena* than any other salinity. However, without any trends to demonstrate why this occurred and re-affirm the validity of these values, they are most likely anomalies.

Table 2: Effect of temperature and salinity on growth

Salinity (ppt)	Average cyanobacteria counts		
	20°C	25°C	35°C
50.0	9.75	8.17	9.25
5.0	11.25	12	10.83
0.5	9.67	9.42	11.5
0.0	9.58	9.67	13

CG: 21.25

Discussion

In the natural environment increases in salinity often kill large populations of aquatic life as do rapid changes from low to high temperatures which force oxygen out of the water, suffocating fish. These two phenomena go hand in hand and often occur during droughts. The additional nutrients from the decay of these organisms contributes to eutrophication (Carpenter et al., 1998). What is remarkable is that though temperature and salinity kill most aquatic life, they leave the akinetes of *Anabaena* relatively unharmed (Tonk et al., 2007). When it came time to count the samples, no filaments could be observed as can be seen in Figure 4.

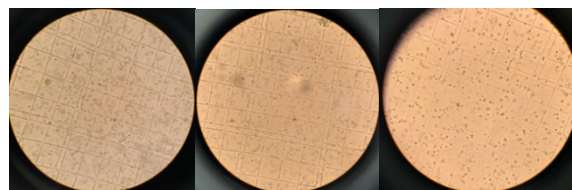


Figure 4: Akinetes observed during experiment

An increase in temperature seemed to have no impact on the number of akinetes of the *Anabaena* with the results observed being random across all salinities. They followed no obvious trends other than in column 35°C where increased salinity negatively influenced the count of *Anabaena*. It is unclear whether salinity had any part to play or whether this was an anomaly as no similar trends were observed in any other columns.

Columns 20°C and 25°C had *Anabaena* counts between 8 and 10 others than at 5 ppt where both columns had greater numbers of *Anabaena* than other salinity levels. However, without any trends to demonstrate why this occurred and reaffirm the validity of these values, they are also most likely anomalies. All the results collected were roughly half the value of the control group. Considering that the solutions of *Anabaena* were diluted by half this is unsurprising.

The formation of akinetes in the cultured sample prior to the application of the test conditions severely compromised the reliability of the study as it may have been that the *Anabaena* were unable to grow during the experiment. If the experiment shows anything, it demonstrated the impressive survival skills of *Anabaena*. The akinetes were able to survive all experimental conditions and survived for the best part of 6-weeks without a food supply.

The COVID-19 national shutdown was unprecedented and could not have been reasonably anticipated. In other research scenarios it would have been possible to recommence the experiment but owing to the school assessment schedule this was not possible. The presence of filaments within the sample was essential to the original experimental design and the formation of akinetes was unexpected. Checking the *Anabaena* for filament development regularly during the culturing process would have improved the protocol of this experiment.

Sukenik (2013) recommends that if akinetes are observed in the sample, the addition of potassium could "re-waken" the sample. However, the formulation and concentration of such an addition has not been tested. Scientist should also further investigate the remarkable survivability of Akinetes which was only touched upon by this experiment.

On the basis of this project, there are many directions for future research about *Anabaena*. The most obvious would be to complete the original experiment with intact filamentous strands and measure the impact on growth under different controlled conditions. Other factors and

their influences on their growth should be tested such as certain nutrients. Researchers could also consider experiments involving the resilience of akinetes as this experiment did not demonstrate that the various akinete samples were viable. Further investigations involving the reawakening of akinetes following treatment with high salinity and high temperatures would be worthwhile.

The most significant limitation of this research was that the capacity of the cyanobacteria to recover was not tested. Had time permitted, it would have been important to provide a potassium source and stimulate growth in the culture. Whilst it has been shown that the akinetes have not been diminished in number, and no visual damage was observed, it is unknown whether these akinetes remain viable and capable of further reproduction. This is now the domain of future research.

Due to the lack of any valid results the proposed hypothesis (that temperature influences the ability of *Anabaena* to mitigate the effects of high salinity) can neither be accepted or rejected without further experimentation. Instead, it has been possible to determine that the number of akinetes is unaffected by changes in temperature and salinity.

Conclusion

The purpose of this experiment was to determine whether temperature aids in the ability of *Anabaena* to manage high salinities. The experiment hoped to determine this by growing *Anabaena* in controlled conditions ranging from high to no salinity and with temperatures of 20°C, 25°C and 35°C. The experiment was designed to determine the effect of temperature on the growth of *Anabaena* at different salinities.

Due to unforeseen circumstances, and the lengthy and unforeseen culturing of the *Anabaena*, the original purpose of the experiment could not be achieved. The extended period of laboratory shutdown resulted in a significant environmental stress affecting the culture, even before the test conditions of salinity and temperature were applied. Instead of testing the response of *Anabaena* filaments to salinity and temperature, the effect of these variables on the number of akinetes was able to be tested. The experiment did demonstrate the resilience of akinetes to temperature and salinity variation.

Due to the lack of filamentous growth, the experimental design did not test the proposed hypothesis (that temperature influences *Anabaena*'s ability to mitigate the effects of high salinity). The hypothesis can thus neither

be accepted or rejected without further experimentation. It is hoped that future research will be conducted to give further insight into this hypothesis.

Acknowledgments

I would like to thank parents for proofreading my work. To Dr Hill for his helpful advice regarding my results and a special thank you to Dr Gates for her continual help throughout the experiment especially with organizing the experiment and maintaining high standards throughout my report.

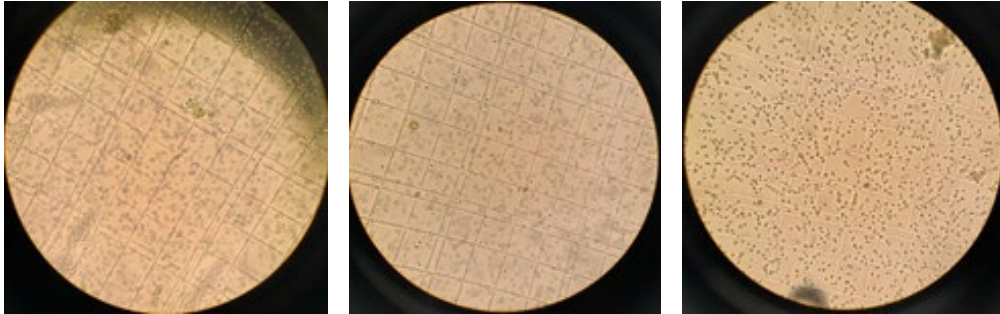
References

- Adams, D.G. and Duggan, P.S., 1999. Tansley Review No. 107. Heterocyst and Akinete differentiation in cyanobacteria. *The New Phytologist*, 144(1), pp.3-33.
- Anne, D., 2019. Murray-Darling fish kill: extreme weather and low river flow led to drop in oxygen levels. *The Guardian*, viewed 27 June 2020, <https://www.theguardian.com/australia-news/2019/jan/24/murray-darling-fish-kill-extreme-weather-and-low-river-flow-led-to-drop-in-oxygen-levels>.
- Capone, D.G. and Carpenter, E.J., 1999. Nitrogen fixation by marine cyanobacteria: historical and global perspectives. *Bulletin-institute oceanography Monaco-Numero special*, pp.235-256.
- Carpenter, S.R., Caraco, N.F., Correll, D.L., Howarth, R.W., Sharpley, A.N. and Smith, V.H., 1998. Nonpoint pollution of surface waters with phosphorus and nitrogen. *Ecological applications*, 8(3), pp.559-568.
- Castenholz, R. W. (1988). [3] Culturing methods for cyanobacteria. In *Methods in enzymology* (Vol. 167, pp. 68-93). Academic Press.
- Checchetto, V., Segalla, A., Allorent, G., La Rocca, N., Leanza, L., Giacometti, G.M., Uozumi, N., Finazzi.
- Francesca Scannone, 2016. What is eutrophication? Causes, effects and control. *eni school energy & environment*, viewed 27 June 2020, <https://www.eniscuola.net/en/2016/11/03/what-is-eutrophication-causes-effects-and-control/>.
- G., Bergantino, E. and Szabò, I., 2012. Thylakoid potassium channel is required for efficient photosynthesis in cyanobacteria. *Proceedings of the National Academy of Sciences*, 109(27), pp.11043-11048.
- Glenn, E.P., Nagler, P.L., Shafroth, P.B. and Jarchow, C.J., 2017. Effectiveness of environmental flows for riparian restoration in arid regions: A tale of four rivers. *Ecological Engineering*, 106, pp.695-703.
- Goss, K.F., 2003. Environmental flows, river salinity and biodiversity conservation: managing trade-offs in the Murray–Darling basin. *Australian Journal of Botany*, 51(6), pp.619-625.
- Haselkorn, R., 1978. Heterocysts. *Annual Review of Plant Physiology*, 29(1), pp.319-344.
- Mur, R., Skulberg, O.M. and Utkilen, H., 1999. Cyanobacteria in the environment.
- Komárek, J., 2016. Review of the cyanobacterial genera implying planktic species after recent taxonomic revisions according to polyphasic methods: state as of 2014. *Hydrobiologia*, 764(1), pp.259-270.
- Perez, R., Wörmer, L., Sass, P. and Maldener, I., 2018. A highly asynchronous developmental program triggered during germination of dormant akinetes of filamentous diazotrophic cyanobacteria. *FEMS microbiology ecology*, 94(1), p. fix131.
- Pretty, J.N., Mason, C.F., Nedwell, D.B., Hine, R.E., Leaf, S. and Dils, R., 2003. Environmental costs of freshwater eutrophication in England and Wales.
- Rachita, 2014. Difference between cyanobacteria and green algae. *DifferenceBetween.net*.
- Rasmussen, B., Fletcher, I.R., Brocks, J.J. and Kilburn, M.R., 2008. Reassessing the first appearance of eukaryotes and cyanobacteria. *Nature*, 455(7216), pp.1101-1104.
- Soilage, 2020 Akinetes, viewed 27 June 2020, <https://www.soilalgae.com/pages/akinetes>.
- Sivonen, K. and Jones, G., 1999. Cyanobacterial toxins. Toxic cyanobacteria in water: a guide to their public health consequences, monitoring and management, 1, pp.43-112.
- Suikkanen, S., Pulina, S., Engström-Öst, J., Lehtiniemi, M., Lehtinen, S. and Brutemark, A., 2013. Climate change and eutrophication induced shifts in northern summer plankton communities. *PLoS one*, 8(6), p.e66475.
- Sukenik, A., Kaplan-Levy, R.N., Viner-Mozzini, Y., Quesada, A. and Hadas, O., 2013. Potassium deficiency triggers the development of dormant cells (akinetes) in *Aphanizomenon ovalisporum* (Nostocales, Cyanoprokaryota). *Journal of phycology*, 49(3), pp.580-587.
- Tonk, L., Bosch, K., Visser, P. M., & Huisman, J. (2007). Salt tolerance of the harmful cyanobacterium *Microcystis aeruginosa*. *Aquatic Microbial Ecology*, 46(2), 117-123.
- Vincent, W. J. (2001). Nutrient partitioning in the upper Canning River, Western Australia, and implications for the control of cyanobacterial blooms using salinity. *Ecological Engineering*, 16(3), 359-371.

Appendix 1

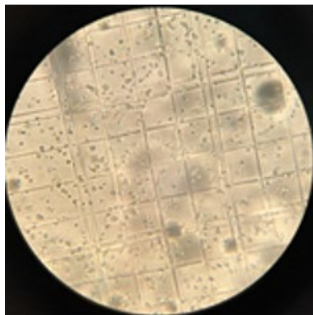
Images of final plates for every sample

Control Group

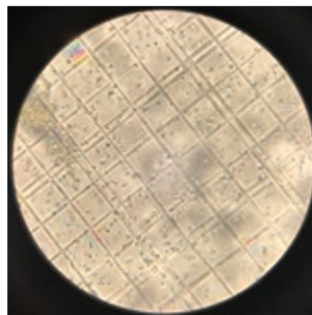


50.0 ppt salinity

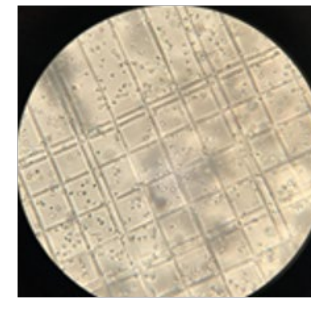
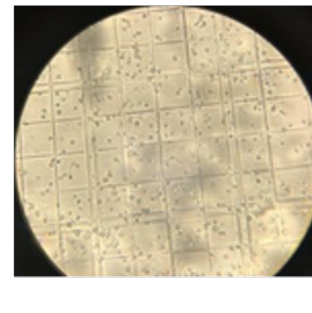
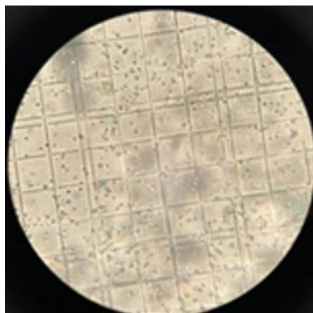
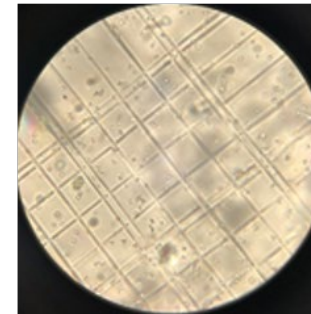
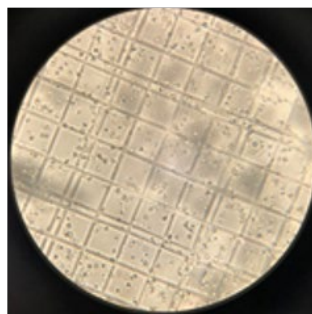
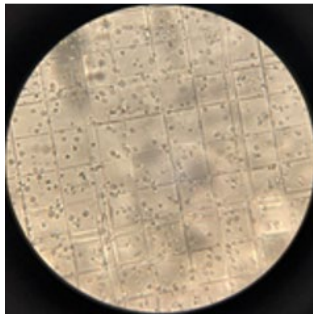
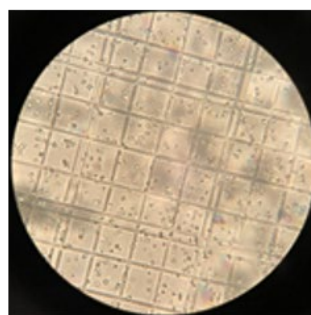
20°C



25°C



35°C

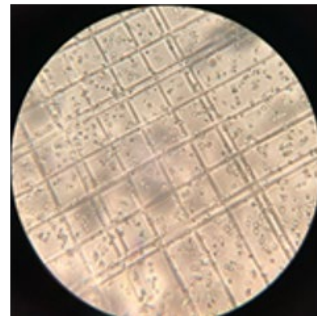
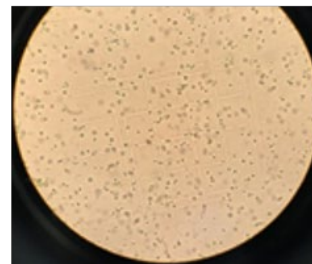
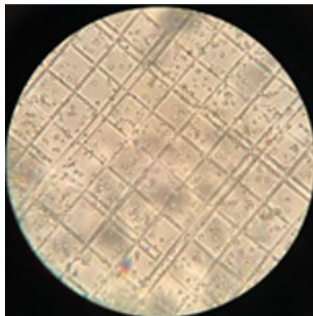
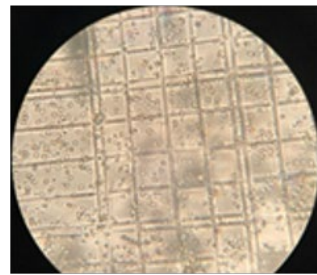
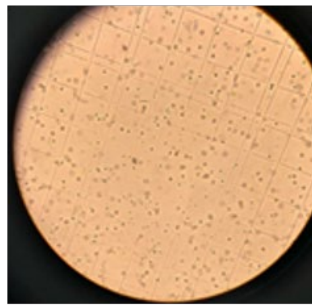
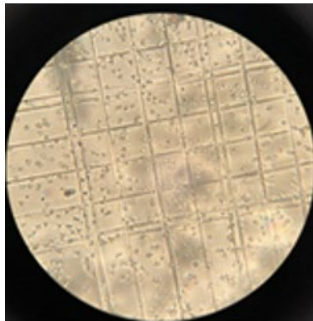
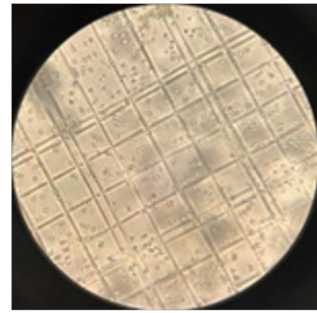
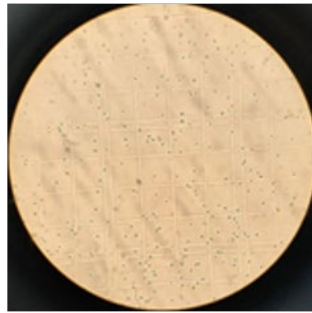
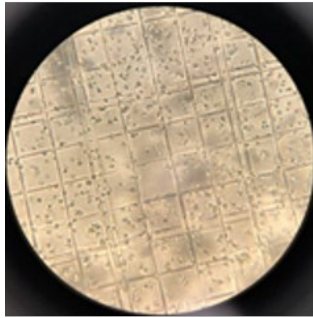


5.0 ppt salinity

20°C

25°C

35°C

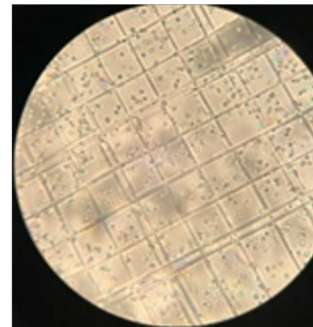
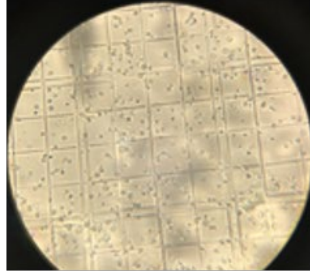
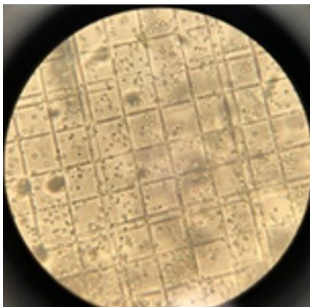
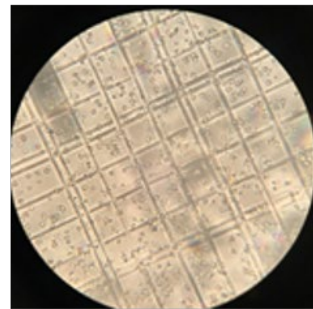
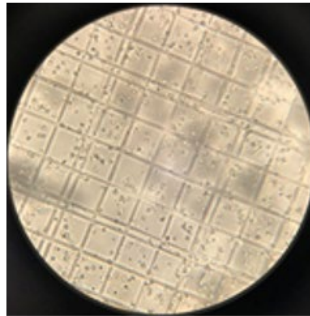
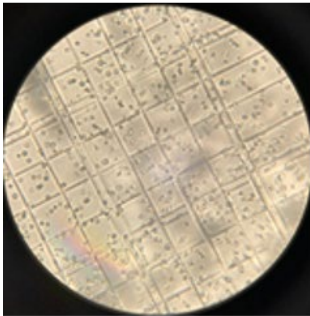
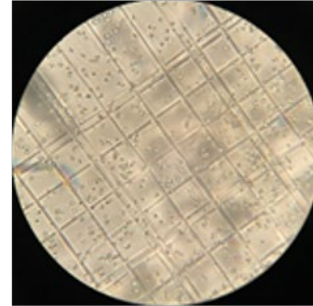
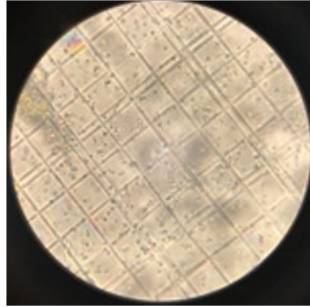
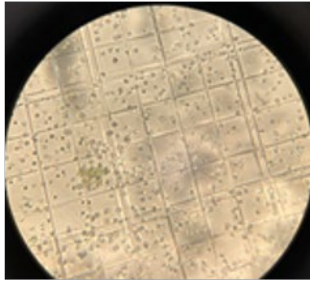


0.5 ppt salinity

20°C

25°C

35°C

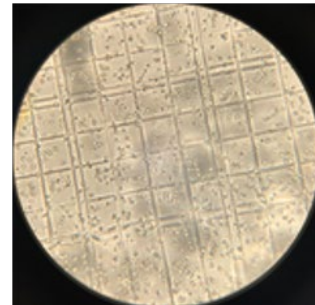
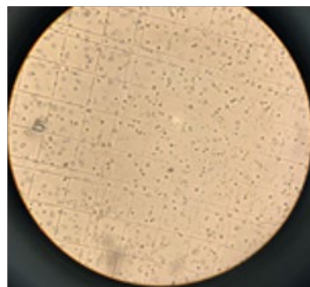
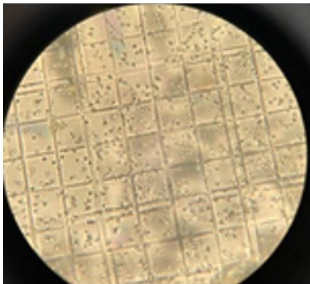
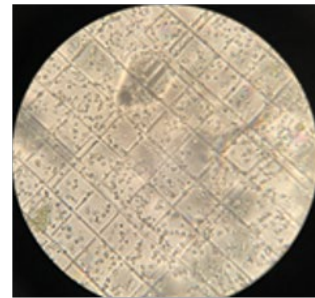
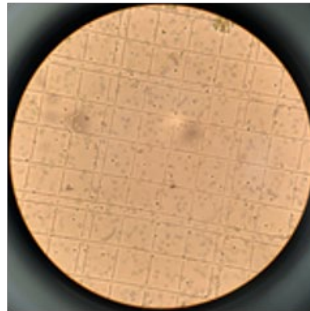
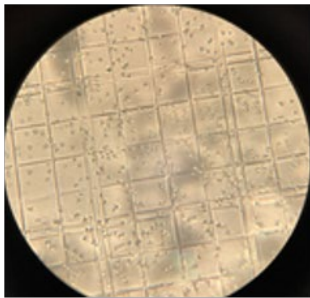
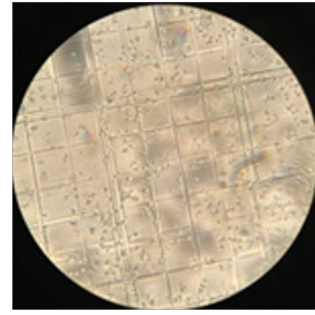
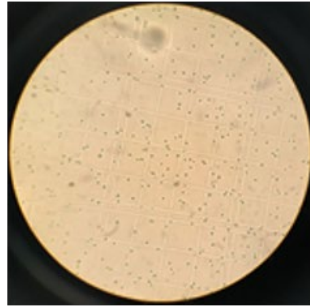
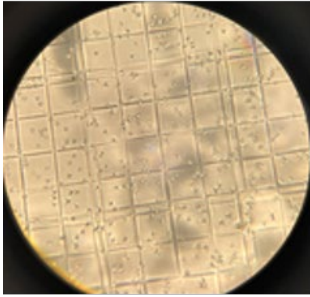


0.0 ppt salinity

20°C

25°C

35°C





Conference Presentations

Dissemination is an essential part of the scientific research process.

Along with publishing in this journal, multiple students have submitted to external journals and conferences. This offers an exciting opportunity for students (and staff) to share their work directly with the academic community. There were three things that were particularly exciting about Arabella's poster being accepted to the Australasian Science Education Research Association (ASERA) conference.

First, she was the only high school student presenting at an international conference for academics and postgraduate students. Second, two academics who Arabella collaborated with for her project were authors of their own paper presentations at the conference. Third, the three Science Extension teachers presented a proposal of a new model of teaching as part of the Science Extension course at the very same conference.

Teachers, student and academics became equal peers for the conference as they shared their work, received feedback and explored brand new research amongst the science education community.

Emotions in the Student Physics Laboratory

The impact of colour and story on secondary school student emotion during physics practical tasks.

Arabella Crowley | Matthew Hill
Barker College, Australia

Barker
Inspiring Tomorrow

Poster presented at the
Australasian Science Education Research Association Conference (ASERA) 2020

Abstract

Facilitating positive student emotions in any classroom is important for many reasons, including supporting their emotional wellbeing and allowing for meaningful learning to occur. Physics is a discipline associated with diverse emotions; some enjoy it, others do not. This is especially true for the laboratory classroom.

This study uses a recent adaptation of the Achievement Emotions Questionnaire, the AEQ-PhysicsPrac, to assess the emotional impact of the inclusion of colour and story in high-school physics laboratory instructional material. Previously the AEQ-PhysicsPrac has only been used to measure emotions at a university level.

As part of a Year 12 Science Extension research project, 69 Year 11 Physics students at a secondary school in Sydney, Australia completed a practical activity using instructional material that was either in black and white (adapted from the existing practical instructional material) or a new set of material that also incorporated green coloured checkpoints, a colourful image, and a historical narrative background information. Results are presented across six achievement emotions: Pride, Enjoyment, Anger, Anxiety, Hopelessness and Boredom. For these particular students, the inclusion of colour and storytelling in practical instructional material had a positive effect on all six measured emotions, which is consistent with the results from research at a university level. More research is needed to investigate the generalisability of this result.

Contact Information



Arabella Crowley
Year 12 Science Extension Student



Dr Matthew Hill
Director of the Barker Institute

Barker College
91 Pacific Highway,
Hornsby NSW, 2077

Phone: +61 2 8438 7585
E-mail: mhill@barker.nsw.edu.au
Web: www.barkerinstitute.com.au

Background Research

Physics education research has revealed that the implementation of colour and storytelling in physics helps to increase student engagement and motivation (Kuh, Cruce, Shoup, Kinzie, & Gonyea, 2008), attention retention and memory performance (Olorinolola & Tayo, 2015), and positive emotions towards physics (Lim, 2019). This suggests that by using colour and story we might increase both positive emotions and also engagement. It is particularly important for subjects such as Physics which is often associated with particularly diverse, and often negative, emotions due to the perceived difficulty (Pekrun, Goetz, Titz, & Perry, 2002; Williams, Stanistreet, Spall, Boyes, & Dickson, 2003).

The Achievement Emotion Questionnaire (AEQ) is an established survey implemented in diverse contexts with sound statistical results (Pekrun, Goetz, Frenzel, Petra, & Perry, 2011). The AEQ has been modified for use in specific contexts (e.g. the Mathematics AEQ (AEQ-M) (Pekrun, Goetz, & Frenzel, 2005) and recently for use in the context of students completing physics practicals (Bhansali & Sharma, 2020). The emotions measured in the AEQ-PhysicsPrac were pride, enjoyment, anger, anxiety, hopelessness, and boredom.

As part of validating the AEQ-PhysicsPrac Bhansali and Sharma (2020) administered the survey to 320 undergraduate Physics students completing two different Physics laboratory activities. One group of students undertook the intervention which consisted of a new newly developed practical on 'heat and thermodynamics' and contained a colourful historical science story. The control was an established practical on 'ultrasound', having a theoretical background with no colour, science story, or historical context. Bhansali and Sharma found that students completing the heat and thermodynamics practical activity reported significantly higher scores on the positive emotions and significantly lower scores on most of the negative emotions (anxiety being the exception).

To what extent is this result generalisable to a wider context? Can colour and story support positive emotions for high school students completing Physics practical tasks too?

Procedure

The research involved an experimental, small-scale procedure, including 69 Year 11 students studying Physics as an elective, 15 to 17 years old, with around 15% females. It was conducted at a single Pre-Kindergarten to Year 12, Independent, coeducational School in Sydney, Australia. The cohort constitutes of 5 mixed ability classes with different teachers. An existing practical activity for Year 11 was selected for this investigation. The activity chosen was 'Measuring Acceleration due to Gravity' which required students to drop tennis balls from various heights while measuring the time taken for them to reach the ground.

The intervention involved the instructional material being modified to include a historical science story with a colourful image (Figure 1). The control had a black and white theoretical background of the same length. Along with recording an initial emotion, the activity was finished by completing the AEQ-PhysicsPrac (Figure 2).



Figure 2: A flow chart comparing the intervention (colour and story) with the control (black and white)



Figure 1: The front page of the intervention version of the material

Results and Discussion

Table 1: Comparing intervention with control for each emotion including the p-value for a one-tailed student's t-test

Emotion	Mean (SD)		Range	p-value
	Intervention (n=37)	Control (n=32)		
Initial emotion	3.1 (0.9)	3.5 (0.6)	1-5	0.048
Pride	14.1 (2.1)	13.5 (2.4)	9-19	0.118
Enjoyment	17.4 (2.4)	16.8 (2.6)	11-22	0.165
Anger	6.5 (1.3)	6.8 (2.4)	3-12	0.222
Anxiety	6.6 (2.1)	6.7 (2.0)	3-13	0.444
Hopelessness	3.9 (1.5)	4.0 (1.7)	2-9	0.331
Boredom	5.2 (1.6)	5.7 (1.8)	2-10	0.110

Mean scores for each emotion if the AEQ-PhysicsPrac.

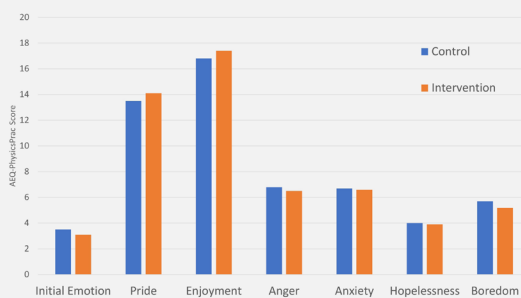


Figure 3: Mean scores for each emotion if the AEQ-PhysicsPrac. Initially the students using the intervention material had a lower overall emotion but after completing the activity had slightly higher positive emotions and slightly lower negative emotions.

Initially the students from the intervention group reported a lower level of happiness prior to the activity (indicated by circling a face on the front page (see Figure 1).

After the experiment, on average, these students exposed to colour and story were measured to have higher scores on the positive emotions (pride and enjoyment) and lower scores on the negative emotions (anger, anxiety, hopelessness, and boredom) than students using the regular black and white material.

The results are consistent with the previous research using the same instrument in a university context (Bhansali & Sharma, 2020). Positive emotions are enhanced and negative emotions decreased when encountering colour and story in the Physics laboratory. It is important to note that the t-tests did not indicate a significant difference between any of the means for the six emotions. This does not suggest the results are not meaningful, they are consistent with previous research in a different context, rather that more research needs to be done to come up with a more universal conclusion on the impact of storytelling in a secondary school Physics context.

Further research

- The same instructional material can be used in future years with Year 11 students and the data combined to increase the sample size. This may affect the p-values.
- Studies in secondary school have a variety of factors that are difficult to control. These include the time of day or day of the week that the class occurred, and the teacher who supervised the class. Dividing each class into students who completed the control and the intervention goes towards mitigating this.
- The research can be expanded to other practical investigations in Year 11 Physics, or those in other Scientific domains.
- Analysis of student qualitative responses about the task and their emotions.

Bhansali, A., & Sharma, M. D. (2020). The Achievement Emotions Questionnaire: Validation and implementation for undergraduate physics practicals. *International Journal of Innovation in Science and Mathematics Education (Formerly CAL-Laborate International)*, 27(9), Article 9. <https://openjournals.library.sydney.edu.au/index.php/CAL/article/view/14011>

Kuh, G. D., Cruce, T. M., Shoup, R., Kinzie, J., & Gonyea, R. M. (2008). Unmasking the effects of student engagement on first-year college grades and persistence. *The Journal of Higher Education*, 79(5), 540-563.

Lim, B. (2019). The Story of Physics: Storytelling for High School Physics Teaching. *Ontario Association of Physics Teachers Newsletter*. <http://newsletter.oapt.ca/files/story-of-physics.html>

Olorinolola, O., & Tayo, O. (2015). Colour in Learning: Its Effect on the Retention Rate of Graduate Students. *Journal of Academic and Practice*, 6(14), 1-5.

Pekrun, R., Goetz, T., Frenzel, A. C., Barchfeld, P., & Perry, R. P. (2011). Measuring emotions in students' learning and performance: The Achievement Emotions Questionnaire (AEQ). *Contemporary Educational Psychology*, 36(1), 36-48. <https://doi.org/10.1016/j.cedpsych.2010.10.002>

Pekrun, R., Goetz, T., Titz, W., & Perry, R. P. (2002). Academic emotions in students' self-regulated learning and achievement: A program of qualitative and quantitative research. *Educational Psychologist*, 37(2), 91-105.

Williams, C., Stanistreet, M., Spall, K., Boyes, E., & Dickson, D. (2003). Why aren't secondary students interested in physics? *Physics Education*, 38(4), 324-329. <https://doi.org/10.1088/0031-9120/38/4/306>

The effect of colour and story on student emotion during physics practical tasks

Arabella Crowley & Dr Matthew Hill*

Barker College

*Corresponding author: mhill@barker.nsw.edu.au

Existing research indicates that the emotional component of the student experience in physics teaching must not be neglected. The use of colour and storytelling in physics instruction has been shown to have positive effects on student attention, retention and memory, engagement, motivation, and positive emotions towards physics. Physics laboratory materials can often be devoid of colour or storytelling and measuring emotions can be difficult. This is currently being investigated at the tertiary level involving the validation of the Achievement Emotions Questionnaire adapted for physics practicals (AEQ-PhysicsPrac) (Bhansali & Sharma, In press).

In this study, 80 Physics students in Year 11 completed one of two modified practical tasks as part of normal instruction. One set of instruction was introduced with a background story and colour was integrated throughout, the other followed the traditional method of practical instruction with information presented simply and in black and white. Student emotions were measured with the AEQ-PhysicsPrac allowing comparisons between levels of pride, enjoyment, anger, hopelessness, boredom and anxiety.

This research is being completed by Arabella Crowley, a high school student studying the NSW Science Extension HSC course being supervised by Matthew Hill who completed his PhD in Physics Education in 2016.

Reference

Bhansali & Sharma, In press, Int Journal of Innovation in Sci and Math Ed

A new frontier in secondary science education: scientific research to high school students

Dr Matthew Hill, Dr Alison Gates & Dr Katie Terrett

Barker College

mhill@barker.nsw.edu.au, agates@barker.nsw.edu.au, kterrett@barker.nsw.edu.au

Science Extension was offered in the NSW HSC for the first time in 2019. This innovative new course posed a fresh set of challenges for secondary Science teachers. Based around a high level individual research project, culminating in a 3000 word scientific report, the course demands that teachers step from their classroom and into the world of research supervision. This paper presentation uses literature and ethnographic methodology to report on the challenges and benefits of amalgamating university-level research and supervision in a high-school context. From our unique perspective as teachers that have transitioned from postgraduate research and academic appointments to the secondary classroom, we feel positioned to contribute to this frontier in science education.

Our research includes a review of the literature on undergraduate research supervision at the tertiary level to inform perspectives on equipping science teachers to meet the demands of this course. By drawing on this research and using an ethnographic frame to explore our own *teaching* experiences, this research identifies crucial skills in undergraduate research supervision and explores how these might translate into secondary settings. We provide a rationale for resourcing and developing specialist supervision skills in secondary science teachers.



91 Pacific Highway
Hornsby NSW 2077
Australia

+61 2 8438 7999
barker.college